Charles University

Faculty of Science

Study program: Physical chemistry

Mgr. Valeryia I. Kasneryk

Design of zeolite materials with tailored interlayer structure and tunable textural properties

Doctoral thesis

Supervisor: Dr. Maksym V. Opanasenko

Adviser: Prof. Ing. Jiří Čejka, DrCs.

Prague, 2018

Univerzita Karlova

Přírodovědecká fakulta

Studijní program: Fyzikální chemie

Mgr. Valeryia I. Kasneryk

Návrh zeolitických materiálů s řízenou strukturou a texturními vlastnostmi

Disertační práce

Školitelé: Dr. Maksym V. Opanasenko

a Prof. Ing. Jiří Čejka, DrCs.

Praha, 2018

Prohlášení:

Na dizertační práci jsem pracovala v Ústavu fyzikální chemie J. Heyrovského, AV ČR.

Prohlašuji, že jsem závěrečnou práci zpracovala samostatně a že jsem uvedla všechny použité informační zdroje a literaturu. Tato práce ani její podstatná část nebyla předložena k získání jiného nebo stejného akademického titulu.

V Praze, 01.06.2018

Acknowledgments

Abbreviations

ADOR	– Assembly-Disassembly-Organisation-Reassembly
BET	– Surface area according Brunauer-Emmet-Teller isotherm
DEDMS	– Diethoxydimethylsilane
DFT	– Density Functional Theory
DMBIH	– 1,2-Dimethyl-3-(3-methylbenzyl)imidazolium hydroxide
DMDH	– Decamethonium dihydroxide
D4R	– Double four ring - secondary building unit
D3R	– Double three ring - secondary building unit
FCC	– Fluid catalytic cracking
HETCOR NMR	– Heteronuclear Correlation Nuclear Magnetic Resonance Spectroscopy
HRTEM	– High Resolution Transmission Electron Microscopy
HMH	– Hexamethonium dihydroxide
IF	– Impact factor
IZA	– International Zeolite Association
FTIR	– Fourier Transform Infrared Spectroscopy
MPPH	– 1,5-bis-(methylpyrrolidinium)pentane
MTH	– Methanol to hydrocarbons
MTP	– Methanol to propene
MAS NMR	– Magic Angle Spinning Nuclear Magnetic Resonance
SDA	– Structure directing agent
S4R	– Single four ring secondary building unit
SEM	– Scanning Electron Microscopy
Si/Ge	– Silicon to germanium atoms ratio
TEOS	– Tetraethyl orthosilicate
TMHDA	– N,N,N′,N′-tetramethyl-1,6-hexanediamine
V_{meso}	– Mesopore volume
V_{micro}	– Micropore volume
V_{tot}	– Total adsorption volume
XRD	– X-ray Diffraction
2D	– two-dimensional

3D — three-dimensional

Abstract

Germanosilicate zeolites attracted a lot of attention during the last decade. The reason is related to the unique structural properties of germanosilicates, which include zeolites of **UTL**, **UOV**, **ITH**, **IWR**, **IWW**, and CIT-13 types. The frameworks of these materials can be described as Si-rich layers connected by double four ring (D4R) units preferentially occupied by Ge atoms. Hydrolytic instability of Ge–O bonds in mentioned frameworks compared with Si–O bonds in conventional zeolites gives the opportunity for controllable chemically selective transformation of the germanosilicate frameworks towards novel types of zeolites including their 2D analogues.

This PhD thesis focuses on modification of the structure and textural prope germanosilicates using different ways of post-synthesis treatment: the ADOR (**A**ssembly – **D**isassembly – **O**rganization – **R**eassembly) transformation and post-synthesis degermanation and alumination. Presented work was carried out in the Department of Synthesis and Catalysis at J. Heyrovský Institute of Physical Chemistry in Prague under the supervision of Dr. Maksym Opanasenko and advising of Prof. Jiři Čejka.

The first post-synthesis treatment applied in this work was the recently developed method of zeolite synthesis – the ADOR transformation. Investigation of germanosilicates **UOV**, CIT-13 and **IWR** possessing Ge-rich D4R units in the frameworks allowed us to expand the "IPC-family" by 3 novel zeolites (IPC-12, IPC-13, and IPC-17, respectively) and confirm versatility of this technique.

It was found that the framework of novel IPC-12 zeolite consists of the same layers as parent **UOV** zeolite, but they are connected by O-bridges in contrast to **UOV** possessing connectivity through the D4R units. The possibility of IPC-12 formation by 2 different ways was demonstrated. The first one is based on a controllable Disassembly under moderately acidic conditions (pH = 1) followed by calcination (Reassembly); the other one consists of direct **UOV**-to-IPC-12 rearrangement at highly concentrated acid (pH < −1).

The frameworks of new zeolites IPC-13 and IPC-17 obtained by the ADOR protocol were shown to have structure similarities. The layers in these materials were connected by the single four ring (S4R) units, in contrast to D4R connectivity for parent CIT-13 and **IWR** germanosilicates (respectively). Thus, the ADOR approach can be applied to control zeolite structure properties, as transformation of D4R units into O-bridges or S4R change the pore system in final materials.

Moreover, modification of the ADOR approach as a method was performed. For the first time, it was demonstrated that the ADOR can be realized under solvent-free conditions. It was achieved by the treatment of zeolite with H_2O/HCl vapours, i.e. without direct contact of material with the respective solution. Application of germanosilicate **IWW** led to the formation of a new zeolite IPC-18. In the zeolite IPC-18 the layers have the same structure as in the parent **IWW** but connected by S4R units in contrast to D4R units in the parent material.

The second part of this work was devoted to post-synthesis modification of germanosilicate zeolites not leading to the frameworks transformation. Germanosilicates **UOV**, **ITH,** and **IWW** possessing the D4R units enriched with Si atoms were applied for tuning of textural properties and design of hierarchical materials. Their acidic degermanation resulted in formation of additional micro- and mesopores, which amount was controlled by appropriate choice of chemical composition of the starting material and conditions of the treatment (pH, temperature and duration).

Post-synthesis alumination was studied for germanosilicates **UOV**, **ITH**, CIT-13, **UTL**, and **IWW**. Incorporation of Al atoms in zeolite framework resulted in formation of both Brønsted and Lewis acid centres. The process was accompanied with formation of additional mesopores and increase in the surface area, which makes obtained materials perspective for investigation in catalysis.

Comparison of post-synthesis alumination with direct synthesis of aluminium containing zeolites showed that the post-synthesis treatment is more suitable method for Al incorporation, as it resulted in introduction of a higher amount of Al atoms into the framework and generation of a higher number of both Brønsted and Lewis acid centres.

For the first time the mechanism of post-synthesis alumination in germanosilicates was studied using XRD, ^{24}Al and ^{29}Si MAS NMR and ICP-OES techniques. Kinetic investigation of post-synthesis substitution of Ge by Al atoms for germanosilicate **UOV** showed that this process proceeds through multi-stage mechanism. The first step consists of degermanation and partial disassembly of the **UOV** framework followed by Al incorporation and healing the silanol defects in the framework in the second step.

Abstrakt

V posledních deseti letech germanokřemičitanů zeolity přitahovaly velkou pozornost vědců. Důvodem pro tento zájem jsou jedinečné strukturní vlastnosti germanokřemičitanů, které zahrnují zeolity **UTL**, **UOV**, **ITH**, **IWR**, **IWW** a CIT-13. Struktury těchto materiálů obsahují křemíkové vrstvy spojené jednotkami „double four ring" (D4R), které jsou přednostně obsazenv atomy germania. Hydrolytická nestabilita chemických vazeb Ge-O ve srovnání s vazbami zeolitech nabízí možnost kontrolovatelné selektivní transformace germanokřemičitanů na nové typy zeolitů včetně jejich 2D analogů.

Tato disertační práce se zabývá modifikací struktury a texturních vlastností germanokřemičitanů s použitím různých způsobů postsyntetické modifikace: ADOR (**A**ssembly – **D**isassembly – **O**rganization – **R**eassembly) přeměnou a postsyntetickou degermanací a aluminací. Práce byla vypracována na Oddělení syntézy a katalýzy Ústavu fyzikální chemie J. Heyrovského AV ČR, v.v.i. pod vedením Dr. Maksyma Opanasenka a prof. Jiřího Čejky.

První metodou postsyntetické úpravy materiálů byla v této práci syntéza zeolitů pomocí ADOR přeměny. Studium germanokřemičitanů **UOV**, CIT-13 a **IWR**, které obsahují D4R jednotky bohaté na germanium umožnilo rozšířit skupinu IPC materiálů o 3 nové zeolity (IPC-12, IPC-13 a IPC-17) a potvrdit univerzálnost této techniky.

Struktura nového zeolitu IPC-12 se skládá ze stejných vrstev jako výchozí zeolit **UOV,** ale vrstvy jsou spojeny přes kyslíkovémůstky na rozdíl od **UOV**, které jsou vázány prostřednictvím D4R jednotek. Dva různé způsoby byly prokázány. První z nich je kontrolovaný rozklad (Disassembly) v neutrálním nebomírně kyselém prostředí (pH = 1) následovaný kalcinací (Reassembly); druhou metodou je přímá přeměna **UOV** na IPC-12 v přítomnosti vysoce koncentrované kyseliny (pH <-1).

Bylo prokázáno, že struktury nových zeolitů IPC-16 a IPC-17 získaných transformací ADOR metodou mají podobnou strukturu. Vrstvy v těchto materiálech jsou spojeny jednotkami „single four ring" (S4R), na rozdíl od spojení přes D4R jednotky typické pro původní germanosilikáty CIT-13 a **IWR**. ADOR metodu lze tedy aplikovat pro syntézu zeolitů s řizenou strukturou, jelikož během transformace dochází k přeměně D4R jednotek na kyslíkové můstky nebo na S4R jednotky, které mění systém pórů konečných materiálů.

V další části práce byla metoda ADOR modifikována. Poprvé bylo prokázáno, že ADOR metodu lze provést bez přítomnosti rozpouštědel. Toho bylo dosaženo zpracováním zeolitu

přítomností par H_2O/HCl, tedy bez přímého kontaktu materiálu s roztokem. Užitím této metody k přeměně germanokřemičitanu **IWW** za vzniku nového zeolitu IPC-18. Vrstvy zeolitu IPC-18 mají stejnou strukturu jako původní **IWW** germanosilikát, ale jsou spojeny jednotkami S4R na rozdíl od jednotek D4R ve výchozím materiálu.

Druhá část práce se zabývá postsyntetickou modifikací germanokřemičitanových zeolitů (bez transformace zeolitových struktur). Germanokřemičitanové zeolity **UOV**, **ITH** a **IWW** obsahující jednotky D4R obohacené křemíkem byly použity pro kontrolu texturních vlastností a návrh nových hierarchických materiálů. Odstranění germania **UOV**, **ITH** a **IWW** v kyselém prostředí vedla k tvorbě dodatečných mikro- a mesoporů, jejich množství bylo řízeno vhodnou volbou chemického složení výchozího zeolitu a podmínek jeho zpracování (pH, teplota a čas).

Postsyntetické aluminace byla zkoumána pro germanokřemičitany **UOV**, **ITH**, CIT-13, **UTL** a **IWW**. Zavedení atomů hliníku do zeolitové struktury vedlo k vytvoření Brønstedových a Lewisových kyselých center. Proces byl doprovázen tvorbou mesoporů a zvětšením plochy povrchu, což činí tyto materiály atraktivní pro použití v katalýze.

Výsledky práce ukázaly, že metoda postsyntetické aluminace je vhodnějším způsobem zavádění Al nežpřímá syntéza germanokřemičitanů obsahujících hliník. Postsyntetické úpravy původních germanosilikátů vedou k syntéze zeolitů s vyšším obsahem Al a tvorbou většího množství Brønstedových a Lewisových center.

Poprvé byl studován mechanismus postsyntetické aluminace v germanokřemičitanech za použití technik XRD, ^{24}Al MAS a ^{29}Si NMR a ICP/OES. Studium kinetiky postsyntetické substituce germania atomy hliníku pro germanokřemičitan **UOV** ukázalo, že tento proces probíhá prostřednictvím vícestupňového mechanismu. Prvním krokem je degermanace a částečný rozklad (disassembly) struktury **UOV**, následovaný ve druhém kroku insercí Al a opravou silanolových defektů ve struktuře.

List of publications

1. <u>Kasneryk, V.</u>; Shamzhy, M.; Opanasenko, M.; Wheatley, P. S.; Morris, S. A.; Russell, S. E.; Mayoral, A.; Trachta, M.; Čejka, J.; Morris, R. E., Expansion of the ADOR Strategy for the Synthesis of Zeolites: The Synthesis of IPC-12 from Zeolite UOV. *Angewandte Chemie-International Edition* **2017,** *56* (15), 4324-4327. (**IF** = 11.994)

2. <u>Kasneryk, V.</u>; Opanasenko, M.; Shamzhy, M.; Musilová, Z.; Avadhut, Y. S.; Hartmann, M.; Čejka J., Consecutive interlayer disassembly–reassembly during alumination of UOV zeolites: insight into the mechanism. *Journal of Materials Chemistry A* **2017**, *5*, 22576-22587. (**IF** = 8.867)

3. <u>Kasneryk, V.</u>; Shamzhy, M.; Opanasenko, M.; Wheatley, P. S.; Morris, R. E.; Čejka, J., Insight into the ADOR zeolite-to-zeolite transformation: the UOV case. *Dalton Transactions* **2018**, *47*, 3084-3092. (**IF** = 4.029)

4. <u>Kasneryk, V. I.</u>; Shamzhy, M. V.; Opanasenko, M. V.; Čejka, J., Tuning of textural properties of germanosilicate zeolites ITH and IWW by acidic leaching. *Journal of Energy Chemistry* **2016,** *25* (2), 318-326. (**IF** = 2.594)

5. Shamzhy, M. V.; Ochoa-Hernandez, C.; <u>Kasneryk, V. I.</u>; Opanasenko, M. V.; Mazur, M., Direct incorporation of B, Al, and Ga into medium-pore ITH zeolite: Synthesis, acidic, and catalytic properties. *Catalysis Today* **2016,** *277*, 37-47. (**IF** = 4.636)

Further publications:

6. Rubeš M.; Trachta M.; Koudelková E.; Bulánek R.; <u>Kasneryk V.</u>; and Bludský O., Methane adsorption in ADOR zeolites: A combined experimental and DFT/CC study. *Physical Chemistry Chemical Physics* **2017**, *19*, 16533. (**IF** = 4.123)

Contents

1. Aims of the study

The PhD thesis focuses on the chemistry of germanosilicate zeolites: their post-synthesis transformation into novel zeolites; and post-synthesis modification resulted in tuning of their textural and acidic properties. The main goals are summarized as follows:

✓ To show general applicability of the ADOR (Assembly – Disassembly – Organization – Reassembly) approach through its expansion on **UOV**, CIT-13, **IWW**, and **IWR** germanosilicates.

✓ To synthesise new zeolite materials based on transformation of mentioned zeolites.

✓ To perform detail characterization of the properties of obtained novel zeolites using X-ray powder diffraction (XRD), nitrogen and argon adsorption, microscopy techniques: scanning electron microscopy (SEM) and transmission electron microscopy (TEM), nuclear magnetic resonance (NMR), Fourier transform infrared spectroscopy (FTIR), inductively coupled plasma atomic emission spectroscopy (ICP/OES).

✓ To elaborate the ADOR approach applying chemical vapour treatment (i.e. "solvent-free conditions").

✓ To design hierarchical zeolite materials based on the post-synthesis treatment of **IWW**, **ITH** and **UOV** germanosilicate. To optimize conditions of the treatment in order to control micro- and mesopore volumes and surface area.

✓ To modify the acidic properties of zeolite **UOV** and its derivative zeolite IPC-12 by post-synthesis incorporation of Al atoms in the framework.

✓ To investigate the mechanism of post-synthesis substitution of Ge in the framework positions by Al atoms.

2. Introduction

2.1. Zeolites

Nowadays, the role of zeolite materials for industrial processes can be hardly estimated. Zeolites are microporous crystalline materials with three-dimensional networks consisting of corner-sharing TO_4 tetrahedra, where T is a tetrahedrally coordinated atom (Al, Si, Ti, Ge, Ga, B, P etc)[1-4]. The structure and chemical composition of zeolites influence their acidic and sorption properties determining their applications in heterogeneous catalysis[4-9], gas separation[10-12] and storage[13-17], and ion exchange[18-20]. Recently, using of zeolites expanded to medicine[21-22], optics[21], chemical sensors[23-24] and electronics[25].

For designation of different types of zeolite materials, the Structure Commission of the International Zeolite Association (IZA)[26] created the unique 3-letter codes (e.g. **FAU**, **MFI**, **BEA**), which is applied in the thesis.

2.2. Short Overview on Historical Development and Zeolites Application

The history of zeolites began from the works of mineralogist Axel F. Cronstedt, who found a new mineral in copper mine in Iceland in 1756. A. F. Cronstedt named it "zeolite" (from Greek ζέω - to boil and λίθος – stone), as a new discovered material seemed to boil when heated. The next big step, which started the era of fabrication of synthetic zeolites, was done in 1930th by Prof. Richard M. Barrer, when he showed the possibility of synthesis of chabazite and mordenite[27-28]. The following turning point was the introduction of organic cations as structure-directing agents (SDAs, also called templates) in 1960s[3], which resulted in the synthesis of a number of previously unknown zeolite topologies with high silicon to aluminium ratios. Industrial application of zeolite materials started by Union Carbide for gas drying in 1954 and for paraffin separation in 1959[29]. At the same time, these materials were firstly applied as the ion exchangers. Since 1962, when zeolites have been firstly applied by Mobil as acid catalysts for FCC process, they became key materials for industrial use.

2.3. Framework Types

The framework of zeolites is characterized by the unique size, shape, connectivity of the channels and presence of cavities. The size of channel system is delimited by the size of the pore opening, which is defined by the number of T-atoms. According to this number, zeolites are classified as small (8-ring pores with diameter ~ 4.0 Å), medium (10-ring, d ~ 5.5 Å), large (12-ring, d ~ 7.0 Å) and extra-large pore (> 12-ring)[30-31]. The textural properties of zeolites also depend on the void spaces and the interconnectivity of the channels. According to these parameters zeolites can have: one-dimensional pore system having no intersections of channels (e.g. **LTL**, **AFI**); two-dimensional channel systems possessing intersections of two channels of different sizes (e.g. **MOR**, **UTL**); three-dimensional channel systems with (e.g. **FAU**) or without cavities at the channel intersections (e.g. **MFI**, **SOD**); or even two independent three-dimensional channel systems (e.g. **PAU**, **MWW**)[1].

The properties of zeolites depend also on chemical composition of framework and distribution of T-elements, presence of guest species in the pores, and stacking faults or defects of the framework. The range of Si/Al ratios varies depending on the material, as some zeolites can be obtained in a broad Si/Al ratio (e.g. **BEA**, Si/Al = 10 – 200) [30], another only at particular values (e.g. zeolite **IWV**, Si/Al = 30)[32]. Distribution of elements can also differ from one zeolite to another. While Al atoms are normally randomly distributed in zeolite frameworks, many heteroatoms preferentially occupy particular T-sites, for example Ge atoms, which are mostly located in double four ring (D4R) or double three ring (D3R) units in germanosilicate zeolites[33].

By now, there are about 235 different structural types, officially accepted by the Structure Commission of the IZA[26].

2.4. Synthesis of Zeolites

Zeolites can be obtained via hydrothermal synthesis. Syntheses are carried out in aqueous media in the presence of sources of silicon and aluminium or other T-elements and SDAs. Suitable silicon reagents for synthesis are fumed silica, precipitated silica, colloidal silica, sodium and potassium silicates, and alkoxy silanes (mainly tetraethyl orthosilicate, TEOS). As aluminium reagents, aluminium hydroxide, gibbsite ($Al_2O_3 \cdot 3H_2O$), boehmite (AlO(OH)), and

salts of aluminium (sulphate, nitrate, chloride), sodium and potassium aluminates, and aluminium alkoxides, such as aluminium isopropoxide are usually used. It should be noticed that some of zeolites may be obtained only in the presence of particular sources of T-elements. For example, germanosilicate **UOV**, which up to now was obtained only using Cab-O-Sil silica[34]. Inorganic (sodium, potassium ions etc.) or organic ions (mainly quaternary ammonium salts) are used as SDAs. The presence of SDA is essential to induce the zeolite formation that would not be formed without its presence. In many cases, an organic SDA acts as a "starting point" around which T-element species began to organize and then form crystalline framework. In some syntheses even T-elements can direct the formation of particular structures. For example, in the syntheses of germanosilicates, Ge atoms play the role of inorganic structure directing agent[35-38].

The crystallization conditions, namely temperature, duration and stirring rate can have a big impact on final phase formation. In most cases, syntheses are carried out in the range of temperatures between 100 and 200 °C and times from several hours to several month[26]. Longer duration and higher temperatures direct the synthesis to more thermodynamically stable, low porous or even non-porous phases. On the other hand, syntheses at short times and low temperatures can result in formation of amorphous or non-fully crystalline materials. Until the last decade, the choice of optimum conditions for synthesis of new zeolite was still based on the "trial-and error" approach[39-40].

2.5. 3D *vs* 2D zeolites

Most of solvothermal zeolites syntheses, which were discussed above, proceed directly to the three dimensional structures. Much rarely, reactions can pass through the formation of two-dimensional (2D) zeolite precursors, topotactic condensation of which leads to the final 3D structure[41]. 2D zeolites represent crystalline materials with thickness from one up to several nm (or 1 – 2 unit cells at maximum along one direction)[41-42]. Lamellar zeolites possess exceptional properties, because they combine the features of zeolites, such as Brønsted and Lewis acidity[43-46], and the advantages of 2D materials, i.e. high external surface area (helping to overcome diffusion limits). Moreover, in contrast to three-dimensional zeolites, zeolite layers can be modified and organized in different ways. Together with calcination, 2D zeolites can be swollen,

pillared, stabilized or delaminated [47-50]; which allows obtaining materials with different structural properties.

A lot of researches developed methods of 2D zeolite preparation (Fig. 1.), Several zeolites were formed via precursor-way using traditional hydrothermal synthesis[51]: **MWW**[52-53], **NSI**[54], **FER**[55], **SOD**[56], **CAS**[57], **RWR**[58], **RRO**[59], **AFO**[60], **CDO**[61-62], and **AST**[63]. The group of R. Ryoo developed another method using specially designed surfactant SDAs[64-66]. Such SDAs contain 2 parts; each of them is needed for different purpose. While the hydrophilic part of the surfactant (usually quaternary ammonium group) directs the zeolite crystallisation, the hydrophobic part of template restricts the crystal growth in one crystallographic direction. As a result, the **MFI** nanosheets were synthesised; obtained materials performed as perfect long-lifetime catalysts for the methanol to gasoline (MTG) conversion. It was also shown that the number of quaternary ammonium species control the thickness of nanosheets, which can be used for the design of materials for specific purposes[41].

Recently, the alternative approach for 3D-to-2D transformation was developed. This top-down method is based on selective disassembly of 3D zeolite with appropriate structure into a 2D layered material[41]. Based on this possible rearrangement and another 2 steps, the ADOR (Assembly-Disassembly-Organisation-Reassembly) approach of zeolite synthesis was discovered.
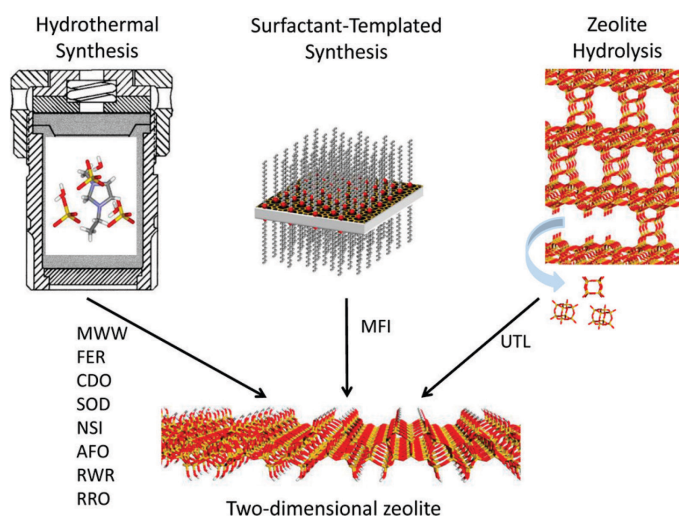

Fig.1. The three main ways of fabrication of 2D zeolites[41].

2.6. The ADOR Strategy for Zeolite Synthesis. IPC Family

The **ADOR** approach consists of 4 principal steps[33]. The first step, the *Assembly*, represent the synthesis of initial 3D zeolite via traditional hydrothermal protocols, described previously. After that, the parent zeolite is ***D**isassembled* under acidic conditions into a lamellar material (top-down synthesis). The next step includes post-synthesis treatment resulted in ***O**rganization* of the layers[67] formed previously. This process provides the layers orientation suitable for their ***R**eassembly*, the condensation into new 3D crystalline materials, which show connectivity between the layers different from the starting one. The scheme of the ADOR process is presented in the Fig. 2.
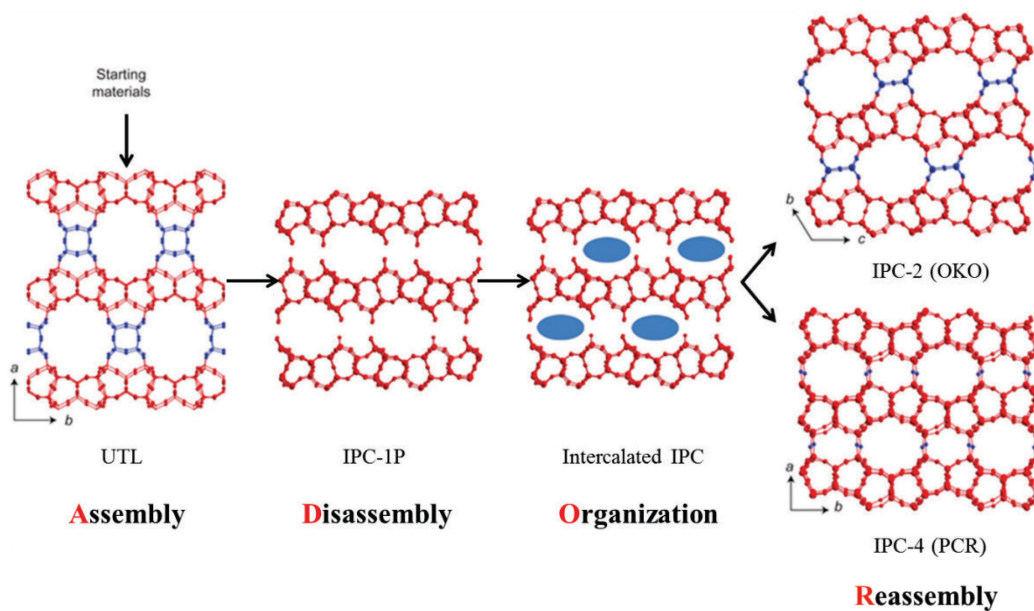
Fig. 2. The scheme of the ADOR strategy for zeolite synthesis, adopted from[68]. There are 4 principal steps of this approach: **A**ssembly, **D**isassembly, **O**rganization and **R**eassembly. Starting with **UTL** germanosilicate having Ge-rich D4R (marked blue) units, 2 new zeolites were obtained: IPC-2, where layers are connected by the S4R (**OKO** topology, on the top); and IPC-4 with direct connectivity (**PCR** topology, on the bottom). Both of them are not available by traditional hydrothermal methods of synthesis.

The structure of parent material, obtained in the Assembly step, is a crucial parameter affecting success of all following steps. To be "ADORable" the framework of starting zeolite must possess some hydrolytically unstable groups of atoms, which have to be located at appropriate positions in the zeolite framework. The first zeolite, which was successfully applied in the ADOR, was germanosilicate **UTL**[68] (see below, Table 1). This zeolite has Ge-rich double four ring (D4R) units, which are located between Si-rich dense layers. Ge-O bonds in D4Rs in

UTL can be simply hydrolysed by water or low concentration acids. But not only zeolite structure properties influence the progress of the ADOR process. For different types of germanosilicates, which potentially can be suitable for the ADOR method, it was demonstrated that intrinsic characteristics of starting material affect the disassembly process[69]. These parameters include chemical composition and distribution of T-elements (Si and Ge) in the framework. The parent zeolite may be hydrolysed to layered precursor only in the case that the amount of Ge atoms presented in the D4R units is more than 4 per unit. Furthermore, location of Ge atoms was demonstrated to be a crucial parameter[70]. While there are 6 possible configurations of 4 Ge atoms in the [4Si, 4Ge] D4R units, only the acidic treatment of 2 of them (D1 and D6) can lead to transformation needed (Fig. 3).
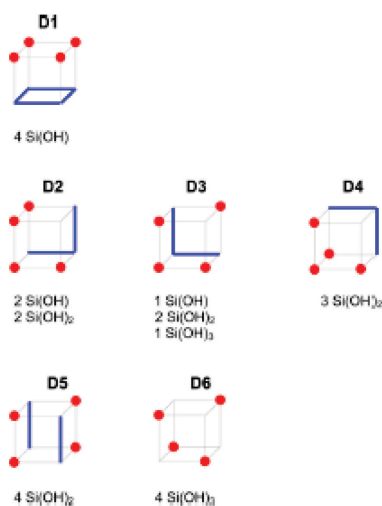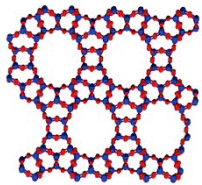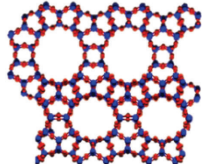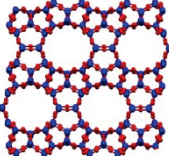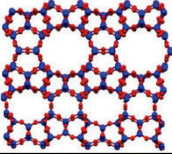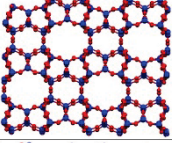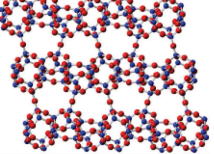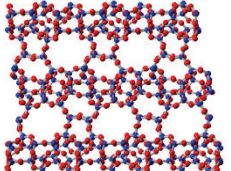
Fig. 3. Possible configurations of Ge atoms (red) in the [4Si,4Ge] D4R units. Blue lines represent Si−O−Si linkages[70].

Based on the transformation of **UTL** zeolite, the set of IPC-x zeolites ("IPC-family") was obtained. The **UTL** disassembly in low acidic conditions resulted in the formation of layered precursor IPC-1P[71]. Its organization with octylamine followed by condensation led to IPC-4[68] zeolite possessing connectivity between the layers through O-bridges (Fig. 2, bottom). It has the channel system made of intersecting 10 and 8- ring pores (Table 1). The Structure Commission of the IZA assigned the acronym to this zeolite material as **PCR**. The layers organization, which was made in the presence of silane-type molecules[68, 72] (this process is also called stabilization procedure[73]), with following calcination resulted in formation of single four ring (S4R) units between the layers. In this material, named as IPC-2[74] (**OKO** topology according to the IZA) the pore system is formed by intersecting 12 and 10-ring channels.

Investigation of the ADOR mechanism for **UTL** zeolite showed the possibility of self-organization of layers under appropriate conditions[33]. Depending on the conditions, the process of self-organization can have 2 possible outcomes: a) de-intercalation of any residual species remaining between the IPC-1P layers followed by their organization; b) rearrangement of the silica species between the layers with their following condensation into a new material. It was shown that control of the rates of these two processes can influence the structure of forming products. The different products were obtained depending on acidity of the treatment. Calcination of the **UTL** sample treated at neutral or slightly acidic conditions (0.1 M HCl) resulted in formation **PCR** zeolite, while E. Verheyen showed that treatment with 12 M HCl directed the process to the **UTL-OKO** transformation[75]. Moreover, applying acidic treatment with molarities between 1.5 M and 5 M, the possibility of formation of IPC-6 and IPC-7 zeolites was shown[76]. Reaction with 5 M HCl and following calcination resulted in formation of zeolite IPC-7, where layers are connected by the alternating D4R and S4R units. In other word this material has 2 kinds of channel system: 14 × 12- and 12 × 10-ring pores (Table 1). Following decrease in the HCl concentration to 1.5 M directed the framework transformation to the IPC-6 structure possessing connectivity between the layers by the O-bridging and the S4R units; and thus, having two independent types of pore system, intersected 12 × 10 and 10 × 8 pores (Table 1).

Table 1: Zeolite **UTL** and IPC-family synthesised by the ADOR methodology based on **UTL** transformation

Structure type	Projections demonstrating connectivity between the layers	Pore system	Reference	Notes
UTL		14 × 12	77-78	IM-12, ITQ-15
IPC-7		14 × 12 12 × 10	76	
IPC-2		12 × 10	68, 72, 74-75	**OKO** topology COK-14

IPC-6		12 × 10 10 × 8	[76, 79]	
IPC-4		10 × 8	[68]	**PCR** topology
IPC-9		7 × 10	[80]	*"Unfeasible"* zeolite
IPC-10		9 × 12	[80]	*"Unfeasible"* zeolite

The ADOR method itself is the computationally predictable method of zeolite transformation. Based on the different possible organization of layered precursors, the theoretical simulation[81-82] proposes several possible final structures having different connectivity between the layers and different pore systems. The shift of the IPC-1P layers was realized in the presence of choline molecules either in the presence (for IPC-10) or absence (for IPC-9) of dimethyldiethoxysilane (DEDMS). IPC-9 and IPC-10 zeolites have odd-ring pores: 7 × 10 and 9 × 12, respectively[80]. The presence of odd pores in zeolite framework is very unusual[83-84] and previously only few such structures have been synthesised[85-87]. Because of high framework energies and densities, IPC-9 and IPC-10 zeolites were named as "unfeasible" zeolites. While all known silica zeolites are located close to one line on energy-density plot ("traditional synthesis vector")[88], both IPC-9 and IPC-10 materials lie away from this correlation (Fig. 4). Thus, one of the main advantages of the ADOR approach consists in possibility of preparing of zeolite materials, which cannot be available via traditional methods of zeolites synthesis.
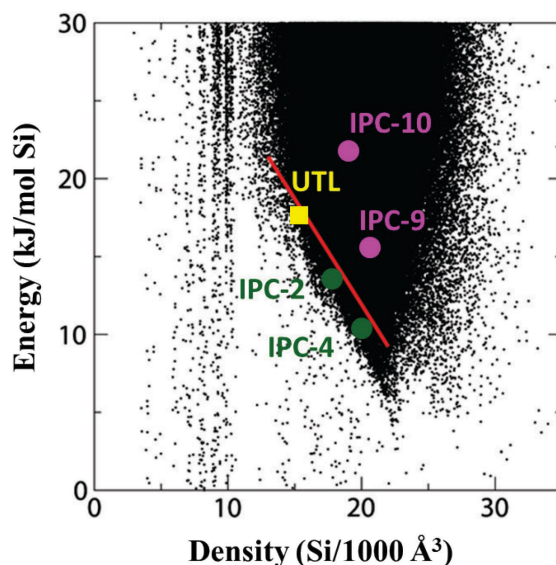
Fig. 4. The energy-density plot adopted from [80, 88]. Black points demonstrate calculated possible zeolites structures, the red line shows the energy-density correlation for all synthesised zeolites, it is also called traditional synthesis vector. While the energies of UTL (yellow), IPC-2 and IPC-4 (green) are still related to the traditional vector, IPC-9 and IPC-10 (violet) lie away from it.

Recently the experimental opportunities of the ADOR method were expanded. It was shown that a variant of **UTL**-to-IPC-6 transformation in acidic conditions via microwave irradiation is possible[89]. IPC-6 samples, obtained by this method, were characterized by 1:1 **PCR** (O-bridges) / **OKO** (S4R connections) layer stacking. Another new route was opened applying the pressure of 1 GPa at 200°C (Walker-type multianvil apparatus) for the transformation[90] (Fig. 5). In this case, in contrast to expected more dense **PCR** structure, the pressure-induced ADOR transformation of 2D zeolite precursor IPC-1P went to **OKO** topology, material possessing a lower density (higher porosity).
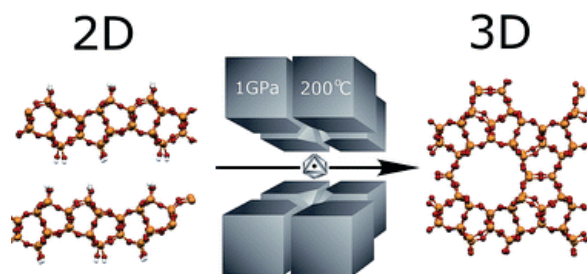
Fig. 5. Schematic presentation of the pressure-induced transformation of IPC-1P precursor[90].

Up to now, the Assembly-Disassembly-Organization-Reassembly technique was limited only by **UTL** germanosilicate used as a starting material. Lately, Firth et al[91] reported an expansion of this technique on the germanosilicate SAZ-1. The authors showed that even the

synthesis of parent zeolite, which possesses appropriate structure properties for the following application in the ADOR may be realized. Initial germanosilicate zeolite SAZ-1 has dense siliceous layers connected by the D4R units. Its pore system is made of 14 × 10-ring pores. The following transformation of this zeolite allowed obtaining of two new "daughter" zeolites: IPC-15 (analogue of **PCR**) and IPC-16 (analogue of **OKO**).

The outlook for the following investigations, which becomes one of the aims of this work, is generalization of this synthetic approach of indirect zeolite preparation. There are several germanosilicates having the double for member units in one direction, which can be perspective starting zeolites: **UOV**[34], **IWR**[92], **IWW**[93], **ITH**[94], **ITR**[95], **IWV**[32], CIT-13[96], etc. It should be noticed, that in contrast to **UTL**, SAZ-1, and CIT-13, having dense layers, the layers of zeolites mentioned above contain pores, which can provide additional lability of the frameworks and cause additional issues in realisation of the ADOR process.

As it was previously discussed, in the ADOR approach only Ge-rich germanosilicates can be possibly applied, i.e. zeolites possessing D4R units with ≥ 4 Ge atoms. On the other hand the post-synthesis treatment of Ge-poor zeolites (having D4Rs with < 4 Ge atoms) may be realised without modifications of the framework topology. Thus, hydrolytic instability of Ge–O–Si bonds can be potentially used for post-synthesis modification of germanosilicates, resulted in degermanation or incorporation of elements into the framework, similar to presented below.

2.7. Demetallation as a Method of Formation of Hierarchical Porous Zeolite

As it was mentioned previously, zeolites are extremely important materials for adsorption, separation and catalysis. Although being extremely beneficial for shape-selective catalysis, presence of micropores restricts the use of conventional zeolites in synthetic applications involving transformations of bulky molecules due to mass transfer limitations. Several different methods were proposed for the development of mesoporosity in zeolites frameworks including top-down and bottom-up, template-assisted and 'template-free' procedures[30, 97].

Demetallation of zeolites can be considered as one of the most effective ways for formation of hierarchical material. This method is based on post-synthesis removal of particular

framework atoms (e.g. Al, Si, B, Ti etc.) to form the additional porosity. Non-uniform mesopores facilitating reactants transport to the active centres of catalysts can be created by post-synthesis treatments; the most common are dealumination, desilication or detitanation.

Controllable leaching of Al, or dealumination, was shown to be achieved by several different ways: acidic treatment of zeolites at elevated temperatures, reactions with $SiCl_4$ vapour or with hexafluorosilicate[98] or by steaming at 450 – 750 °C[99-103]. Together with formation of mesopores the removal of aluminium increases thermal stability of material. However, it significantly increases Si/Al ratios and decreases concentration of acid sites in the final material. Following zeolites were successfully applied in dealumination procedure: mordenite, beta and ferrierite[97]. Dealumination of zeolite Y (**FAU**) is commercially used for preparation of more stable zeolite **USY**, which is used in the FCC process.

The method of desilication is used more often for synthesis of hierarchical catalysts[104-110] (Fig. 6). In contrast to dealumination, this method does not reduce the acidity of material. Silicon leaching is realized in organic or inorganic (or even both) alkaline solutions at different temperatures and times. Thus, applying different conditions of the treatment the tuning of zeolite pore system may be realized. Properties of initial zeolites (Si/Al ratio[105] and morphology of the crystals[97]) were shown to be important for control of mesopores formation. For aluminosilicate **MFI**, the limited amount of mesopores was formed when Si/Al ≤ 15, while mesopores in the range of 20-50 nm and large meso- and micropores were designed for the materials with Si/Al ~ 25-50 and Si/Al ≥ 200, respectively.
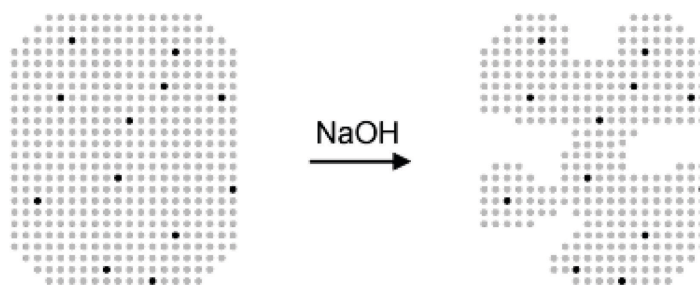
Fig. 6. Scheme of formation of mesopores by desilication procedure[105].

The possibility of partial removal of Ti atoms from the framework by H_2O_2 was shown in [111-113]. Treatment time and concentration of H_2O_2 controlled the pore development. These treatments resulted in interruption of titania chains and the consequent formation of larger micro- and mesopores without substantial degradation of crystallinity. The modified ETS-10 material

exhibited improved performance in the Beckmann rearrangement of cyclohexanone oxime to ε-caprolactam.

Hydrolytic instability of Ge–O linkages can also be used for the development of extra-porosity in germanosilicate framework. Burel at al. demonstrated that treatment of germanosilicates **IWW** with Si/Ge = 3 – 16.5 under strong acidic conditions resulted in degermanation accompanied with formation of mesopores[114]. Also they showed that formed numerous framework defects can be used for the following Al incorporation. However, up to now investigation in the area of formation of additional porosity by degermanation process was limited only by zeolites **IWW**.

2.8. Post-synthesis Incorporation of Elements into Frameworks of Germanosilicate Zeolites

Not only extraction of Ge atoms from zeolite frameworks can take place [114-116] but also they can be post-synthetically isomorphously substituted by different elements. Previously, germanosilicates **UTL**, **IWW**[117], **IWR**[118], **ITH**[119-120] and **BEC**[121] were successfully post-synthetically aluminated. This method has several advantages and results in:
- Generation of strong acid centres;
- Increase in the hydrolytic stability of zeolite framework;
- Formation of additional mesopores, similar to discussed previously.

Combination of these phenomena allows designing of hierarchically porous catalyst materials. It was observed that the properties of starting materials (chemical composition and morphology of the crystals) and the conditions of treatment (temperature, duration, and pH) control the concentration of generated Lewis and Brønsted acid centres and micro- and mesopore volumes. Before, it was shown that very narrow range of Si/T-elements ratios can be used for the direct synthesis of aluminogermanosilicate (Al-Si-Ge) zeolites[122]. Post-synthesis alumination expanded this range, which is also an advantage of discussed method.

Post-synthetically modified zeolites were investigated in tetrahydropyranylation of alcohols as model reaction[117-119]. The catalytic activity depended on the type of zeolite framework and enhanced with increasing total concentration of acid centres. Moreover, germanosilicate **IWR** was catalytically active and selective for benzene alkylation with

propylene and dealkylation-transalkylation of heavy reformate[123]. Germanosilicate **ITH** samples were also used as an additive to E-Cat catalyst for the reactions of cracking of vacuum gasoil[124], where they showed an increase in LPG yield at the expense of gasoline.

In addition to alumination, possibility of post-synthesis introduction of Ga was described for **IWR** germanosilicate by Shamzhy et al[118]. Final material showed high catalytic activity in acylation of p-xylene with benzoyl chloride. The yield of 2,5-dimethylbenzophenone in Friedel-Crafts acylation for Ga-**IWR** was several times higher in comparison with Al-**IWR**: 99 *vs.* 33 % respectively.

Recently, post-synthesis substitution of Ge atoms by Sn was reported for **UTL** zeolite. Obtained Sn-**UTL** samples demonstrated a high catalytic activity in the Meerwein-Pondorf-Verley reaction and Baeyer-Villiger oxidation of ketones using H_2O_2[125]. In comparison with conventional Sn-**BEA** zeolite, Sn-**UTL** was more efficient in Baeyer-Villiger oxidation using bulky oxidant – tert-butylhydroperoxide. Xu et al[126] showed the way of post-synthesis stabilisation of **UTL** framework via Ge substitution by Si atoms, which significantly increased the Si concentration (from Si/Ge = 3.7 to Si/Ge = 233), resulted in improved framework hydrolytic stability. Recently, possible stabilization with TEOS was also reported for **ITT** germanosilicate[127].

2.9. Zeolites Studied in This Investigation

*Zeolite **UTL*** (Tables 1, 2) was independently discovered in 2004 by two research groups and was named as IM-12[77] and ITQ-15[78]. This germanosilicate was the first zeolite synthesised with two-dimensional channel system formed by extra-large 14- (9.5 × 7.1 Å) and large 12-ring (8.5 × 5.5 Å) channels. It may be obtained using different sorts of spiroazocompounds as SDAs[128-129]. Synthesis of IM-12 was carried out in the presence of (6R,10S)-6,10-dimethyl-5-azoniaspiro[4.5]decane hydroxide, and the template for ITQ-15 was 1,1,3-trimethyl-6-azoniatricyclo-[3.2.1.4^{6,6}]decane hydroxide. As a single phase, **UTL** can be synthesised only in the presence of Ge atoms (i.e. it has not been yet prepared in pure siliceous form) from reaction mixtures with Si/Ge molar ratios from 1 to 5. The range of possible **UTL** chemical compositions was expanded when heteroatoms such as B, Al, Fe, Ga, In, Ti[130-131] were added into reaction mixtures.

Introduction of heteroatoms into **UTL** framework opened the possibility of its application in catalytic reactions, where **UTL** samples demonstrated the advantage of extra-large pore channel system. In comparison with commercially available **BEA** and **MFI** zeolites, **UTL** zeolites isomorphously substituted with Al, Ga, Fe showed lower conversions but higher selectivities to xylenes in toluene disproportionation and trimethylbenzene disproportionation/isomerization reactions[132]. Acylation of p-xylene with benzoyl chloride and Beckmann rearrangement of 1-indanone oxime were performed using B, Al, Ga, Fe containing **UTL** samples as catalysts[133]. Aluminium containing **UTL** zeolite exhibited higher activity and selectivity in benzoylation of p-xylene in comparison with conventional **BEA** zeolite. **UTL** zeolites showed 100% selectivity to 3,4-dihydroquino-lin-2(1H)-one in the Beckmann rearrangement of 1-indanone oxime. Moreover, in order to investigate **UTL** as a catalyst for acidic conversion of larger organic molecules, theoretical investigation of the properties of **UTL** with Al, B, Ga was done by Kang et al[134]. The authors showed that Brønsted acidity increased in the order: B–IM-12 < Ga–IM-12 < Al–IM-12. **UTL** zeolite was also tested in the Baeyer–Villiger oxidation of 2-adamantanone and cyclohexanone with hydrogen peroxide in liquid-phase[135], where it exhibited higher catalytic activity in comparison with germanosilicates **UWY** and **IWR**. In this reaction, the tetrahedrally coordinated Ge ions acted as Lewis acid sites. Preparation of bifunctional **UTL** supported metal catalyst showed a high stability for n-decane hydroisomerization/hydrocracking reaction [136].

Zeolite CIT-13. The synthesis of extra-large pore germanosilicate CIT-13 (Table 2), zeolite with properties suitable for transformations via the ADOR process, was reported by the group of Davis[96]. It was found that Ge atoms in CIT-13 are located primarily in the D4R units connecting dense layers enriched with silicon. The structure of CIT-13 is closely related to SAZ-1[91] and NUD-2[137] materials discovered independently in 2016. All mentioned zeolites contain *cfi*-type layers and possess high degree of the D4Rs disorder in the framework. Schematically it presented in the Fig. 7 showing 2 possible connections of the layers: AAAA and ABAB.
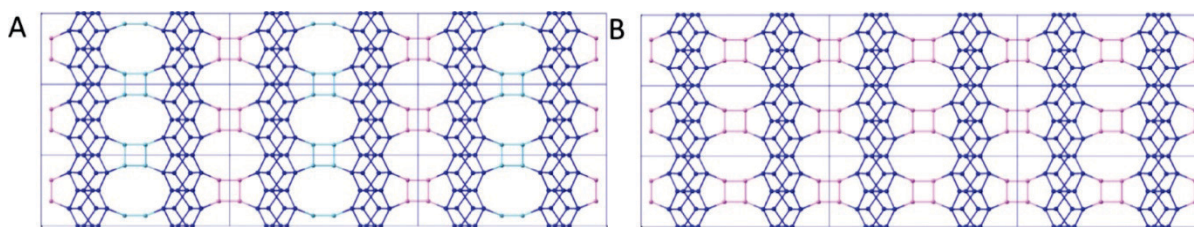
Fig. 7. View along y direction showing two possible connections of layers by the D4R units (pink and light blue): A) ABAB, B) AAAA sequence[96].

CIT-13 has a two-dimensional pore system formed by perpendicular intersecting 14- and 10-ring channels (9.1 × 7.2 Å and 6.2 × 4.5 Å respectively). This germanosilicate was obtained using a family of methyl-benzylimidazolium cations as SDAs (Fig. 8) from the reaction gels with Si/Ge = 3 − 8, H_2O/T = 5 − 7.5 in presence of HF or NH_4F as source of F^- ions.
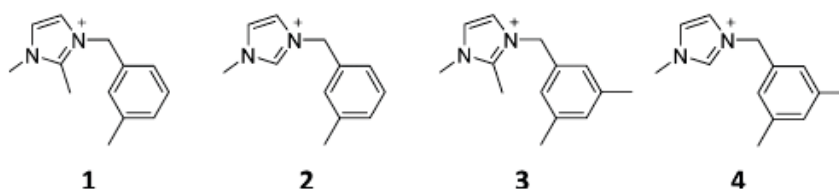
Fig. 8. The structure-directing agents used for the synthesis of CIT-13 germanosilicate: 1) 1,2-dimethyl-3-(3-methylbenzyl)imidazolium, 2) 1-methyl-3-(3-methylbenzyl)-imidazolium, 3) 1,2-dimethyl-3-(3,5-dimethylbenzyl)imidazolium, 4) 1-methyl-3-(3,5-dimethylbenzyl)-imidazolium hydroxides[96].

Zeolite UOV (Table 2). In 2014 Lorgouilloux et al. reported the synthesis of the new germanosilicate zeolite – IM-17[34] also having in its framework the D4R units enriched with Ge atoms. The IZA Structure Commission assigned the code **UOV** for this zeolite material. It was synthesised from concentrated reaction gels (H_2O/T < 10, T = Si + Ge) with Si/Ge = 1.5 − 4 using decamethonium dihydroxide (DMDH) as a SDA. IM-17 possesses a 3-dimensional pore system composed of large 12- (7.7 × 6.0 Å and 5.9 × 7.1 Å) and small 8- (2.9 × 3.1 Å) ring channels along (100) direction intersected by 10-ring (5.9 × 4.7 Å) pores along (001).

Zeolite IWW was firstly prepared in the forms of germanosilicate ITQ-22 and aluminogermanosilicate Al-ITQ-22 using 1,5-bis-(methylpyrrolidinium)-pentane (*SDA-1*) as an SDA by group of Corma[93]. Despite attempts of preparation of **IWW** zeolites from reaction mixtures with Si/Ge = 0.5 − 2, all final samples were characterized by equal Si/Ge = 3.2, which indicates saturation of the framework with Ge atoms. This zeolite possesses the 3D pore system with 8- (4.52 × 3.32 Å), and 12- (6.66 × 6.66 Å) ring channels, which both are intersected by a

sinusoidal 10-ring channels (5.86 × 4.98 Å) as it is presented in the Fig. 9. It was shown that using different SDAs, **IWW** samples with different morphology of crystals may be obtained. The syntheses in the presence of *SDA-1* or hexamethonium dihydroxide (HMH) (Fig. 10, A)[138] lead to the formation of tiny ellipsoid crystals with size of 0.2 µm; in the presence of 5-azonia-spiro[4,5]decane the crystals with the shape of fragmented sheet-like with size up to 4 µm in length and 1 µm in width can be formed[139].
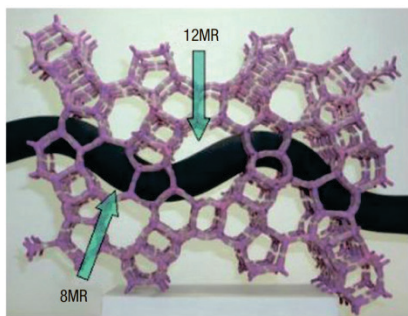
Fig. 9. Three-dimensional structure model of **IWW** zeolite showing the 8 and 12 MR channels intersected by the sinusoidal 10-ring pore showed as a black ribbon[93].

Al-containing ITQ-22 samples were investigated in m-xylene isomerization and disproportionation reactions[93], where they showed an intermediate catalytic behaviour for the m-xylene isomerization in comparison with zeolites **BEA** and ZSM-5. ITQ-22 showed a unique behaviour as a multipurpose alkylation catalyst in alkylation of benzene with ethanol and benzene with isopropanol or propylene in gas or liquid phases[140-141]. Al-ITQ-22 exhibited a higher selectivity to cumene in comparison with ZSM-5 and **BEA** zeolites.

^{19}F solid-state NMR analysis of germanosilicates samples after their post-synthesis fluorination is an indirect method allowing to study distribution of Ge atoms into zeolite framework. Investigation of **IWW** sample (Si/Ge = 4.35) presented in ref. [142] showed that Ge atoms were exclusively located in the D4R units ([4Ge,4Si] and [5Ge, 3Si] D4Rs), which makes this material perspective for the ADOR transformation. Ge-rich samples of **IWW** (Si/Ge=3.1) were shown to be disassembled into the lamellar precursor IPC-5P under acidic conditions[143]. However, any attempts to reassemble the structure resulted in structure collapse. Application of the stabilisation procedure with diethoxydimethylsilane (DEDMS) also did not lead to the formation of new material, as the initial **IWW** framework was restored.

Zeolite **IWR**, which has a three dimensional channel system formed by interconnected 12- (5.8 × 6.8 Å), 10- and 10- (4.6 × 5.3 Å) rings, was firstly synthesised as aluminogermanosilicate Al-ITQ-24 in hydroxide media using HMH (Fig. 10, A) cation as an SDA[92]. Applying different approaches and structure-directing agents for the synthesis, the chemical composition of **IWR** zeolite can be varied. Syntheses in fluoride media with SDA-A allowed to obtain ITQ-24 as borogermanosilicate in broad range of Si/Ge and B/(Si+Ge) ratios. The possible preparation of Ge-free borosilicate **IWR** was reported using the seeding method. Synthesis in the presence of SDA-B (Fig. 10, B) allowed to obtain the pure silica ITQ-24 polymorph[123]. Besides, **IWR** zeolite can also be prepared with other SDAs, such as SDA-C[144] (Fig. 10, C) and SDA-D (Fig. 10, D)[122].
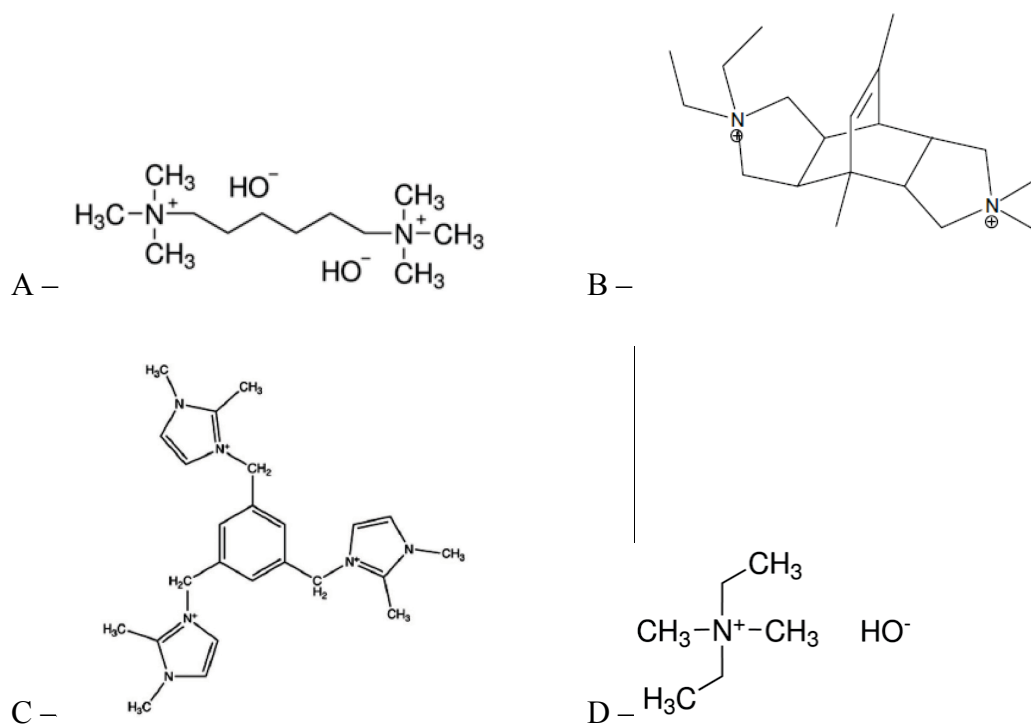
Fig. 10. Templates, which can be used for the synthesis of **IWR** zeolite: SDA-A − HMH[92]; SDA-B − 4,8-(2-methyl)ethenobenzo[1,2-c:4,5-c′]dipyrrolium-4-methyl-2,2,6,6-tetraethyl-1,2,3,3a,4a,5, 6,7,7a,8a-decahydro dihydroxide[123], SDA-C − 1,3,5-tris(1,2-dimethylimidazolium)benzene hydroxide[144], SDA-D − diethyldimethylammonium hydroxide[122].

Several works were devoted to structural studies and investigation of Ge location in **IWR** zeolite[144-145]. Similar to other germanosilicates, it was shown that Ge atoms is located in the D4R units; with increasing of Ge concentration in the framework, they start to occupy other T-sites[145]. Pinar et al. showed for **IWR** sample with Si/Ge = 2.5, that Ge atoms replace some of the Si in

the D4R and in one of them in the S4R, while the other S4Rs contain only Si atoms[144]. The presence of Ge atoms in the layers makes this zeolite highly hydrolytically unstable. Group of Wu showed that when ITQ-24 (Si/Ge = 1.8) reacted with water at room temperature, its crystalline structure was completely degraded to amorphous material[126]. The acidic treatment of borogermanosilicate **IWR** (Si/Ge = 6.9, 14.8% B) showed that it has been disassembled even after 5 minutes of the treatment, according to the XRD data. However, the formation of lamellar precursor was accompanied with partial layers destruction, which may limit their following use for the ADOR approach[69].

*Zeolite **ITH*** was another germanosilicate, which was investigated in this work. It possesses three intersecting medium-size channels: 9-ring channels with the size of pore of 4.0 × 4.9 Å along (100) direction; and two 10-ring channel systems (4.8 × 5.7 Å and 4.7 × 5.1 Å) along (001) and (010) directions, respectively. This zeolite was firstly obtained as a pure silicate ITQ-13 and borosilicate B-ITQ-13 from concentrated reaction mixtures (H_2O/T < 10) in the presence of HMH (Fig. 10, A). Al-containing ITQ-13 was shown to be obtained by ion exchange of B-ITQ-13 with Al[94]. Later on, direct incorporation of Al atoms in **ITH** framework was achieved in the presence of Ge atoms in reaction mixture[146]. It resulted in formation of Brønsted and Lewis acid sites, and Al-**ITH** demonstrated good selectivity and activity in reactions of isomerisation of xylenes, disproportionation of toluene to benzene and xylenes,[147-148], catalytic cracking of vacuum gasoil and 1-butene for propylene and ethylene production[146, 149], conversion of methanol to propene (MTP)[150] and methanol to hydrocarbons (MTH)[151].

In all **ITH** syntheses described above, TEOS was used as a source of silicon. Thermally stable pure silica ITQ-13 zeolite was obtained using fumed silica, which significantly facilitated the gel-making process[152]. As germanosilicate **ITH** can be obtained in the presence of two different templates: hexamethonium dihydroxide for Ge poor samples (Si/Ge > 6)[153-154] and N,N,N′,N′-tetramethyl-1,6-hexanediamine (TMHDA) for the samples enriched with Ge (2 < Si/Ge < 6)[155]. Different SDAs influenced the crystal size: Ge-rich samples obtained using HMH were characterized by large platelet-like crystals, which size reaches 40.0 × 5.0 × 5.0 μm, while syntheses of Ge-poor materials in the presence of TMHDA resulted in formation of agglomerates of tiny crystals with ~10 times smaller size (5.0 × 0.5 × 0.5 μm)[119].

Crystallographic and ^{19}F MAS NMR study showed that Ge atoms preferentially occupy the D4R units in **ITH** framework. However, regardless the concentration of Ge atoms in the

framework, some of them are always located in layers, namely in $[4^1 5^2 6^2]$ cages[142, 153, 156]. Recently, Liu et al. reported the 2D ^{19}F{^{29}Si} HETCOR NMR study of **ITH** zeolite made from pure silica and samples with Si/Ge = 10 (Fig. 11) and 5. Depending on the chemical composition of samples, **ITH** framework can possess different types of the D4R units with different amount and location of Ge atoms. Acidic treatment of respective materials can result either in total hydrolysis of bonds in the D4Rs and formation of lamellar material[69], or only in leaching of Ge atoms from the framework[157].
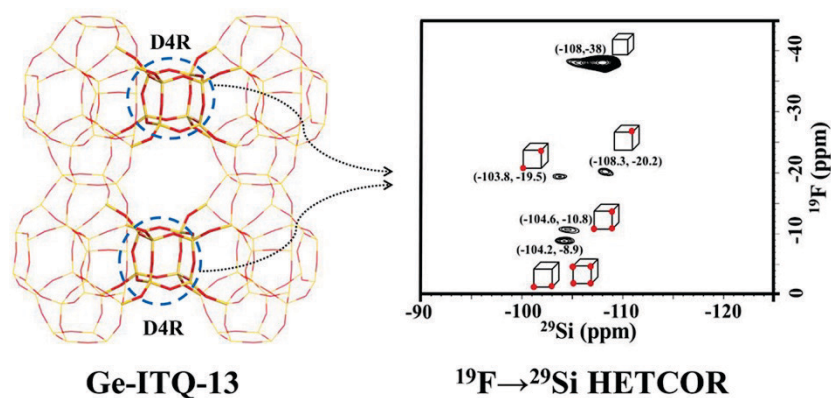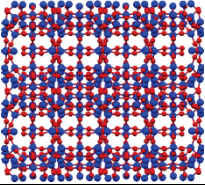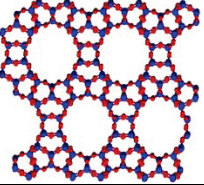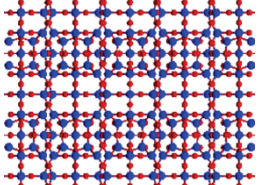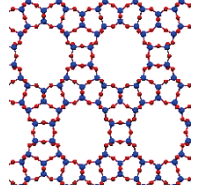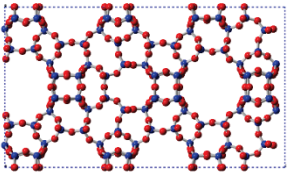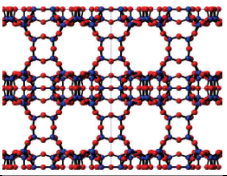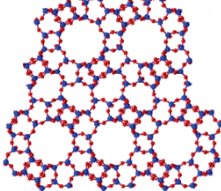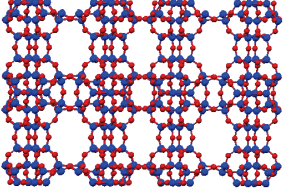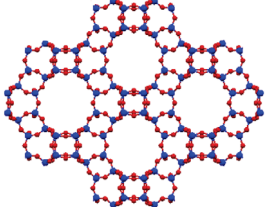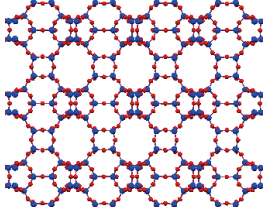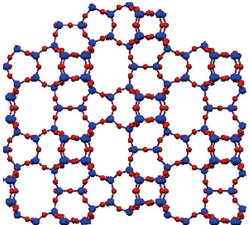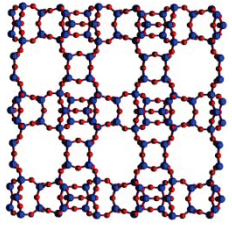
Fig. 11. Left – the framework of **ITH** with indicated the D4R units, right – 2D ^{19}F{^{29}Si} HETCOR NMR spectra of Ge-ITQ-13 with Si/Ge = 10. The chemical shifts of correlation peaks and possible composition of D4R units are shown (Ge atoms are indicated by red balls)[157].

All discussed zeolites possess special structural properties because of the presence of the D4R units connecting layers enriched with Si atoms. Based on the choice of appropriate chemical composition, zeolite may be potential starting material for the ADOR transformation, generation of mesopores by degermanation, or post-synthesis incorporation of Al atoms. In this thesis, syntheses of several new zeolites will be firstly demonstrated based on Assembly-Disassembly-Organisation-Reassembly route for Ge-rich germanosilicates **UOV**, CIT-13, **IWR** and **IWW**.

Tuning of textural properties by leaching of Ge atoms will be presented for Ge-poor **UOV**, **ITH** and **IWW** germanosilicates. The post-synthesis alumination will be firstly described for the zeolite **UOV** and CIT-13. In this work special attention will be paid to investigation of the mechanism of post-synthesis substitution of Ge atoms with Al never discussed before.

Table 2: Structures of investigated germanosilicates

Zeolite	Top view	Side view	Pore system	Space group
UTL			14×12	C2/m
CIT-13			14×10	Cmmm
UOV			$12 \times 10 \times 8$	Ammm2
IWW			$12 \times 10 \times 8$	Pbam
IWR			$12 \times 10 \times 10$	Cmmm
ITH			$10 \times 10 \times 9$	Ammm2

3. Experimental part

3.1. Reagents and Solvents

Origin and purity of the reagents and solvents used for the preparation and post-synthesis modification of zeolites are presented in the table 3.

Table 3: List of used chemicals

Chemical	Purity	Producer	Formula
1,4-Dibromobutane	99%	Aldrich	
1,5-Dibromopentane	97%	Sigma Aldrich	
1,6-Dibromohexane	96%	Sigma Aldrich	
1,2-Dimethylimidazole	98%	Sigma Aldrich	
(2R,6S)-2,6-Dimethylpiperidine	98%	Sigma Aldrich	
3-Methylbenzyl chloride	98%	Sigma Aldrich	
Acetone	99.99%	Lachner	
Aluminum hydroxide	Al_2O_3, 50-57%	Sigma Aldrich	$Al(OH)_3$
Aluminum nitrate nonahydrate	98.5%	Sigma Aldrich	$Al(NO_3)_3 \cdot 9H_2O$
Ambersep® 900(OH)		Acros Organics	
Boric acid	>99.5%	Sigma	H_3BO_3
Chloroform	99.92%	Lachner	$CHCl_3$
Decamethonium bromide	>98.0%	TCI	
Diethyl ether	99.97%	Lachner	$(C_2H_5)_2O$
Ethyl acetate	99.97 %	Fisher Scientific	$CH_3COOC_2H_5$
Germanium oxide	99.99%	Sigma Aldrich	GeO_2
Hydrochloric acid	36%, ANALPURE®	Analytika	HCl
	p.a.	Penta	HCl
Hydrofluoric acid	37%	Sigma Aldrich	HF
	48%, ANALPURE®	Analytika	HF
Methanol	99.98%	Lachner	CH_3OH
N-Methylpyrrolidine	97%	Sigma Aldrich	
N,N,N′,N′-Tetramethyl-1,6-hexanediamine	99%	Sigma Aldrich	
Nitric acid	>70%	Sigma Aldrich	HNO_3
	67%, ANALPURE®	Analytika	HNO_3
Orthophosphoric acid	85%	Fluka	H_3PO_4
Silica (Cab-O-Sil M5)		Supelco Analytical	SiO_2
Sodium hydroxide	p.a. 98%	Penta	NaOH
Sodium sulphate anhydrous	99%	Sigma Aldrich	Na_2SO_4
Sulfuric acid	95.0–98.0%	Sigma Aldrich	H_2SO_4
Tetraethyl orthosilicate	98%	Aldrich	TEOS
Toluene	99.93%	Lachner	
Trichloroacetic acid	99.0%	Sigma Aldrich	CCl_3COOH
Trimethylamine	31–35 % in ethanol	Sigma Aldrich	

3.2. Synthesis of Structure Directing Agents

3.2.1. Synthesis of Hexamethonium Dihydroxide (HMH)

HMH, template for the syntheses of **ITH** and **IWR** zeolites, was prepared based on the method described elsewhere [138]. For preparation of hexamethylene-bis(trimethylammonium) dibromide, 37.4 g of 1,6-dibromohexane was mixed with 82.5 g of trimethylamine solution (31-35 wt. % in ethanol) and 200 ml of ethanol with a magnetic stirrer for 2 days at ambient temperature. After that, the reaction mixture was washed with ethyl acetate and diethyl ether. The final product was separated by filtration and dried at ambient for 12 h.

Hexamethylene-bis(trimethylammonium) dibromide was transformed into hydroxide form using Ambersep® 900(OH) anion exchange resin (0.8 mmol of SDA per 1 g of anion exchange resin). The solution of HMH was concentrated under low pressure (35 Torr) at 30 °C until the hydroxide concentration grown to > 1.0 M.

3.2.2. Synthesis of 1,5-Bis-(methylpyrrolidinium)pentane Dihydroxyde (MPPH)

The SDA for **IWW** synthesis was obtained according to the methods presented in the Ref.[93]. 40 g of N-methylpyrrolidine were mixed with 37.5 g of 1,5-dibromopentane in 300 ml of acetone and heated under reflux during 24 h. After that, obtained 1,5-bis-(methylpyrrolidinium)pentane dibromide was ion-exchanged into hydroxide form using Ambersep® 900(OH) anion exchange resin (with the same anion exchange resin to zeolite ratio as for HMH). Solution was concentrated under low pressure (35 Torr) at 30 °C until the hydroxide concentration was equal to approximately ~1.0 M.

3.2.3. Synthesis of (6R,10S)-6,10-Dimethyl-5-anizoporo[4.5]decane Hydroxide (DMAD)

(6R,10S)-6,10-dimethyl-5-azoniaspiro[4,5] decane hydroxide, the SDA for the UTL synthesis, was prepared according to the method reported in [129]. 16.07 g of (2R,6S)-2,6-dimethylpiperidine was added drop-wise to 140 ml of water solution of sodium hydroxide (5.68 g) and 1,4-dibromobutane (30.66 g). After that, the mixture was refluxed under intensive stirring for 12 hours. After cooling in an ice bath an ice-cooled 50% (wt.) solution of NaOH (70 ml) was added and further solid NaOH was added until the oil product was formed. After crystallization the solid was filtered and extracted with chloroform. The organic fraction was dried using

anhydrous sodium sulphate and partially evaporated (50 – 100 mL of residual volume), then diethyl ether was added to the remaining mixture. Final solid product was washed 3 times with diethyl ether. The bromide salt was ion-exchanged into hydroxide form using Ambersep® 900(OH) anion exchange resin and concentrated by evaporation in order to obtain 1 M solution.

3.2.4. Synthesis of 1,2-Dimethyl-3-(3-methylbenzyl)imidazolium Hydroxide (DMBIH)

Synthesis was carried out according to the procedure presented in[96]. 14.4 g of 1,2-dimethylimidazole was dissolved in 300 ml of toluene and heated up to 45 °C. After that, 21.1 g of 3-methylbenzyl chloride were added dropwise under intensive stirring and the reaction mixture was stirred for 30 min. Then, the temperature was increased to 105 °C and the reaction mixture was stirred for 24 h. After cooling and filtration, obtained product was washed for several times with diethyl ether and dried. The chloride anions were exchanged with hydroxyl anions using Ambersep® 900(OH) anion exchange resin, resulting SDA solution was concentrated (to 1 M solution) by evaporation.

3.3. Synthesis of Zeolites

3.3.1. Zeolite UOV

Samples of germanosilicate **UOV** were obtained based on ref.[34] from the reaction mixtures with the following composition:

x SiO_2 : (1-x) GeO_2 : 0.25 DMDH : y H_2O, where x = 0.33 – 0.66, y = 5 or 10,

using decamethonium dihydroxide (DMDH) as the structure-directing agent (SDA). DMDH was prepared from the bromide form by ion exchange using Ambersep® 900(OH) anion exchange resin. The solution of DMDH was concentrated under low pressure (25 Torr) at 30 °C until the SDA concentration grown to > 1.5 M. Certain amount of germanium oxide was dissolved in a mixture of water and DMDH. Silica (Cab-O-Sil M5) was added progressively to the solution, and the mixture was stirred at room temperature for 30 min. The reaction gels were autoclaved at 175 °C for 7 – 14 days under static conditions. The solid product was recovered by centrifugation, washed several times with distilled water till pH of solution became neutral, dried at 65 °C during 12 h and finally calcined at 550 °C for 6 h with a temperature ramp of 2 °C/min

under air flow (200 ml/min). The prepared **UOV** samples are denoted as **UOV**-n for diluted starting gels (y = 10) and **UOV**-n-c for concentrated (y = 5), where *n* is the Si/Ge ratio in the starting reaction mixture.

Starting gels with following compositions:

x SiO_2 : (1-x) GeO_2 : 0.005 Al_2O_3 : 0.25 DMDH : 10 H_2O, where x = 0.33 or 0.6, were used for the synthesis of aluminium-containing samples based on the same procedure as for germanosilicate **UOV** but adding aluminium hydroxide in the reaction mixture. The final samples in this case were denoted as Al-**UOV**-n, where *n* is the Si/Ge ratio in the starting reaction mixture.

3.3.2. Zeolite IWR

The synthesis of boron containing **IWR** zeolites was performed according to Ref. [138] in the presence of HMH as an SDA. The starting gel had the following composition:

(1-x) SiO_2 : x GeO_2 : 0.1 $BO_{1.5}$: 0.225 HMH : y HF : 5 H_2O, where x = 0.33 or 0.17, y = 0 or 0.1.

Typically, boric acid and germanium oxide were dissolved in 1.0 M HMH solution. TEOS was then added and the mixture was gently stirred at room temperature until complete evaporation of the alcohol formed. After that, 49 wt. % solution of hydrofluoric acid was added. The resulting gel was autoclaved at 175 °C under tumbling (~ 60 rpm) for 10 days. The obtained solid was separated by filtration, washed with distilled water, and dried overnight at 95 °C. The occluded hexamethonium was removed from the samples by its heating from room temperature to 300 °C at a rate of 1 °C min^{-1} and that latter temperature was maintained for 3 h. The next step involved increasing the temperature at a rate of 1 °C/min up to 580 °C; the product was kept at this temperature for 3 h, to burn off the remaining organic.

Obtained samples were then used as seeds for boron-free **IWR** synthesis, which were carried out from gels:

(1-x) SiO_2 : x GeO_2 : 0.225 HMH : 5 H_2O : 0.1 (**IWR** seeds), where x = 0.11 − 0.33, following the same procedures, except adding boric and hydrofluoric acids.

IWR samples were denoted as **IWR**-n-(B)-(m)-(s)-(F), where *n* is the Si/Ge ratio in the starting reaction mixture; B and F were used for designation of samples obtained from boron or

fluorine containing reaction mixtures, m – percentage of used B; *s* was used for designation of samples obtained with seeds.

3.3.3. Zeolite ITH

Method A. *Ge-rich zeolite ITH-2[155]* was obtained from following reaction gel:

0.66 SiO_2 : 0.33 GeO_2 : 7 TMHDA : 1.4 HF : 44 H_2O.

Commercially available N,N,N′,N′-tetramethyl-1,6-hexanediamine (TMHDA) was used as the SDA. Germanium oxide was dissolved in the mixture of water and TMHDA. After that, TEOS was added and the mixture was stirred at room temperature until alcohol was completely evaporated. Then, 49 wt. % solution of hydrofluoric acid was added to the reaction mixture. Finally, the reaction mixture was autoclaved at 175 °C for 6 days under static conditions. The solid product was washed with distilled water and dried at 65 °C during 12 h.

Method B. Synthesis of *Ge-poor ITH* samples was based on the same procedure as Method A, but the SDA in this case was HMH[94]. Reaction mixture had a following composition:

(1-x) 0.86 SiO_2 : x GeO_2 : 0.25 HMH : 0.5 HF : 5 H_2O, where x = 0.09 or 0.14.

The resulting fluid gel was heated at 175 °C for 20 days under agitation (~ 60 rpm). Final product was separated by centrifugation, washed with distilled water and dried overnight at 65 °C. Final samples were calcined at 650 °C for 8 h with a temperature ramp of 1 °C/min under air flow (200 ml/min). The synthesised **ITH** samples were denoted as **ITH**-n (*n* is the Si/Ge ratio in the initial reaction gel).

Aluminium-containing samples were prepared from initial starting gels with compositions:

0.91 SiO_2 : 0.09 GeO_2 : 0.005 Al_2O_3: 0.25 HMH : 10 H_2O

using the same procedure (Method B) and adding aluminium hydroxide in the reaction mixture. The obtained sample was denoted as Al-**ITH**-10.

3.3.4. Zeolite IWW

IWW zeolites were prepared according the procedure presented in [93] from reaction mixture

(1-x) SiO_2 : x GeO_2 : 0.25 MPPH : 15 H_2O,where x = 0.33 or 0.2.

Appropriate amounts of germanium dioxide and TEOS were added to MPPH solution under stirring. The resulting mixtures were stirred to evaporate the ethanol formed by the hydrolysis of TEOS. Then, the gels were heated in Teflon-lined stainless steel autoclaves at 175 °C for 11 days. The final products were recovered by centrifugation, washed with water and dried at 60 °C overnight. The resulting solids were calcined at 580 °C for 6 h in air.

Final samples were denoted as **IWW**-n, where *n* is Si/Ge ratio.

Aluminium-containing **IWW** samples were prepared using the same procedures only adding the aluminium hydroxide in the amount required for 1 % or 2 % Al molar concentration in reaction mixture. Al-**IWW**-n was used for the designation of directly synthesised aluminium containing samples.

3.3.5. Zeolite UTL

Synthesis of **UTL** samples was based on the method reported in Ref.[129] by the crystallization of a gel with the composition of

$0.83\ SiO_2 : 0.17\ GeO_2 : y\ Al_2O_3 : 0.25\ DMAD : 30\ H_2O$, where y = 0 or 0.005,

at 175 °C for 6 days under agitation (60 rpm). The solid products were separated by filtration, washed out with distilled water, and dried overnight at 95 °C. Final solids were calcined at 550 °C for 6 h with a temperature ramp of 2 °C/min under air flow (200 ml/min). Samples were named as **UTL**-5 if y = 0 or Al-**UTL**-5 for aluminium containing sample (y = 0.005).

3.3.6. Zeolite CIT-13

Detailed method of CIT-13 preparation is described in [96]. In our work CIT-13 samples were synthesised from gels with following compositions:

$0.8\ SiO_2 : 0.2\ GeO_2 : 0.5\ DMBIH : 0.5\ HF : 10\ H_2O.$

The needed amounts of germanium oxide and TEOS were dissolved in aqueous solution of SDA. The mixtures were stirred in order to hydrolyse all TEOS and dried under a continuous air flow to evaporate excess water and ethanol until the gel contained required amount of water. After that, hydrofluoric acid was added dropwise. The final mixtures were thoroughly mixed and additionally dried for 2 days and then crystallized at 175 °C for 9 days under static conditions. After filtration, washing with water and drying at 60 °C, final products were calcined at 580 °C for 6 h in air atmosphere.

Aluminium-containing CIT-13 samples were prepared using the same procedure and from the reaction mixtures with the same compositions by adding needed amount of aluminium hydroxide. Samples of CIT-13 were named as (Al)-CIT-13-4, where Al was used for the designation of the samples obtained from aluminium containing mixture.

3.4. Post-synthesis Treatment

0.1 g of calcined zeolite was treated with 10 ml of acid solution (0.1 – 12 M HCl, 0.1 –1 M HNO$_3$, 0.146 M CCl$_3$COOH, 1.4 M H$_3$PO$_4$ or 0.09 M H$_2$SO$_4$) under chosen conditions (T = 25 – 175 °C, τ = 5 min – 168 h). The solid products were recovered by centrifugation, washed thoroughly with methanol and acetone, dried at 25 °C. The obtained solids were calcined at 550 °C for 6 h with a temperature ramp of 2 °C/min.

Post-synthesis alumination of zeolite samples was carried out by:

• stirring of the parent zeolite in 1 M solution of Al(NO$_3$)$_3$ (1 g of zeolite per 100 ml of solution) at T = 80 °C and pH = 2.0 for the period from 5 min to 15 days.

• treatment of germanosilicate zeolite in 1 M solution of Al(NO$_3$)$_3$ (1 g of zeolite per 100 ml of solution) at T =175 °C and pH = 2.0 for 24 h in an autoclave.

For post-synthesis alumination of **UTL,** two-step procedure was used [117]. 0.5 g of calcined zeolite was treated with 50 ml of 1 M HCl solution in ethanol. Under stirring, an additional Si source was added into the mixture (1 mmol of TEOS per 1 g of zeolite). The mixture was stirred for 30 min, then transferred to Teflon-lined autoclave and heated at 170 °C for 24 h. After the treatment, zeolites were filtered and washed with ethanol and water, dried at room temperature. After that, samples were aluminated with 1 M Al(NO$_3$)$_3$ solution at 80 °C for 24 h. The final samples were filtrated and washed with 0.01 M HCl and distilled water.

UOV samples subjected to post-synthesis alumination were named as **UOV**-n-Al-T-t, where n – Si/Ge ratio, T – temperature and t – duration of the treatment. Aluminated samples of **IWW**, **UTL**, CIT-13 were named as ABC-n-Al-post, where ABC – three letter code of zeolite and n – Si/Ge ratio.

3.5. Characterization

The structure and crystallinity of zeolite samples under study were determined by powder X-ray diffraction (XRD) using a Bruker AXS-D8 Advance diffractometer with a graphite monochromator and a position sensitive detector (Våntec-1) using CuKα radiation in Bragg-Brentano geometry at a scan rate of 0.25 2θ/min.

Synchrotron X-ray diffraction data were collected on beamline I11 at the Diamond Light Source, UK. The wavelength of the radiation was 0.82604 Å. Rietveld refinement of the computationally-derived model for novel zeolites against this data converged satisfactory to RF2 = 0.1086, wRp = 0.0259 and Rp = 0.0189 using the GSAS suite of refinement programs. Bond distance restraints of Si-O, O-O and Si-Si of 1.61, 2.63 and 3.07 Å, respectively, with a weighting factor of 100 in GSAS. The isotropic displacement parameters (Uiso) were fixed at 0.04 and 0.05 for Si and O, respectively. The structural model refinement then converged to a reasonably chemically sensible structure.

The chemical compositions of zeolite samples were determined by ICP/OES (ThermoScientific iCAP 7000) analysis. 50 mg of a zeolite were dissolved in a mixture of 2 ml of 48% HF, 4 ml of 67% HNO_3, and 4 ml of 36% HCl in a microwave. After cooling, the HF excess was eliminated by complexation with 15 ml of a saturated solution of H_3BO_3 and the final mixture was treated in the microwave again. Thereafter, the solutions under analysis were collected and diluted with ultrapure water to total volume of 250 ml.

Nitrogen and argon adsorption/desorption isotherms were measured using an ASAP 2020 (Micromeritics) static volumetric apparatus at –196 °C for nitrogen and –196 °C for argon. Prior to the sorption measurements, all samples were degassed with a turbomolecular pump at 300 °C for 8 h. BET area (S_{BET}) was evaluated by BET method[158] using adsorption data in the p/p_0 range of 0.05 – 0.20. The t-plot method[159] was applied to determine the volume of micropores (V_{micro}). The volumes of mesopores in the range from 2 to 20 nm were calculated from the desorption branch of the isotherm using BJH method[160] with Halsey equation. Micropore size distribution was evaluated using NLDFT method (Carb Cylinder Pores MWNT kernel). To calculate the adsorption isosteres, Ar sorption isotherms (at -196/-186 °C) were transformed to log(p) – a coordinates, where a – adsorbed amounts; a = 5, 10, 15,..., 55 cm^3/g STP. The values of log(p) were calculated using a polynomial interpolation procedure. The isosteric heats of adsorption

(Q_{st}) were calculated from the slope of the adsorption isosteres using the equation

$$\frac{d(\log p)}{d(1/T)} = -\frac{Q_{st}}{2.303 \cdot R} \quad (R - \text{gas constant}).$$

The concentrations of Lewis (c_L) and Brønsted (c_B) acid sites were determined after adsorption of pyridine (Py) by FTIR spectroscopy using a Nicolet Protégé 460 Magna with a transmission MCT/B detector. The zeolites were pressed into self-supporting wafers with a density of 8.0 – 12 mg/cm^2 and activated in situ at T = 450 °C and p = $5 \cdot 10^{-5}$ Torr for 4 h. Pyridine adsorption was carried out at 150 °C and a partial pressure of 3.5 Torr for 20 min, followed by desorption for 20 min at the same temperature. Before adsorption, pyridine was degassed by freeze–pump–thaw cycles. All spectra were recorded with a resolution of 4 cm^{-1} by collecting 128 scans for a single spectrum at room temperature. The spectra were recalculated using a wafer density of 10 mg/cm^2. c_L and c_B were evaluated from the integral intensities of bands at 1454 cm^{-1} (c_L) and 1545 cm^{-1} (c_B) using extinction coefficients, $\varepsilon(L) = 2.22$ cm/μmol and $\varepsilon(B) = 1.67$ cm/μmol[161]. For determination of the strength of different acid sites, desorption of pyridine was carried out at 150, 250, 350 and 450 °C and followed by FTIR measurement.

Scanning electron microscopy (SEM) was used to study size and shape of zeolite crystals (SEM, JEOL JSM-5500LV microscope). For the measurement the crystals were coated with a thin layer of platinum (~10 nm) in a BAL-TEC SCD-050 instrument.

The ^{19}F solid-state MAS NMR spectra were acquired using a Bruker Advance III 600 MHz spectrometer equipped with a wide bore 14.1 T magnet. Prior the NMR measurement, 0.1 g of zeolite was ground in the mortar with 0.1 g of NH$_4$F. Samples were loaded into 2.5 mm rotors and rotated at MAS rates of 25 kHz. The chemical shift scale was shown relative to CCl$_3$F.

The solid state ^{27}Al and ^{29}Si MAS NMR spectra were recorded on an Agilent DD2 500WB spectrometer at resonance frequencies of 130.24, and 99.30 MHz, respectively. All MAS NMR were carried out with a commercial 3.2 mm triple resonance MAS probe. The chemical shifts of ^{29}Si are referenced to tetramethylsilane (TMS) at 0 ppm and for ^{27}Al to a 1.1 mol/kg solution of Al(NO)$_3$ in D$_2$O on a deshielding scale. Saturation combs were applied prior to all repetition delays. All ^{27}Al MAS spectra were conducted using a single pulse excitation (1D) at a sample spinning frequency of 15 kHz. Typical 90° pulse lengths for the ^{27}Al central transition were 1.25 us and recycle delays of 1.0-15.0 s. Similarly, ^{29}Si 1D experiments were acquired at a sample spinning frequency of 10 kHz using a pulse length of 3 us and a recycle delay of 60 s.

During the ^{29}Si acquisition period proton broadband decoupling were applied with a continuous wave sequence using a nutation frequency of 100 kHz. Total 6000 and 1000 number of scans was acquired for ^{27}Al and ^{29}Si, respectively.

High resolution transmission electron microscopy (HRTEM) was made on a JEOL JEM-2011 electron microscope operating at an accelerating voltage of 200 kV. The HRTEM images were recorded using a 9 Gatan 794 CCD camera. The measurements were carried out in Advanced Microscopy Laboratory, Nanoscience Institute of Aragon, University of Zaragoza, Spain.

4. Results and discussion

The outcome of the tuning of zeolite porosity by the ADOR methodology or post-synthesis treatment (degermanation, or alumination) depends on the several factors:

- intrinsic properties of starting materials such as framework type, chemical composition, and distribution of Si and Ge atoms in the framework;

- treatment conditions applied, which include the way of the treatment (in the presence or absence of solvent), type of reactant (H_2O, acids or bases), pH, temperature, and duration.

The first challenge of this work was to prepare zeolites possessing properties appropriate for each of these treatments. For application of the ADOR approach, starting zeolites should be easily hydrolysable giving stable layered materials. In **UOV**, **IWR,** and **IWW** germanosilicate, Ge atoms were located not only in the D4R building units but also in the layers. Thus, for each of germanosilicate, the syntheses conditions should be optimized to prepare samples containing the D4Rs having $\geq$ 4 Ge atoms, as it was previously discussed, and on the other side, to minimize its amount into the layers. On the other hand, zeolite frameworks must be preserved during mesopore formation by post-synthesis degermanation and for that purpose zeolite samples should possess the D4R units enriched with Si atoms.

4.1. New Zeolites Obtained by the ADOR Approach

4.1.1. Application of UOV Germanosilicate in the ADOR

4.1.1.a. Synthesis of New Zeolite IPC-12

Based on ref.[34], the reaction mixtures with the range of ratios Si/Ge = 0.5 – 6 and different water amount (H_2O/T^{IV} = 10 for diluted and 5 for concentrated gels) were used for the preparation of **UOV** samples (Table 4).

Table 4: Chemical and phase compositions of obtained **UOV** zeolites

Sample name	H_2O/T^{IV} ratio in reaction mixture	Si/Ge ratio		Phase composition
		Starting gel	Final sample[a]	
UOV-0.5	10	0.5	3.1	**UOV**
UOV-0.5-c	5	0.5	1.3	**UOV**
UOV-0.75	10	0.75	3.0	**UOV**
UOV-1	10	1	3.3	**UOV**
UOV-1-c	5	1	1.4	**UOV**
UOV-1.5	10	1.5	3.1	**UOV**
UOV-2	10	2	3.3	**UOV+MFI**
UOV-2-c	5	2	3.2	**UOV+MFI**
UOV-3	10	3	12.6	**MFI**
UOV-3-c	5	3	4.1	**UOV+MFI**
UOV-6-c	10	6	6.2	**UOV+MFI**

[a]Si/Ge ratio obtained by ICP/OES analysis.

As the main product, **UOV** zeolites were obtained from reaction mixtures with ratios Si/Ge = 0.5 – 1.5. Further increase in the silicon concentration in reaction gels resulted in the formation of **MFI** phase as the admixture or even as the main product (for **UOV**-3 sample). Water amount used for syntheses significantly influenced the chemical composition of final samples. Si/Ge ratios in samples obtained from concentrated starting gels (H_2O/T^{IV} = 5) were twice as low in comparison with the samples prepared from gels with H_2O/T^{IV} = 10 (Table 4). The "concentrated" **UOV**-n-c materials showed low framework stability, as they were sequentially hydrolysed even in presence of air moisture under ambient conditions (presented in details in Enclosure). That indicates that Ge atoms in the framework of **UOV**-n-c samples were located not only in the D4R units, but also in the layers.

UOV zeolites obtained from concentrated reaction mixtures were hydrolytically instable, thus, we focused on the **UOV**-n samples with optimal chemical composition both for the following disassembly and post-synthesis modification. The structural changes taking place during the disassembly of **UOV** layers were investigated by XRD. All lines in the XRD pattern can be assigned as the interlayer (peaks positions are affected by the change in interlayer distance) or intralayer (peaks positions are maintained upon manipulation with the layers) signals. In the case of **UOV**, (h00) reflexes relate to the interlayer signals which correspond to the distance between the individual layers, while intralayer peaks (all other combinations of hkl) fit the positions of atoms in the layers. Removing the D4R units from the framework during

disassembly causes the decrease in the interlayer distance. Thus, the change of the positions of the interlayer peaks (we followed the (100) signal located at 7.07° 2θ for the starting **UOV**) to the higher 2θ values provides us information about the success of the disassembly step. The Fig. 12 represents the scheme of structure transformation taking place during acidic treatment of **UOV** and the XRD patterns of **UOV** zeolite before and after the treatment.
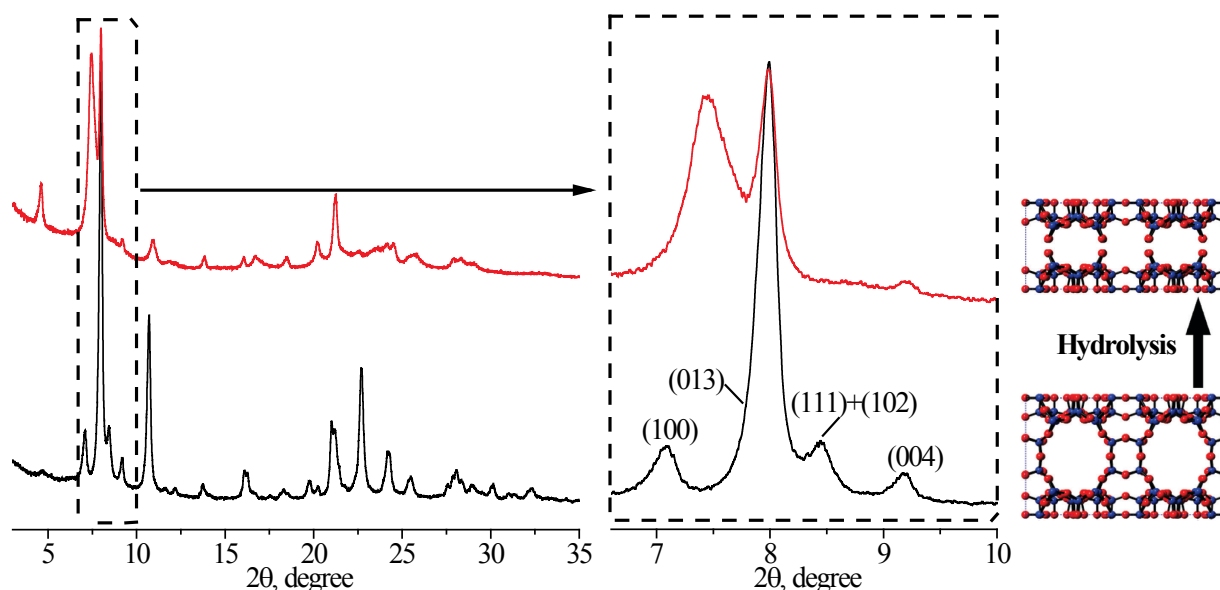
Fig. 12. XRD patterns and corresponding structures of parent **UOV** zeolite (black), and the precursor IPC-12P obtained after hydrolysis (red).

Even though the chemical compositions of the reaction mixtures were significantly varied (Table 4), the ICP/OES analysis showed that samples obtained from diluted reaction mixtures were characterized by very similar content of Ge (Si/Ge = 3.0 – 3.3). But, according to the ^{19}F NMR spectroscopy (Fig. 13) these **UOV** samples after post-synthetic fluorination exhibited significant differences in the location of Ge atoms. The spectra of all fluorinated samples were characterized by the presence of the peaks at -10 ppm corresponding to F$^-$ occluded in the [4Si, 4Ge] D4Rs units; and at -30 ppm typically assigned to F$^-$ ions located in the siliceous layers surrounded only by Si atoms. With increase in the Si/Ge ratio in reaction mixture from 0.5 to 2, the gradual increase in the peak intensity at -20 ppm attributed to the [7Si, 1Ge] D4R units can be noticed.

The differences in the location of Ge atoms in the **UOV** samples significant changed their stability. The XRD patterns of small angle region for the samples treated with 0.1 M HCl are presented in the Fig. 13 B and show preservation of the (013) lines corresponding to intralayer

signals, but the positions of (100) reflections differed. The highest degree of hydrolysis was observed for the materials obtained from reaction mixtures with Si/Ge = 0.5 and 0.75, as it is indicated by the maximal right-shift of the interlayer (100) peak. Hydrolysis of these samples resulted in the formation of layered material IPC-12P. Calcination of IPC-12P leads to its condensation to new zeolite IPC-12, as all interlayer signals were additionally shifted to high-angle region on the XRD pattern (Fig. 13, C). While in the parent **UOV** zeolite layers are connected through the D4R units, in IPC-12 they are linked by oxygen atoms, i.e. material possess direct connectivity of the layers.
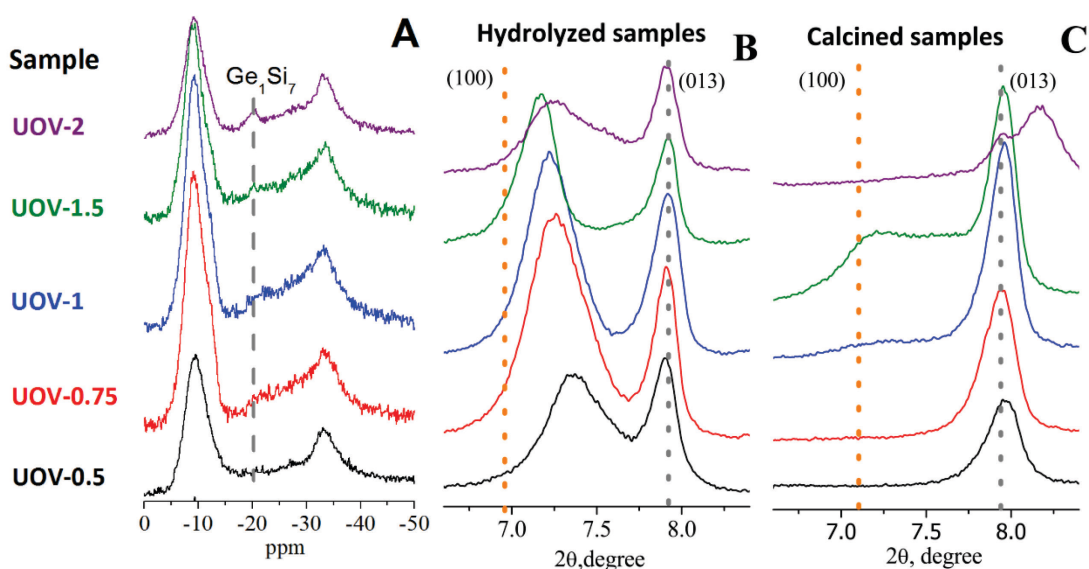
Fig. 13. A) ^{19}F MAS NMR spectra of fluorinated **UOV** zeolite samples synthesised from different reaction mixtures; B) characteristic low-angle region of diffraction patterns for the samples hydrolysed with 0.1 M HCl at 25 °C for 24 h; C) diffraction patterns of respective calcined samples. Orange and grey dotted lines correspond to the positions of (100) and (013) reflections in parent **UOV**, respectively.

On the other hand, the acidic treatment of the samples possessing Si-enriched D4Rs i.e. synthesised from initial gels with Si/Ge = 1 – 2, resulted in insignificant shifts of (100) signal and its preservation on the XRD after following calcination. It indicates that **UOV** framework remained practically intact after the treatment, which makes respective samples perspective materials for the development the extra-porosity, as it will be presented below.

To obtain highly crystalline IPC-12 material, optimisation of the treatment conditions on the disassembly step was made for **UOV** sample with starting Si/Ge = 0.5. Type of reactant used for disassembly (solutions of 0.1 M HCl, 0.1 M HNO$_3$, 0.146 M CCl$_3$COOH, 1.4 M H$_3$PO$_4$ and 0.09 M H$_2$SO$_4$, all are characterized by pH = 1) practically did not affect the final phase

formation, as the obtained IPC-12 samples were characterized by similar crystallinity (Enclosure). Per contra, it was observed that pH of solution significantly influenced the degree of disassembly and even the direction of zeolite framework transformation. When concentration of hydrochloric acid was increased in the order 0.1 M – 1 M – 4 M, the process of hydrolysis was inhibited, as the right-shift of (100) interlayer peak decreased (Fig. 14). Such inhibition is especially pronounced for the sample treated with 4 M acid and may be related to the decrease in germanium solubility with increasing pH, similar to the results reported for germanium (IV) oxide[162]. Using of 12 M HCl for the treatment resulted in a maximum change in the interlayer distance. Kinetic study of the treatment with 12M HCl showed that the prolongation of experiment unpredictably led to the formation of the same IPC-12 material obtained previously by calcination of IPC-12P precursor.
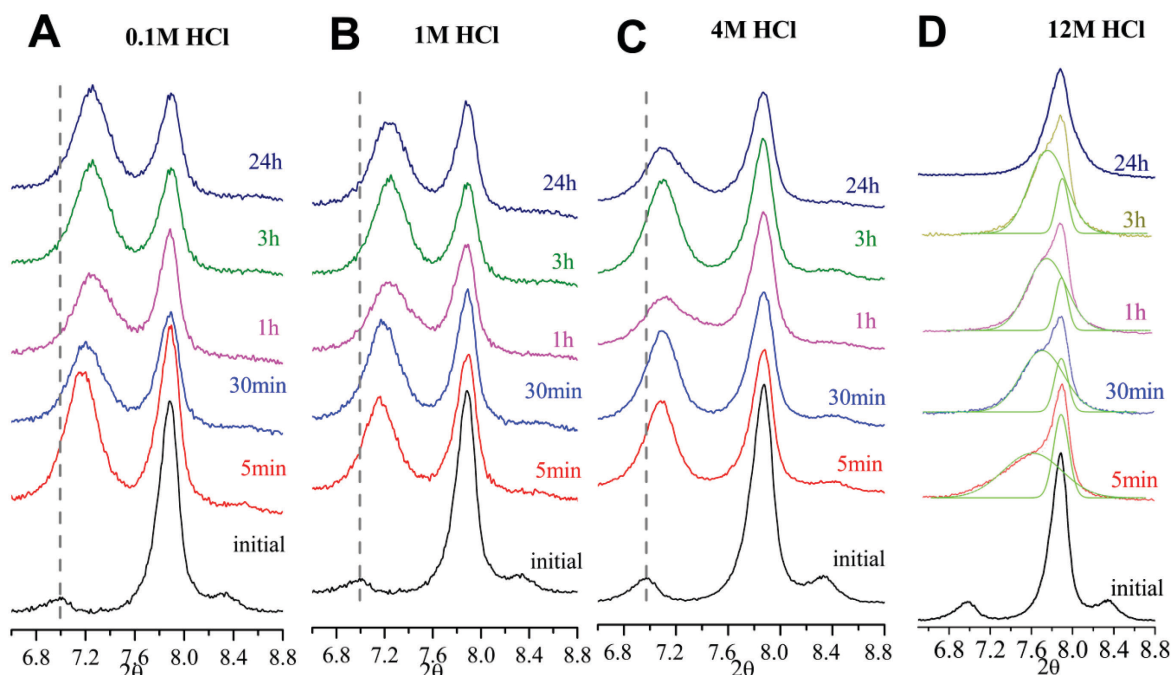
Fig. 14. XRD patterns of **UOV**-0.5 treated at 25 °C with A) 0.1 M, B) 1 M HCl, C) 4 M HCl, D) 12 M HCl for different times (with deconvolution for evaluation of the peak positions). Grey dotted lines correspond to the positions of (100) reflections in parent **UOV**.

Thus, we observed that IPC-12 can be formed *via* two different ways. First one is based on consecutive disassembly-reassembly steps that means through the formation of stable layered precursor; or IPC-12 synthesis can be realized by direct framework rearrangement without detectable intermediate steps at pH < 0 (Fig. 15). In the latter case, silica mass-transfer takes place under highly acidic conditions similarly to the "inverse sigma transformation" process for zeolite **UTL**, which was discussed previously in details (see Introduction, 2.6). Noticeably, the

outputs of the treatments of **UOV** and **UTL** are different: while for **UOV** the change of the treatment conditions leads to the formation of the same material (IPC-12), in the case of **UTL**, 2 different treatment conditions provides two different materials (**OKO** at very low pH and **PCR** via multistep disassembly-reassembly).
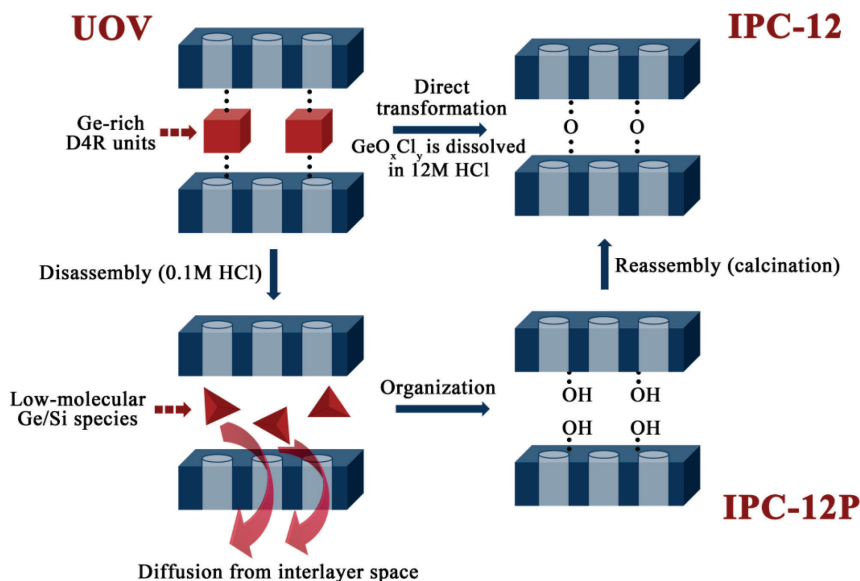
Fig. 15. Schematic presentation of mechanisms of **UOV**-to IPC-12 rearrangement in 0.1 vs. 12 M HCl.

4.1.1.b Properties of New Zeolite IPC-12

Formation of new zeolite IPC-12 was confirmed by comparison of the X-ray diffraction pattern obtained using synchrotron source with theoretical predicted one. They matched well and based on these data the Rietveld refinement for IPC-12 was carried out (Fig. 16).
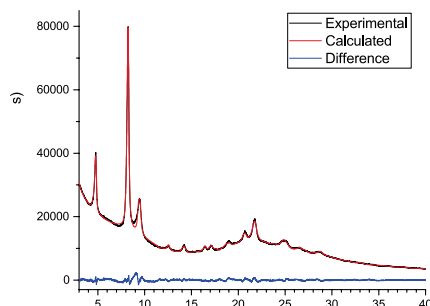
Fig. 16. Experimental and calculated XRD patterns (Rietveld refinement) and the difference between them. Unit cell parameters a = 7.511(11) Å, b = 21.638(4) Å, c = 37.736(29) Å, $\alpha = \beta = \gamma = 90.0°$, space group Amm2.

The structure of IPC-12 (Fig. 17) was investigated by STEM-HAADF electron microscopy with atomic resolution. As the zeolite layers are assumed to be intact during the ADOR transformation, 12 and 8-ring pores located perpendicularly to the **UOV** layers have to remain unchanged. The 12-ring channels are organized in a pseudo-hexagonal arrangement with 8-ring channel in the middle of such hexagon. Fig. 18A shows STEM-HAADF image of the layers from the top view confirming the preservation of the pore arrangement in the final IPC-12 zeolite.
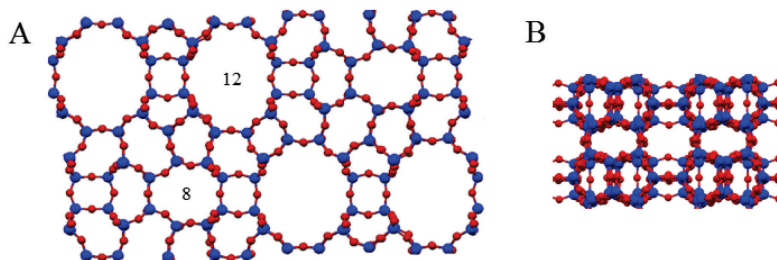
Fig. 17. Crystallographic model of IPC-12 A) in the *ab* projection; 12 and 8-ring pores are designated by respective numbers, B) in *ac* projection representing direct connectivity between the layers.

The 12- and 8-ring channels in parent **UOV** zeolite intersect with 10- ring pores located along (001) direction. After **UOV**-to-IPC-12 rearrangement, 10-rings were transformed into 6-rings due to the removal of the D4R units. STEM-HAADF image (Fig. 18, B) shows that a repeating distance between the layers is about 1.054 nm, which confirms the absence of the D4R domains in final IPC-12. The d-spacing for parent **UOV** was 1.78 nm.
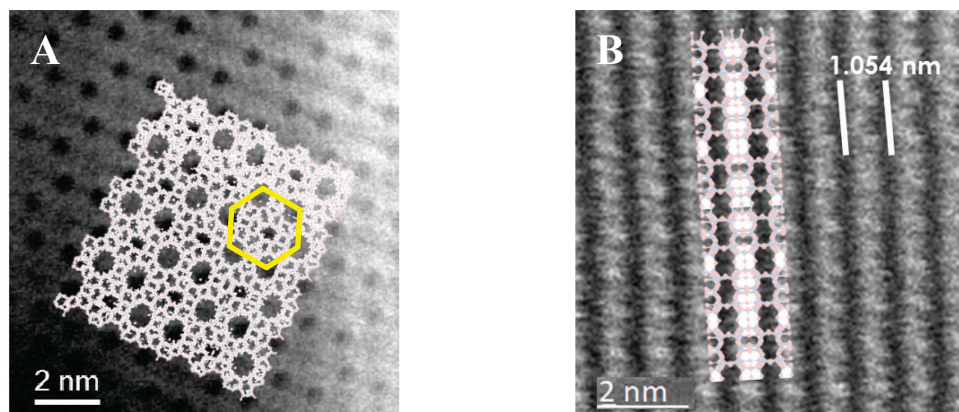
Fig. 18. STEM-HAADF images of IPC-12 viewed A) in *ab* projection, showing top view of the layers (yellow hexagon shows pseudo-hexagonal arrangement of 12-ring pores); B) in the *ac* projection showing the arrangement of layers in the final material.

Removing the D4Rs resulted in the change in pore system from 3-dimensional to two independent set of channels (both are 1-dimentional and are along (100) direction). This

transformation has to be accompanied with the significant loss in micropore volume, which was confirmed by the results of nitrogen adsorption-desorption experiments presented in the Fig. 19. Both **UOV** and IPC-12 zeolites exhibit the isotherms of I type with loop at $p/p_0 = 0.9 - 1$ related to the interparticle adsorption. Expectedly, V_{micro} for IPC-12 material was two-times lower (0.052 cm^3/g) in comparison with **UOV** zeolite (0.111 cm^3/g). Both materials possess comparable volume of mesopores: 0.153 *vs.* 0.145 cm^3/g for IPC-12 and **UOV** respectively indicating that only microporous system of the latter was affected during the ADOR transformation. IPC-12 formation influences also the pore size distribution (Fig. 19, B), showing the decrease in average channel diameter from 0.605 nm for **UOV** to 0.575 nm for IPC-12.
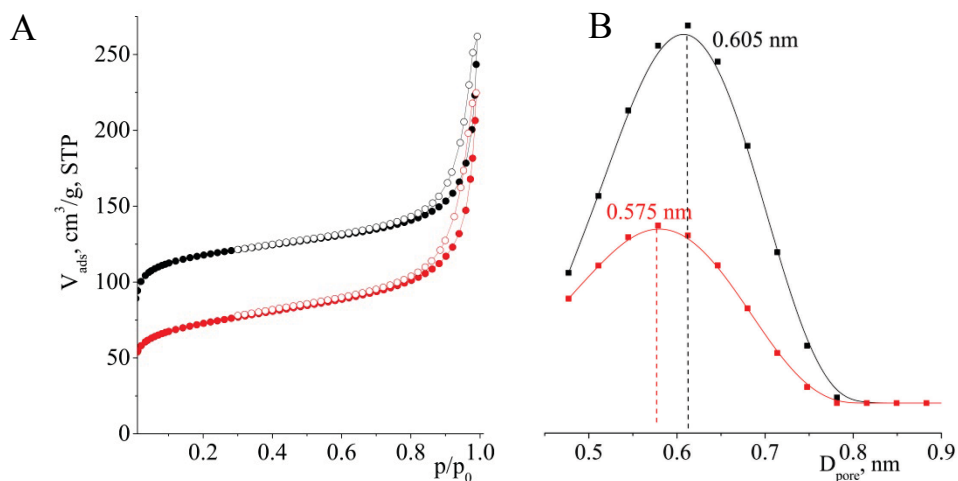
Fig. 19. A) Nitrogen adsorption and desorption isotherms and B) Pore size distribution for: initial **UOV**-0.5 (black) and final IPC-12 (red).

The ADOR transformation practically did not impact the crystal morphology. Similarly to the initial **UOV**, IPC-12 was characterized by tiny plate-like crystals with size of 0.5 x 0.4 x 0.1 µm (Fig 20).
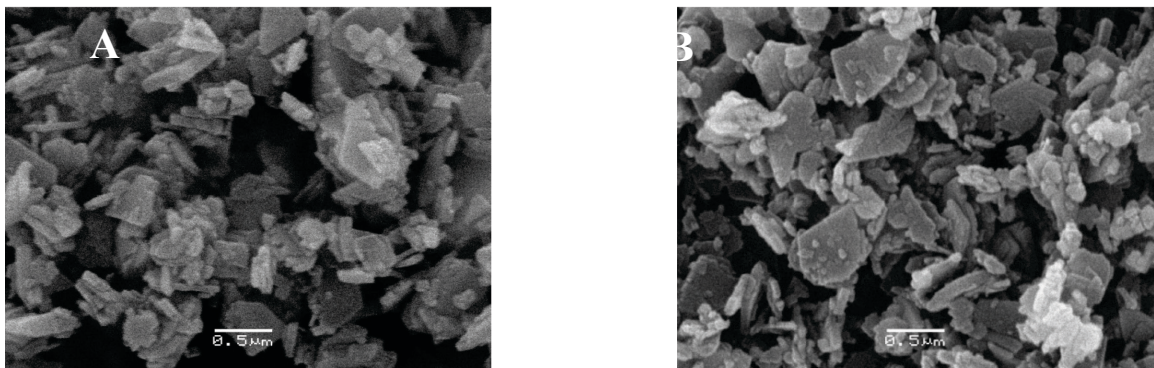
Fig. 20. SEM images of A) **UOV**-0.5 and B) IPC-12 zeolite obtained by the ADOR.

4.1.2. IPC-13 Obtained Starting from Germanosilicate CIT-13

As it was previously mentioned, the structure of CIT-13 is closely related to the structure of zeolite SAZ-1. These zeolites possess the same structure of layers but differ in their connections by the D4Rs (similar to presented in the Fig. 7). Thus, application of CIT-13 in the Assembly-Disassembly-Organization-Reassembly procedure is expected to lead to the formation of the products similar to reported by D. S. Firth et al[91] for SAZ-1: IPC-15 (with connectivity between the layers by O bridges) and IPC-16 (where layers are connected by the S4Rs).

In order to investigate germanosilicate CIT-13 in the ADOR approach, the sample with Si/Ge = 4 was synthesised based on [96] (Fig. 21, A, B, black patterns). It was subsequently transformed into a lamellar material under acidic conditions. The original position of interlayer (200) signal in CIT-13 was 6.45° 2θ; after hydrolysis with 0.1 M HCl it was shifted up to 7.78° 2θ, with 12 M HCl – 7.42° 2θ, which indicates change of the interlayer structure, probably a hydrolysis of Ge–O–Si bonds and hence disintegration of the D4R units. On the other hand, the positions and intensities of intralayer signals remained intact meaning the preservation of the silicate layers during hydrolysis.
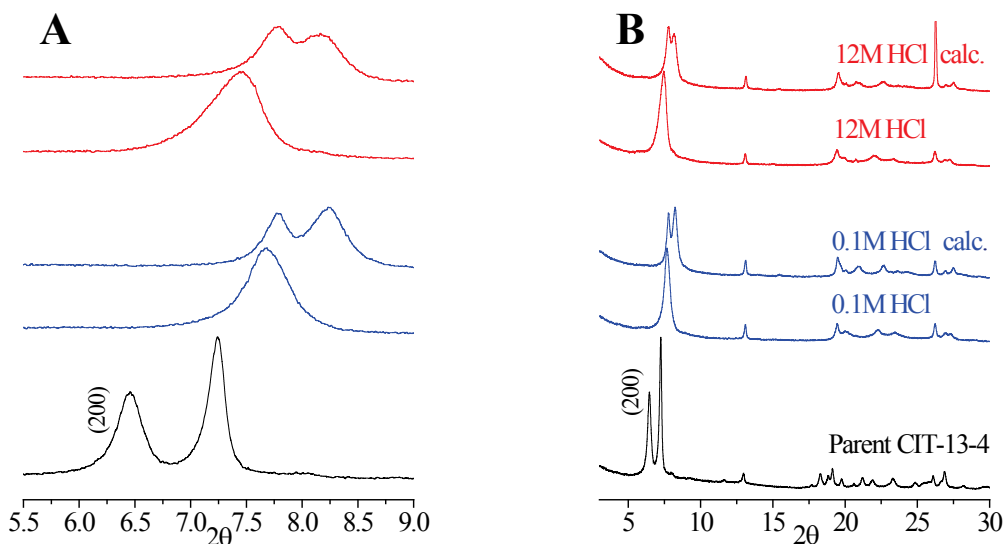
Fig. 21: A) Small angle region, B) full region of the XRD pattern CIT-13-4 sample: initial (black), before (lower) and after (upper) calcination treated with 0.1 M (blue) and 12 M HCl (red) for 16 h.

Despite the difference in deepness of hydrolysis with 0.1 and 12 M HCl, following calcination of the treated samples resulted in formation of the same material, which we named IPC-13. The comparison of its XRD pattern with the patterns of products derived from SAZ-1

showed that the structure of obtained material corresponded to IPC-16. Fig. 22 shows the models of parent CIT-13 and final IPC-13 zeolites. The formation of IPC-13 having additional S4R linkages may be explained by the presence of the remaining Si and Ge species between the layers after hydrolysis. It should be noticed that final IPC-13 samples differed in chemical composition (according to ICP/OES analysis): material obtained after calcination of CIT-13-4 treated with diluted acid was characterized be Si/Ge = 23, while that prepared with concentrated acid had Si/Ge = 9.
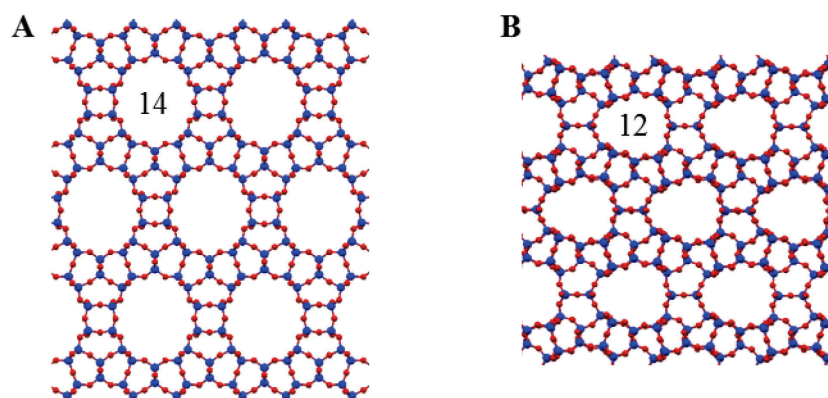
Fig 22. Crystallographic model of A) initial CIT-13 and B) IPC-13 zeolites.

Based on the results of theoretical simulation of the ICP-13 framework and the corresponding XRD pattern, the Rietveld refinement was carried out (Fig. 23). The space group in the final material was P-1, which differed from Cmmm for initial CIT-13. Parameters of units cells were following: a = 9.953(6) Å, b = 13.668(7) Å, c = 13.5562(30) Å, α = 120.21(5)°, β = 89.71(8)°, γ = 69.21°.
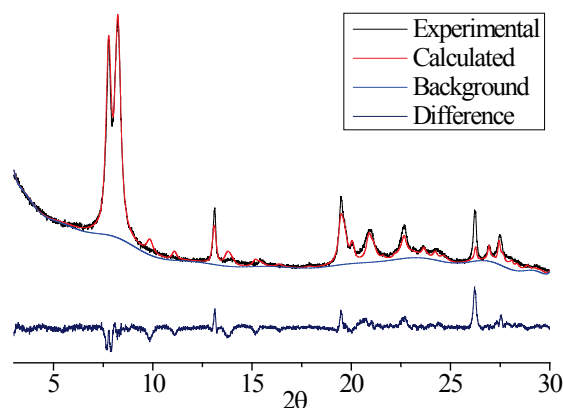
Fig. 23. The XRD data: experimental pattern (red), calculated pattern (black) from the final Rietveld refinement, and the difference between them (navy).

The CIT-13-to-IPC-13 rearrangement was confirmed by the results of STEM-HAADF microscopy presented in the Fig. 24. As it is clearly seen from the side view on the layers, the interlayer distance decreased from 1.335 nm for CIT-13 to 1.088 nm for IPC-13, which indicates transformation of the D4R into the S4R units.
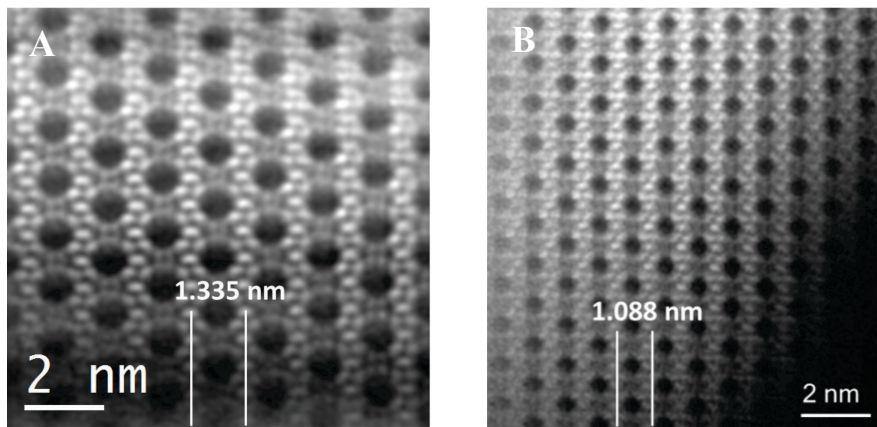
Fig. 24. STEM-HAADF images of A) CIT-13 and B) IPC-13 zeolites showing the connection of layers by the D4R and the S4R units respectively.

The results of adsorption-desorption experiments also provide information about structure transformation. The Fig. 25 A shows the nitrogen adsorption isotherms of initial and final materials: both possess the isotherm of I type. As the pore system was changed from 14×10 for CIT-13 to 12×10 for IPC-13, micropore volume decreased from 0.06 to 0.04 cm^3/g, while BET area decreased from 250 to 203 m^2/g respectively. Similarly to discussed previously for **UOV**-to-IPC-12 transformation, we observed the decrease in the average channel diameter (Fig. 25, B): for IPC-13 it was less by 0.061 nm.
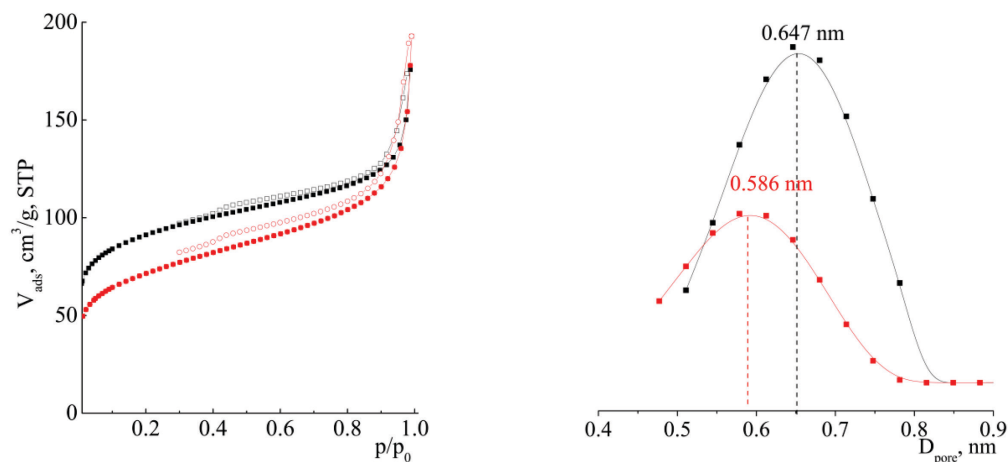
Fig. 25.A) Nitrogen adsorption and desorption isotherms and B) Pore size distribution for: initial CIT-13-4 (black) and final IPC-13 (red).

4.1.3. IWR Zeolite in the ADOR Strategy. Approaches for Synthesis of Parent Zeolite

Presence of different framework elements in the parent zeolite and their concentration are important parameters for the disassembly step. Previously, a possibility of disassembly of **IWR** borogermanosilicate in acid conditions was reported[69]. However, obtained 2D material possessed a high lability of layers, as the disassembly process was accompanied with partial layers degradation due to the presence of boron. This instability of layers restricted **IWR** application in following steps of the ADOR approach. To exclude negative impact of framework boron and improve stability of the layers several approaches were proposed, such as: i) decrease in the boron amount and variation of Si/Ge ratio in **IWR** zeolite samples through the change of chemical composition of starting reaction mixtures, ii) adding source of fluorine, or iii) using seeding approach.

For this purpose, we synthesised samples from reaction mixtures with Si/Ge ratios from 2 to 5 in the presence of 5 – 10% B based on[123]. Any attempts to decrease percentage of boron to 1 – 2% resulted in the formation of **IWW** as a main phase instead of **IWR** zeolite. Synthesised **IWR**-n-B-m samples were crystalline single phase materials, except **IWR**-2-B-10 having an admixture of **IWW** zeolite (Fig 26). Following treatment of the samples with 12 M HCl resulted in all cases in framework transformation. The interlayer (001) peak was shifted to the high-angle region, indicating the decrease in the distance between the layers. However, it was also accompanied with degradation of layers, as intensities of all peaks corresponding to intralayer signals dropped. Another way of layer stabilization was based on the idea of adding of fluorine source in reaction mixture, which can possibly change distribution of Ge atoms in the framework by coordinating them into the D4R units. However, similar to the synthesis in boron medium, the framework destruction was observed when **IWR**-2-B-5-F sample was treated with 12M HCl (Fig. 26 C, D).

Stabilization of the **IWR** layers was achieved using the seeding approach for syntheses. They were carried out using boron-free reaction mixtures (Si/Ge = 2 – 5) containing 10% of sample **IWR**-5-B-5 as seeds. Acidic treatment of these samples with 12 M HCl resulted in preservation of layers. Formation of stable **IWR** germanosilicate is related to the decrease in the boron amount in the framework, because chemical analysis of **IWR**-n-s samples showed that the amount of boron in final sample was less than 0.1%. Sample **IWR**-2-s, i.e. obtained from

reaction mixture with Si/Ge = 2, gave a stable lamellar material after the disassembly (in comparison with other IWR samples). The XRD pattern of treated IWR-s shows (Fig. 26, C, D) the preservation of all signals corresponding to intralayer reflections.
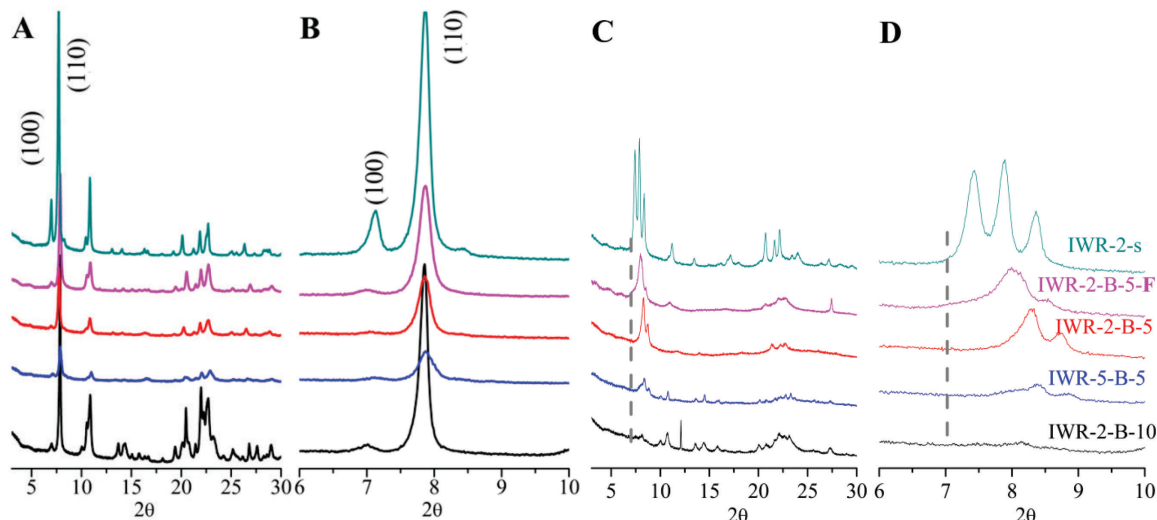
Fig. 26. **IWR** sample obtained by seeding (IWR-2-s) and B-containing **IWR** samples A) before and C) after the treatment with 12 M HCl at RT for 6 h; B) and D) are low-angle regions corresponding to A) and C), respectively
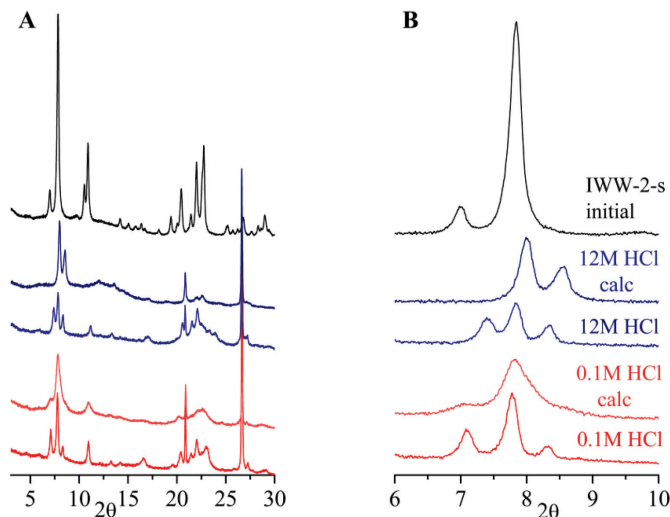
Fig. 27. A) The XRD patterns and B) corresponding low-angle region for **IWR**-2-s sample: initial (black), before and after calcination treated with 0.1 M (red) and 12 M HCl (blue) for 16 h.

Acidity of solution was important parameter for the disassembly of **IWR**-2-s. When **IWR** zeolite was treated with 0.1 M HCl, interlayer (001) reflection was only slightly shifted to high angle region (Fig. 27, red patterns). The XRD pattern of resulting material had 2 additional lines at 20.8° and 26.7° 2θ attributed to GeO_2 phase, which indicates the leaching of Ge atoms from zeolite framework. Nevertheless, the samples after calcination corresponded to defective

parent **IWR** phase. In contrast, (100) interlayer signal was significantly right-shifted, when **IWR**-2-s germanosilicate was treated with 12 M HCl (Fig. 27, blue patterns). Following calcination of this sample led to the formation of new zeolite material – IPC-17 (Fig. 28), where layers are linked by the S4R units.
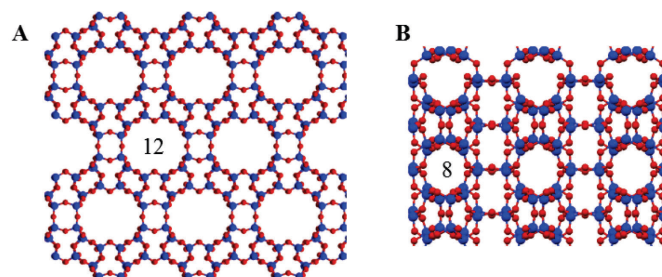
Fig. 28. Crystallographic model of IPC-17 A) in the *ab* projection, showing top view on the layers with 12-ring pores, B) in *bc* projection (the side view on the layers) demonstrating connection between the layers by the S4R. After the transformation 8-ring pores appear in this direction.

Thus, we observed that the ADOR transformation depends on the framework type and chemical composition of initial zeolite. Applying highly acidic conditions for **UOV**, the D4R units can be removed from the framework giving IPC-12 zeolite. On the other hand, in the case of **UTL**, CIT-13 and **IWR** it leads to the framework rearrangement into zeolites possessing connectivity between the layers through the S4R units.

4.1.3.a. Properties of IPC-17

Fig. 29 shows comparison of the XRD patterns obtained with synchrotron source for parent **IWR** and the new zeolite IPC-17. Several intralayer signals for final IPC-17 were significantly less intensive in comparison with **IWR** complicating the refinement of the structure.
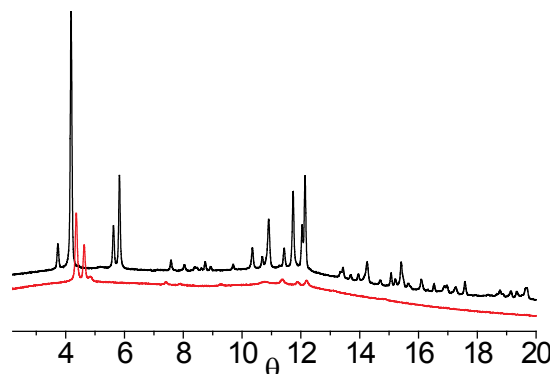
Fig.29. Comparison of the X-ray diffraction patterns obtained with synchrotron source: initial **IWR** (black) and final IPC-17 (red) zeolites.

Based on the topology of initial **IWR** zeolite, several possible structures of IPC-17 were predicted by Density Functional Theory (DFT) method[143]. Fig. 30 shows the comparison of experimental and theoretically simulated XRD patterns, which matches quite good in number, positions (except those at 13 – 15 ° 2θ) and intensities of signals.
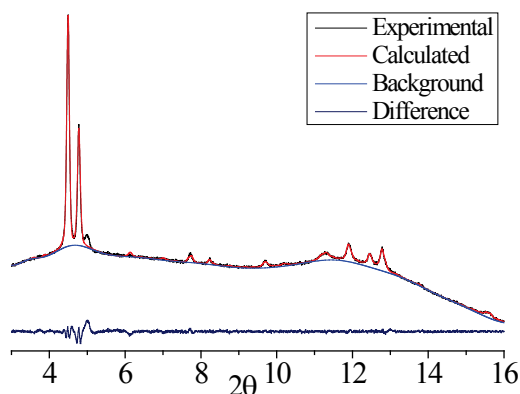
Fig. 30. Comparison of the XRD patterns for IPC-17 zeolite: experimental (black) and theoretically predicted by DFT (red), the difference between them (navy).

Zeolite **IWR** has a three dimensional channel system, which is formed by interconnected 12- (along (001) projection) and 10- (along (010) and (100) directions) ring pores. 12-ring channels were not changed during **IWR**-to-IPC-17 transformation, while 10-ring channels become 8-ring one due to the transformation of D4Rs into S4Rs. This change in the pore system resulted in the decrease in the micropore volume and change of average pore size (Fig. 31). Similarly to the results presented before for IPC-12 and IPC-13, micropore volume was found to be 2 times lower in comparison with the starting zeolite (0.150 *vs.* 0.086 cm^3/g for **IWR** and IPC-17). The average channel diameter decreased from 0.619 nm for **IWR** to 0.566 nm for IPC-17.
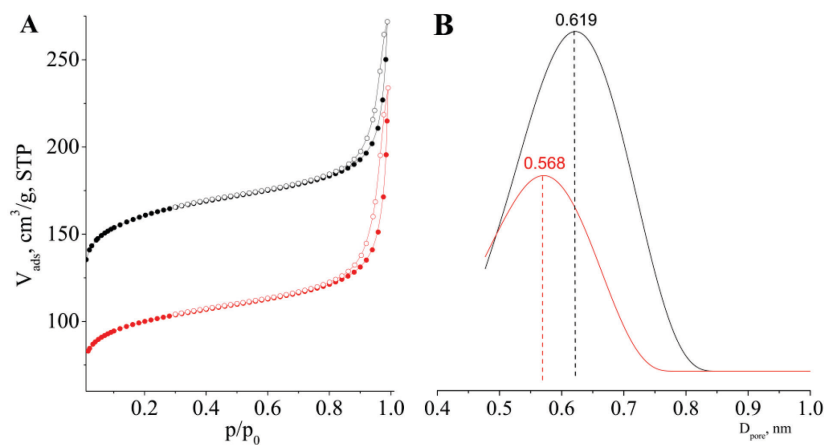
Fig. 31. A) Nitrogen adsorption and desorption isotherms and B) Pore size distribution for: initial **IWR**-2-s (black) and IPC-17 (red) zeolites.

Formation of new zeolite IPC-17 was also confirmed by the results of STEM-HAAD microscopy (Fig. 32). From the top view, the layers of zeolites **IWR** and IPC-17 should look the same (Fig. 32, A); 12-ring pores in final IPC-17 can be clearly recognized. Fig. 32, B, C shows HRTEM images from the side view on zeolite framework. D-spacing decreased from 1.05 to 0.97 nm for initial **IWR** and IPC-17 materials, respectively.
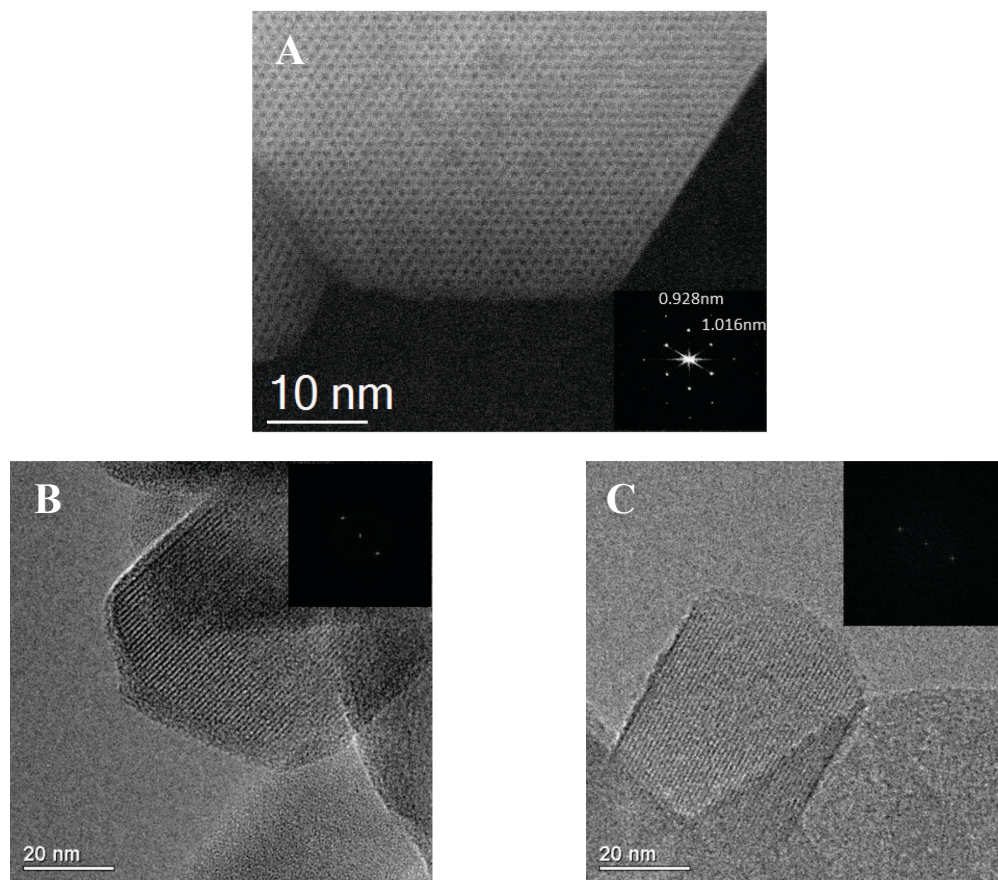
Fig. 32. A) STEM-HAADF image showing top view on the layers of IPC-17 zeolite, which remain intact after the rearrangement; and the side view on the layers (HRTEM images): B) for initial **IWR** zeolite, d-spacing = 1.05 nm, and C) for IPC-17 zeolite, d-spacing = 0.97 nm.

Evolution of the degree of condensation in the process of **IWR**-to-IPC-17 zeolites rearrangement was studied by ^{29}Si MAS NMR analysis (Fig. 33). The ^{29}Si MAS NMR spectrum of starting **IWR**-2-s was characterized by the presence of distinct signals at -107 and -115 ppm corresponded to Q^4 Si atoms in $Si(OSi)_4$ and $Si(OSi)_3(OGe)$ coordination, and shoulder at -101 ppm related to Q^3 Si atoms ($Si(OSi)_3(OH)$). Treatment of **IWR**-2-s with 12 M HCl resulted in hydrolysis of Si–O–Ge bonds and formation of IPC-17P precursor. Significant increase in the intensity of deficient silanol groups (Q^3 atoms) was observed on the spectra of this material. Moreover, the signal at -92 ppm corresponding to Q^2 Si atoms ($Si(OSi)_2(OH)_2$) was detected.

Following calcination of precursor and formation of IPC-17 zeolite leads to the decrease in intensity of signal attributed to silanol groups, which is explained by their condensation. There are 3 signals on the spectra of final IPC-17: Q^4, Q^3 and low intensive Q^2.
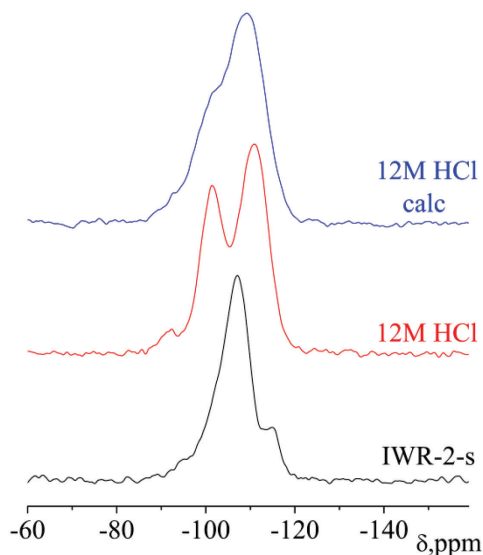
Fig. 33. ^{29}Si MAS NMR of **IWR** sample before and after treatment

4.1.4. From the ADOR in Solution to the "Non-contact" Transformation: Synthesis of IPC-18 Based on IWW Rearrangement

IWW germanosilicate containing Ge-rich D4R units in its framework was another perspective starting materials for the investigation in the ADOR transformation. Previously, the variation of chemical composition of parent **IWW** showed that acidic treatment of the samples with composition having Si/Ge = 3.1 leads to the formation of the lamellar precursor IPC-5P [143]. However, any attempts of organisation or reassembly resulted in either reconstruction into initial **IWW** framework (but enriched with Si), or layers recrystallization. Challenge for us was to find those mild conditions of the treatment, which allow transformation of the zeolite framework by the ADOR, but on the other hand preserving of the **IWW** layers. It was achieved when the solvent-free conditions were applied for transformation. The idea was based on possible hydrolysis of Ge–O bonds by limited amount of water molecules adsorbed in the zeolite pores. The process was catalysed by vapour of 12M HCl without contact of solid with solution. It was

realized at room temperature when **IWW**-2 zeolite was placed on the PTFE filter over the solution of hydrochloric acid, as it schematically presented on the Fig. 34.
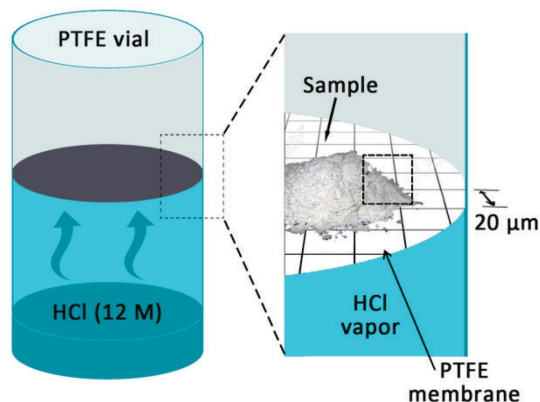
Fig.34. Scheme of treatment of **IWW**-2 germanosilicate on PTFE filter

Investigation of kinetics of **IWW**-2 zeolite treatment with 12M HCl on the PTFE filter at 25 °C (Fig. 35) showed that (001) interlayer signal[1] has already changed its position to high angle region after 5 minutes of the treatment. Intensities of (111), (211), (311), (213) interlayer signals decreased with prolongation of experiment. Furthermore, unexpectedly, the intensity of (210) intralayer signal also dropped with increasing of treatment time from 5 min to 5 h, and after that time this reflection was not presented on the spectra. The XRD pattern after 1 d was unchanged, which indicates that bonds in the D4Rs were finally hydrolysed and the precursor IPC-18P was formed.
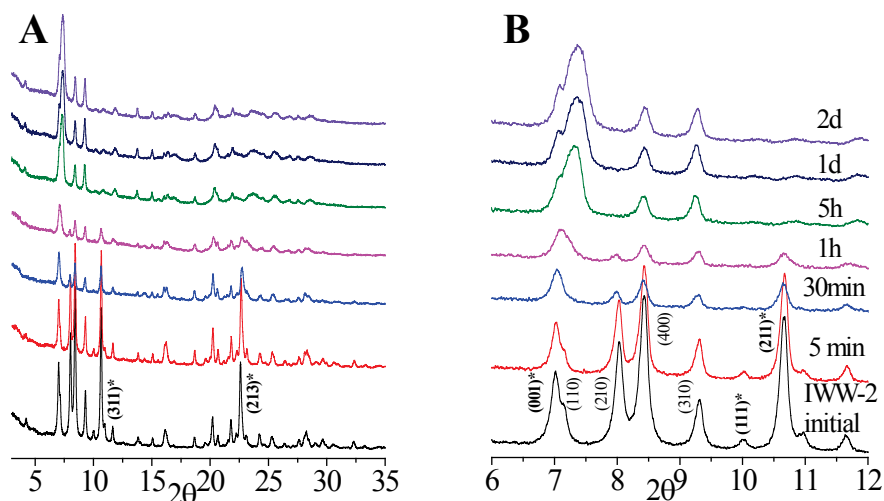
Fig. 35. A) The XRD patterns of **IWW**-2 treated at 25 °C by vapour of 12 M HCl on PTFE filter, B) the respective low angle region. Interlayer signals are marked by asterisk.

---

[1] For IWW zeolite interlayer signals are those, which have hkl, l≠0.

49

Calcination of IPC-18P (**IWW**-2 treated for 1 d) resulted in the formation of new zeolite IPC-18, which possesses connectivity between the layers through the S4R units. Formation of this product can be explained by several reasons. From one side, theoretical simulation presented in[82] showed that the energy of formation of the product with the S4Rs, is lower than one with the completely removed D4Rs (4.5 and 8 kJ/mol respectively), i.e. the former product is energetically more preferable. On the other hand, under conditions applied, the mass transport is inhibited in the course of transformation. Products of hydrolysis of the D4Rs still stay in the pores of zeolite and afterwards take part in following formation of the S4Rs. The crystallographic model of IPC-18 is presented on Fig. 36. Fig. 36 A shows the top view on the layers, which is the same for parent **IWW** zeolite, and Fig. 36 B – side view, where the S4Rs connect the zeolite layers.
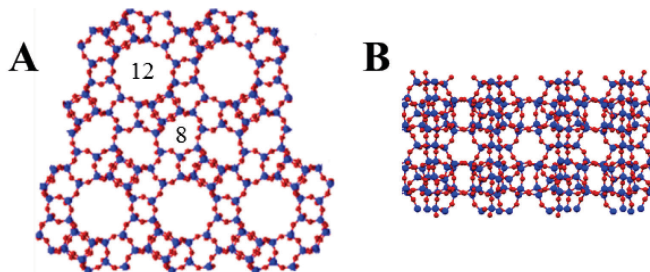
Fig. 36. Crystallographic model of IPC-18 A) in the *ab* projection, demonstrated 12 and 8-ring pores, B) in *ac* projection, showing connectivity between the layers by the S4R units.

The XRD pattern of IPC-18 matched well with theoretically predicted. Based on that the Rietveld refinement for final structure was done (Fig. 37). The space group differed from initial **IWW** (Pbam) and was $P2_1/c$, parameters of the cell were following: a = 9.606(4) Å, b = 12.7280(21) Å, c = 40.717(7) Å, α = 90.0°, β = 94.97°, γ = 90.0°.
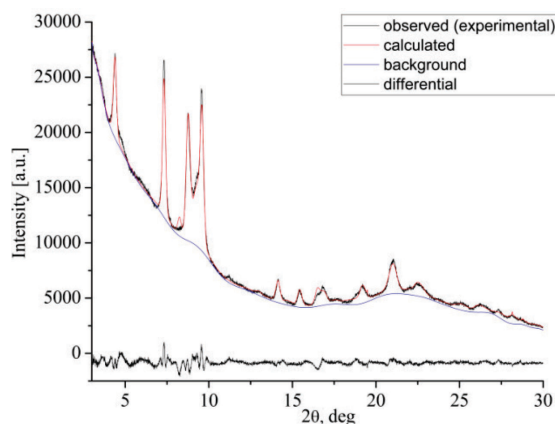
Fig. 37. Plot showing the X-ray diffraction data: experimental patterns for IPC-18, calculated pattern from the final Rietveld refinement, and the difference between them.

Formation of this new well-ordered zeolite based on the transformation of **IWW** was also confirmed by the results of HRTEM presented in the Fig. 38. The images A, B, and C show the different coordination on initial **IWW**, D, E, and F correspond to IPC-18 zeolite. The Figures A and D, B and E give comparable values of d-spacing: 1.20 *vs.* 1.20 nm and 0.95 *vs.* 0.90 nm for **IWW** and IPC-18 respectively. The Figures C and F demonstrate the "ADOR-changeable" view on the IWW zeolite framework. While for initial **IWW** the d-spacing was 2.02 nm, for final IPC-18 the repeating distance between the layers decreased to 1.92 nm.
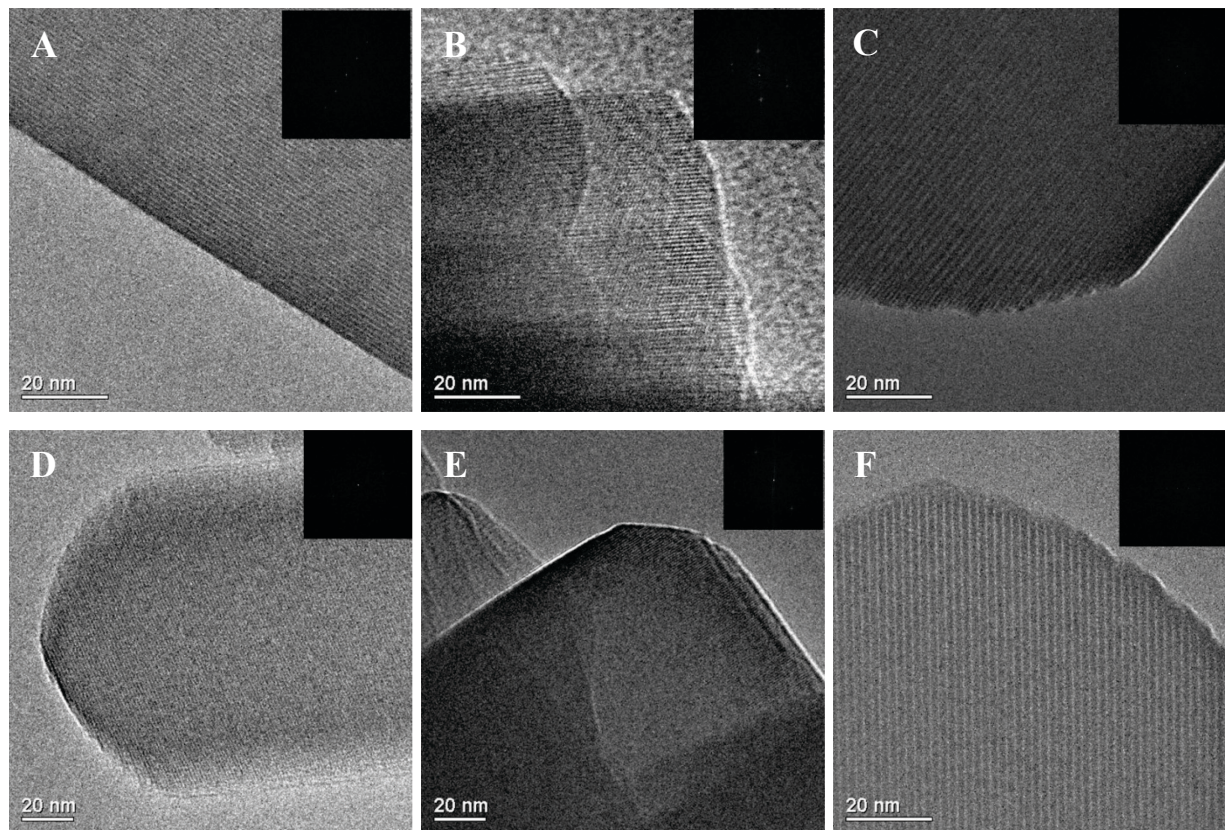
Fig. 38. HRTEM images of initial IWW: A) d-spacing = 1.20 nm, B) d-spacing = 0.95 nm, C) d-spacing = 2.02 nm; and final IPC-18: D) d-spacing = 1.20 nm, E) d-spacing = 0.90 nm, F) d-spacing = 1.92 nm

4.2. Degermanation as a Method of Synthesis of Hierarchical Materials

Ge-rich germanosilicate zeolites were perfectly applied in the ADOR approach as they can hydrolyse into lamellar materials. On the other hand, germanosilicates possessing the D4R units enriched with Si cannot be fully disassembled that means the 3D framework of parent material is partially preserved after an acidic treatment. This feature can be used for tuning of textural properties and design of hierarchical materials, as it is schematically presented in the Fig. 39. It should be noticed that topology of starting material is an important parameter influencing the direction of transformation (the ADOR *vs.* degermanation). For example, acidic treatment of both Ge-poor and Ge-rich samples of germanosilicate **UTL** always leads to the framework rearrangement (towards IPC-2/6/7 zeolites, see above, section 2.6.). For this investigation we chose germanosilicates **ITH**, **IWW** and **UOV**, where Ge atoms are located not only in the D4R units in frameworks, but also in the layers.
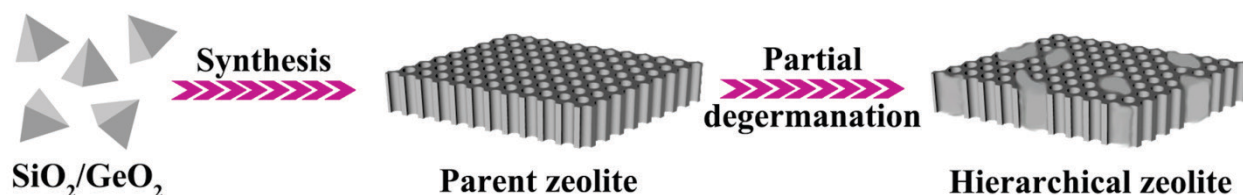
Fig. 39. Scheme of formation of hierarchical zeolite by degermanation method.

We studied the influence of the acidic treatment conditions such as pH (0.01 and 1M HNO_3, H_2O), duration (from 1 h to 96 h), and temperature (25, 80, 175 °C) on the textural properties of degermanated derivatives. Change of the treatment pH from 7 (H_2O) to 2 (0.01 M HNO_3) did not influence significantly formation of additional micro- and mesopores and the obtained samples were characterised by comparable V_{micro} and S_{BET} (Table 5). Following increase in the concentration of HNO_3 till 1 M resulted in an inhibition of Ge leaching for all **ITH** and **IWW** samples. This result agreed with suppression of hydrolysis for Ge-rich zeolites with the pH decrease discussed above (section 4.1.1.a). This inhibition is related to the decrease in solubility of germanium oxide species with increasing pH[162]. Ge-rich and Ge-poor **ITH** and **IWW** samples subjected to degermanation by 1 M HNO_3 were characterized by increased mesopore volumes (by 1.3-2.5 times, Table 5), but volumes of micropores were comparable with those of initial zeolite.

Table 5. Textural characteristics of **ITH** and **IWW** samples after the treatment at different pH

Sample	Chemical composition, Si/Ge ratio	S_{BET}, m²/g	V_{micro}, m³/g	V_{meso}, m³/g
ITH-2	3.4	313	0.125	0.050
ITH-2-0-80	15.1	339	0.142	0.086
ITH-2-0.01-80	15.9	344	0.147	0.070
ITH-2-1-80	13.7	358	0.106	0.090
ITH-6	5.8	321	0.138	0.130
ITH-6-0-80	19.7	418	0.166	0.311
ITH-6-0.01-80	18.0	404	0.161	0.299
ITH-6-1-80	16.6	412	0.15	0.324
IWW-2	3.3	279	0.109	0.137
IWW-2-0-80	14.3	449	0.162	0.181
IWW-2-0.01-80	15.0	424	0.156	0.183
IWW-2-1-80	13.7	371	0.113	0.194
IWW-4	4.2	425	0.161	0.284
IWW-4-0-80	23.4	579	0.199	0.374
IWW-4-0.01-80	22.2	560	0.194	0.372
IWW-4-1-80	16.9	486	0.161	0.376

*Samples are denoted as zeolite-a-b-c, where a – Si/Ge ratio in synthesised zeolite, b – concentration of HNO_3, c – temperature.

Study of kinetics of degermanation at pH = 2 and T = 80 °C showed that hydrolysis has optimal duration, 24 h. Formation of additional mesopores was observed with increasing treatment time from 1 h to 24 h. At the same time, the increase of micropore volume was found under the same conditions that can be explained by the increase of micropore size. Prolongation of the treatment was accompanied with the drop of these parameters (for samples obtained after 96 h), which can be explained by reinsertion of Si atoms into the framework.

Fig. 40 represents the isotherms of the initial and degermanated samples **IWW**, **ITH**, and **UOV** obtained after the treatment at 80 °C and 175 °C. All parent samples exhibited isotherms of type I corresponding to microporous solids, having the uptake in the range of p/p₀ = 0.8–1.0 related to interparticle adsorption in the voids between small crystals. Temperature of the treatment significantly influenced the adsorption characteristics of the final samples. Increase in the temperature to 175 °C resulted in the increase in mesopore volumes for Ge-rich samples, and drop of mesopore volumes for Ge-poor **IWW** and **ITH** samples. Extraction of Ge under hydrothermal conditions at 175 °C was accompanied with a dramatic decrease in micropore volumes for all samples, which can be explained by the deposition of leached species in zeolite

pores. In the case of **UOV**-1.5, treatment at 175 °C resulted in total destruction of the zeolite framework.

Thus, the ratio between micro-and mesopore volumes can be controlled by the choice of suitable chemical composition of starting materials and conditions of the treatment. Acidic treatment with 0.1M HNO_3 at 80 °C for 24 h was found to be the optimal conditions for fabrication of micro-mesopore porous materials. Under these conditions the rates of two competing processes, degermanation (leads to the development of intracrystalline porosity) and reinsertion (heals formed defects), are optimized.
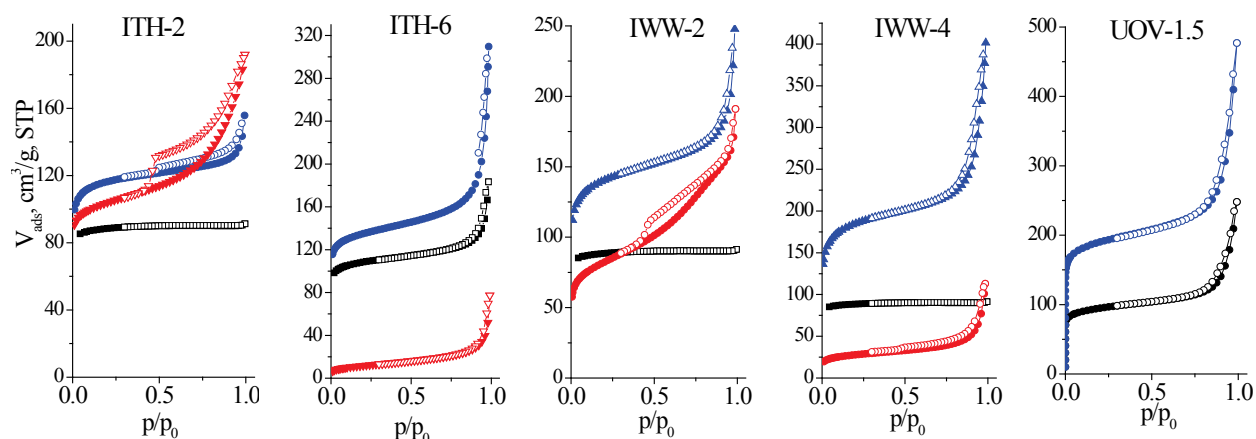
Fig. 40 Nitrogen adsorption (•) and desorption (○) isotherms of **ITH**-2, **ITH**-6, **IWW**-2, **IWW**-4 and **UOV**-1.5 germanosilicates. Initial zeolites (black), samples treated by 0.01 M HNO_3 for 24 h at 80 °C (blue) at 175 °C red).

4.3. Post-synthesis Alumination

4.3.1. Incorporation of Al Atoms into Zeolite Framework as a Method for Generation of Acid Centres and Extra-porosity

As it was previously discussed, the hydrolytic instability of Si–O and Ge–O bonds in germanosilicate zeolites can be used for their post-synthesis alumination. As acidic treatment of Ge-rich germanosilicate samples leads to their disassembly into lamellar materials, post-synthesis alumination with $Al(NO_3)_3$ in acidic medium (pH = 2) results in preservation of zeolites frameworks. It indicates that Al cations stabilize frameworks as they heal up the defects formed after hydrolysis of Ge–O bonds. Additionally, incorporation of Al atoms into

germanosilicates framework leads to generation of acid centres, which opens the opportunity of their application in catalysis.

Samples of zeolites **UOV** (Si/Ge = 0.5 and 1.5) and IPC-12 (Si/Ge = 12) were subjected to alumination with 1 M $Al(NO_3)_3$ at 80 °C and 175 °C for 24 h and 96 h. These treatment conditions were chosen in accordance with references [118-119]. Formation of acid centres was studied using FTIR spectroscopy. There were 2 absorption bands on the spectra of parent **UOV** samples in the region of hydroxyl groups (4000 – 3200 cm^{-1}) (Fig. 41, I, II). The band at 3745 cm^{-1} corresponds to silanol groups; the broad absorption shoulder at 3685 – 3630 cm^{-1} is characteristic for bridging hydroxyl to external Ge-OH groups.
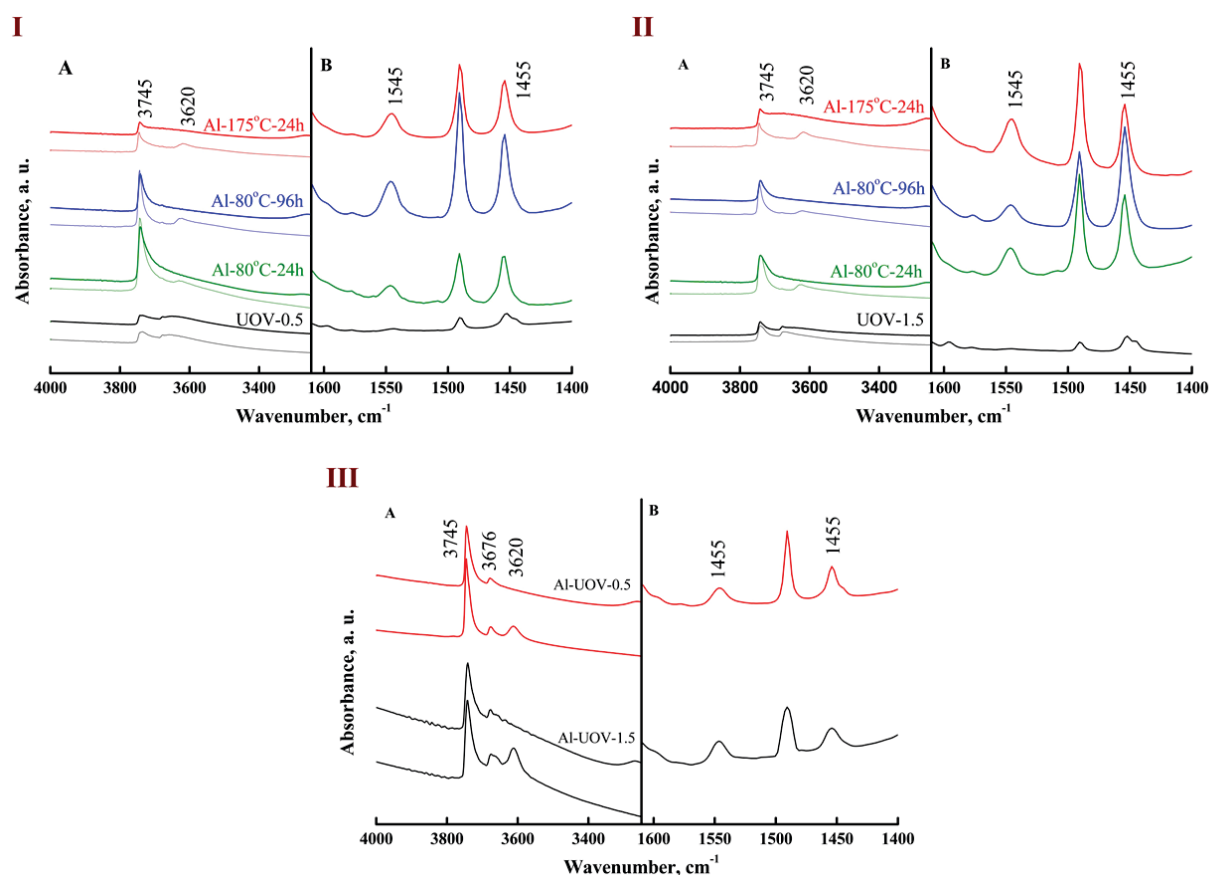
Fig. 41. IR spectra of I) **UOV**-0.5, II) **UOV**-1.5, III) IPC-12 zeolites: parent samples (black), **UOV**-n-Al-80-24h (green), **UOV**-n-80-96h (blue), **UOV**-n-175-24h (red). A) regions of hydroxyl vibrations; B) regions of pyridine vibrations. Bottom thin lines spectra show the spectra before and top bold lines – after adsorption of pyridine.

Degermanation/alumination of **UOV** samples resulted in increasing intensity of the band at 3745 cm^{-1} meaning formation of additional amount of silanol defects related to breaking of Si–O–Ge linkages. Furthermore, the spectra were characterized by the presence of absorption bands

at 3620 cm^{-1} attributed to bridging Si–(OH)–Al groups. Intensity of this band increased with rise of either temperature or time of the treatment (independently on chemical composition of initial **UOV**) indicating acceleration of incorporation of Al atoms into the framework.

The nature and concentration of acid centres in aluminated derivatives were studied by FTIR spectroscopy of adsorbed pyridine. Fig. 41 I, II B show the region of pyridine vibration. Adsorption of pyridine molecules leads to the appearance of several absorption bands in the region of 1400 – 1600 cm^{-1} on the spectra of Al-containing materials: the absorption band at 1455 cm^{-1}, characteristic for coordinatively bonded pyridine, at 1545 cm^{-1} for pyridinium ions adsorbed on Brønsted acid sites. Initial **UOV**-n zeolites possessed similar amounts of acid centres (~0.04 – 0.05 μmol/g). Post-synthetically aluminated **UOV** samples were characterized by increased concentration of both Brønsted (~0.10 – 0.25 μmol/g) and Lewis (~0.11 – 0.29 μmol/g) acid sites (Table 6). The increase in the alumination temperature accelerated Al incorporation, **UOV**-n (where n = 0.5 or 1.5) samples treated at 175 °C possessed higher total concentrations of acids sites (Table 6). On the other hand, samples treated at 80 °C for 96 h were characterized by increased amount of Lewis acid sites in comparison with those treated for 24 h.

Table 6. The concentrations of Lewis and Brønsted acid centers in **UOV** derivatives and IPC-12 obtained by the FTIR spectroscopy of adsorbed pyridine

Sample	c(Brønsted sites), μmol/g	c(Lewis sites), μmol/g	c(Total), μmol/g
UOV-1.5	0.01	0.03	0.04
UOV-1.5-Al-80-24h	0.17	0.17	0.34
UOV-1.5-Al-80-96h	0.12	0.29	0.41
UOV-1.5-Al-175-24h	0.25	0.17	0.42
Al-**UOV**-1.5	0.10	0.10	0.20
UOV-0.5	0.02	0.03	0.05
UOV-0.5-Al-80-24h	0.10	0.11	0.21
UOV-0.5-Al-80-96h	0.24	0.21	0.45
UOV-0.5-Al-175-24h	0.22	0.18	0.40
Al-**UOV**-0.5	0.11	0.12	0.23
IPC-12-Al	0.07	0.22	0.29

IPC-12 material treated with 1M Al(NO$_3$)$_3$ at 80 °C for 96 h also possessed Brønsted and Lewis centres. In comparison with the parent **UOV**-0.5 treated under the same conditions, concentration of Brønsted sites in IPC-12 was significantly lower: 0.07 vs. 0.24 for IPC-12 and **UOV**-0.5 respectively. It is related to removal of the D4Rs from the **UOV** framework and, thus,

decreasing amount of germanium, which potentially can be substituted with aluminium. While all substituted aluminium atoms are located in the layers in the case of IPC-12-Al, majority of Al atoms are probably located in the D4R units for **UOV**-0.5-Al zeolite.

Post-synthesis alumination of **UOV** samples led not only to creation of acid sites but also to formation of additional mesopores. For aluminated **UOV**-1.5 zeolites mesopore volumes and surface areas were significantly increased (Table 7). This development of porosity related to the high level of degermanation (similar to that discussed in the previous section) and non-equivalent replacement of leached framework Ge atoms with Al. Unexpectedly, **UOV**-0.5 samples after alumination showed adsorption characteristics similar or lower than the parent zeolite. It can be related with deposition of Si or Ge compounds in pores after the treatment.

Table 7. Textural properties of **UOV** samples subjected to direct and post-synthesis alumination

Sample	V_{micro}, cm^3/g	V_{meso}, cm^3/g	S_{BET}, m^2/g
UOV-1.5	0.15	0.12	330
UOV-1.5-Al-80-96h	0.13	0.19	380
UOV-1.5-Al-175-24h	0.12	0.21	420
UOV-0.5	0.11	0.21	310
UOV-0.5-Al-80-96h	0.10	0.20	340
UOV-0.5-Al-175-24h	0.07	0.17	200

Thus, the c (Brønsted sites) / c (Lewis sites) ratio and textural properties of post-synthetically aluminated derivatives can be tuned by appropriate choice of chemical composition of parent **UOV** germanosilicate and post-synthesis treatment conditions.

4.3.2. Post-synthesis *vs.* Direct Alumination. NMR Study

The method of post-synthesis substitution of Ge with Al atoms was presented above. Alternatively, aluminium atoms may be incorporated in zeolite framework via direct syntheses. According to the Table 8, showing Si/Al ratios in directly and post-synthetically treated germanosilicates, the concentration of aluminium atoms in post-synthetically treated samples depended on the zeolite topology and reached the value of 7 % (or Si/Al = 13). In contrast, the amounts of aluminium, which can be incorporated in direct syntheses of aluminogermanosilicate zeolites, were limited to 1 %, which is the main disadvantage of the direct synthesis. Any

attempts of increasing Al content in starting reaction gels resulted either in formation of undesired phase: for example, **EUO** phase in the synthesis of Al-**ITH;** or presence of Al_2O_3 in final sample. ^{27}Al MAS NMR (Fig. 42) demonstrates that the increase of aluminium concentration in reaction gels from 1 to 2 % for Al-**IWW** syntheses resulted in the formation of high amount of extra-framework pentacoordinated Al species (signal at 14 ppm), which indicates saturation of the zeolite framework with Al.

The difference in Al content in samples obtained by two methods influenced the acidity of materials. As it presented in the Table 7, samples of **UOV** subjected to post-synthesis substitution were characterized by ~2 times higher total amount of Brønsted and Lewis acid sites.

Table 8. Si/Al ratios in **IWW**, **UTL**, CIT-13, **UOV** and **ITH** germanosilicates subjected to direct or post-synthesis Al substitution

Sample	Way of synthesis	Si/Al ratio
2%Al-**IWW**-7-direct	Direct, 2% Al	34
1%Al-**IWW**-7-direct	Direct, 1% Al	40
IWW-7-Al-post	Post-synthesis, 1M Al(NO$_3$)$_3$, 96 h, 80°C	25
Al-**UOV**-0.5-direct	Direct, 1% Al	43
UOV-0.5-Al-post	Post-synthesis, 1M Al(NO$_3$)$_3$, 96 h, 80°C	13
Al-**UTL**-7-direct	Direct, 1% Al	105
UTL-7-Al-post	Post-synthesis, 1M Al(NO$_3$)$_3$, 96 h, 80°C	56
Al-CIT-13-4-direct	Direct, 1% Al	83
CIT-13-4-Al-post	Post-synthesis, 1M Al(NO$_3$)$_3$, 96 h, 80°C	34
Al-**ITH**-10-direct	Direct, 1% Al	59
ITH-10-Al-direct	Post-synthesis, 1M Al(NO$_3$)$_3$, 96 h, 80°C	13

^{27}Al MAS NMR analysis (Fig. 42) also showed differences in aluminium coordination in directly synthesised and post-synthetically obtained Al-containing zeolites. In the case of **IWW**, **UOV**, **UTL** and CIT-13 zeolites subjected to treatment with 1M Al(NO$_3$)$_3$ solution, dominated signals were those at 55 ppm attributed to Al (IV) in tetrahedral coordination indicating isomorphous incorporation of Al atoms into zeolites frameworks. In contrast, samples obtained by direct syntheses from Al containing gels were characterised by dominant signals corresponded to extra-framework Al species. In the case of **IWW** (1%Al-**IWW**-7-direct) and **UOV**, there were Al atoms in octahedral coordination (peak at 0.8 ppm), for **UTL** and CIT-13 – signals at 14 ppm characteristic of pentahedral coordinated aluminium. Thus, post-synthesis

incorporation of aluminium was shown to be more appropriate method for Al incorporation, as it resulted in introduction of higher amount of framework aluminium.
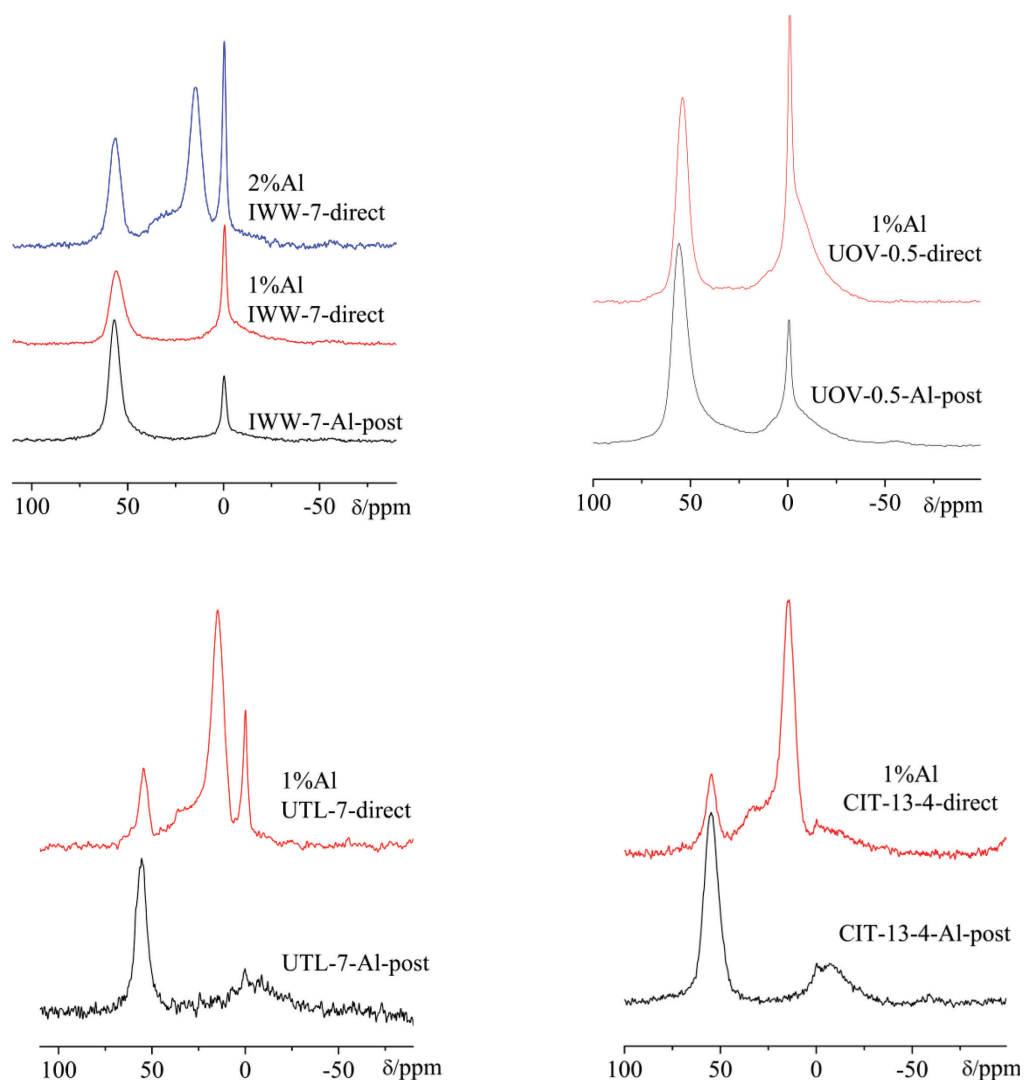
Fig. 42. ^{27}Al MAS NMR spectra of aluminium containing **IWW**-7, **UOV**-0.5, **UTL**-7 and CIT-13-4 zeolites: obtained by adding of Al source in reaction mixtures (direct, black) and post-synthesis alumination at 80°C for 96h (post, red).

4.3.3. Mechanism of Incorporation of Aluminium Atoms in UOV Zeolite Framework

The mechanism of alumination was studied using the treatment of germanosilicate **UOV**-0.5 at 80 °C as a model process. We followed kinetics of this process by XRD, ^{27}Al and ^{29}Si MAS NMR techniques.

The XRD patterns presented in the Fig. 44 show that after 5 minutes of the treatment the interlayer (100) signal has been already right-shifted. Moreover, the patterns of samples subjected to alumination for 5 min, 30 min and 3 h had the additional reflections at 16.56° and 24.38° 2θ, which can be related to the lamellar material IPC-12P[163] discussed previously. With increasing the treatment time to 24 h, these two lines disappeared, while (100) signal was gradually left-shifted up to the interlayer peak position of initial **UOV**. That indicates the reassembly of **UOV** framework. The XRD pattern of **UOV**-0.5 aluminated for 24 h corresponded to pure **UOV** phase. We assume that the first step of alumination consists of acidic hydrolysis of the bonds in the D4R units and extraction of Ge atoms from the framework. Short times of alumination are not suitable for deep incorporation of Al atoms in the framework. In contrast to small proton cations (quickly penetrating into the zeolite pores and catalysing process of hydrolysis), bulky hydrated aluminium cations undergo relatively high diffusion constraints. On the second step of alumination, aluminium cations go into the pores and start to heal up the defects. Schematically this process presented in the Fig. 44, C.
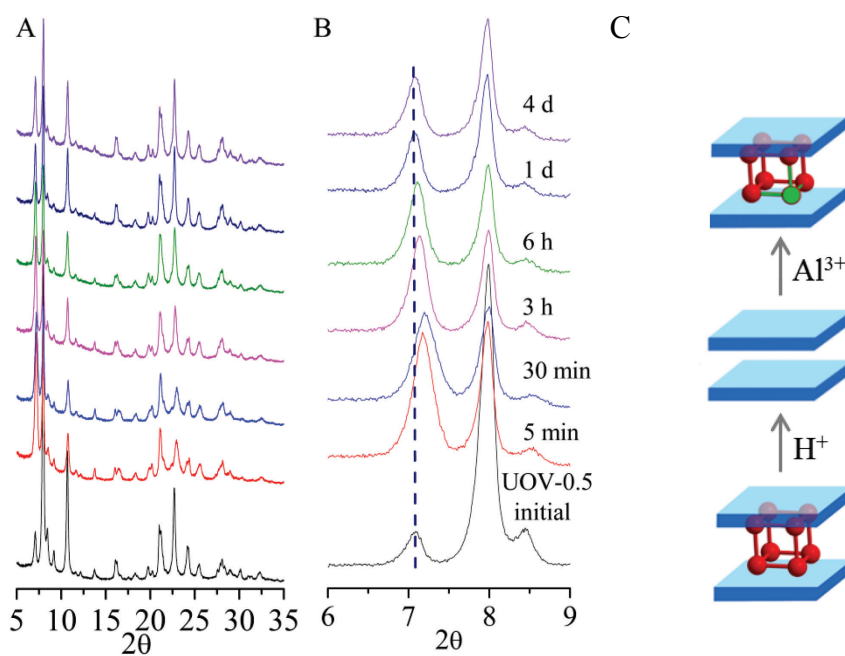
Fig. 44: Kinetic investigation of the alumination with 1M $Al(NO_3)_3$ at 80°C: A) XRD patterns of initial and treated **UOV**-0.5, B) respective small angle region (black dotted line corresponds to the positions of (100) reflection in parent **UOV** sample). C) Schematic representation of the process of post-synthesis alumination.

Chemical analysis of samples showed that amount of Al increased from 2.08 to 2.97 % for samples treated for 5 min and 96 h respectively. Despite similar concentrations of aluminium,

according to the results of ^{27}Al MAS NMR these 2 samples differed in Al coordination. As it is seen on the Fig. 45, A, there are 2 signals on all spectra: at 55 ppm attributed to Al (IV) in tetrahedral coordination; and at 0.8 ppm related to octahedral Al (VI) species. The fraction of tetrahedral aluminium species is significantly lower for calcined **UOV**-0.5 treated for 5 min. Moreover, its spectrum was characterized by the presence of the peak attributed to aluminium in pentahedral coordination (at 14 ppm). That means, for **UOV** sample treated for the short time, most of aluminium was extra-framework. In contrast, most of aluminium atoms were incorporated into zeolite framework after 96 h, as the dominant signal on the spectrum was the one corresponding to Al (IV).

Evolution of Si–O–X (X = H or Si) groups was studied by ^{29}Si MAS NMR presented in the Fig. 45 B. Prolongation of the treatment time from 5 min to 96 h resulted in the decrease in the intensity of the signal at -100 ppm corresponded to Q^3 silicon atoms (deficient silanol groups). It indicates the silanol defects were hilled up with time. Similar effect was observed after calcination of samples: ^{29}Si MAS NMR spectra of calcined **UOV** samples were characterized by dominating signal at -110 ppm attributed to Q^4 silicon atoms, while intensity of Q^3 Si atoms signal was negligible.

The results of MAS NMR agree with the results of the XRD and confirm the proposed multi-stage mechanism of aluminium incorporation.
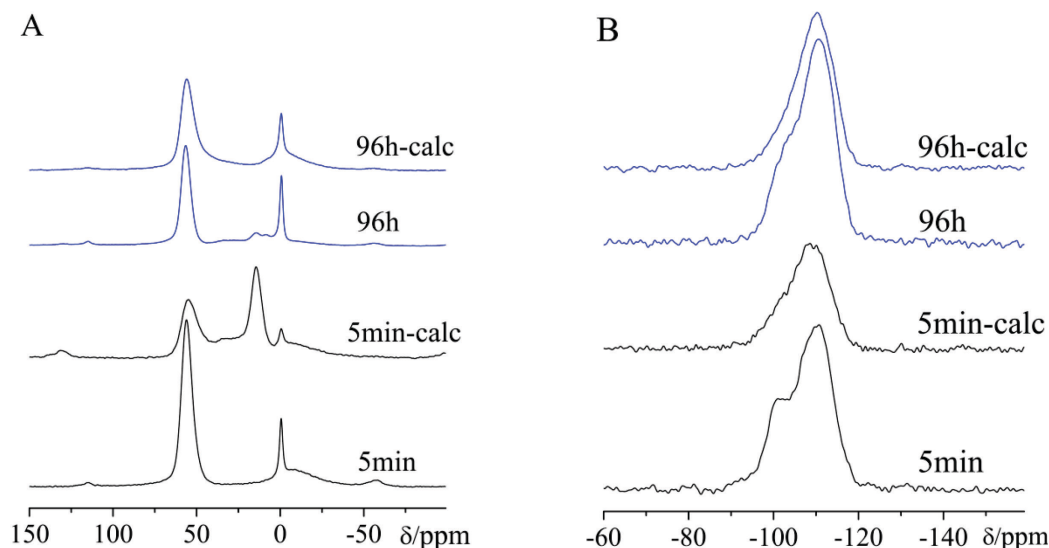
Fig. 45 ^{27}Al MAS NMR (left) and ^{29}Si MAS NMR (right) spectra of **UOV**-0.5 aluminated at 80°C for 5min and 96h before and after calcinations.

5. Conclusions

This thesis was devoted to control the structure and textural properties of zeolites using different ways of post-synthesis treatment: the ADOR (Assembly – Disassembly – Organization – Reassembly) transformation and post-synthesis modification resulted in degermanation and alumination. It was shown that initial zeolites should possess particular structural features depending on the type of the process applied. In order to investigate suitability of germanosilicates **UOV**, **IWR**, CIT-13, and **IWW** for the ADOR approach, respective materials containing Ge-rich D4R units in the frameworks were obtained. Application of mentioned zeolites in the ADOR resulted in obtaining of 4 new zeolites: IPC-12, IPC-13, IPC-17 and IPC-18.

Germanosilicate **UOV** synthesised from reaction mixture with Si/Ge = 0.5 was controllably disassembled by 0.1 M HCl into a lamellar material IPC-12P. Following calcination of obtained layered precursor resulted in formation of new zeolite IPC-12. This zeolite is composed of the same layers as parent zeolite, but layers are connected by O-bridges in contrast to **UOV** possessing connectivity through the D4R units. Variation of treatment conditions opened a possibility of direct **UOV**-to-IPC-12 rearrangement under highly acidic conditions (12 M HCl). The pore system of zeolite IPC-12 consists of two independent 1-dimensional channels (12- and 8-ring pores).

Treatment of germanosilicate CIT-13 (Si/Ge = 4) in the ADOR process resulted in formation of IPC-13 zeolite isostructural to IPC-16 material independently synthesised starting from zeolite SAZ-1. The formation of isostructural zeolites is related to similarity of the layer's structure in SAZ-1 and CIT-13. Framework rearrangement resulted in the change of pore system from 14 × 10 channels for CIT-13 to 12 × 10 rings for IPC-13, which is connected with transformation of the D4Rs to the S4R units.

Another zeolite possessing layers connected by the S4R units was obtained based on the consecutive Disassembly – Reassembly of germanosilicate **IWR**. In order to synthesise parent **IWR** zeolite with stable layers enriched with Si atoms, optimization of the Assembly step conditions was performed. The seeding technique was shown to be appropriate for that purpose. Acidic treatment of obtained **IWR**-s (Si/Ge = 2) with 12 M HCl followed by calcination resulted in formation of IPC-17 zeolite.

Thus, possibility of application of zeolites with layers containing pores in the ADOR approach was firstly demonstrated. As this method was limited only by germanosilicate **UTL** before, expansion of this technique on germanosilicates **IWR**, **UOV** and CIT-13 from one side increased the number of known zeolite structures ("IPC-family" members) and, on the other hand, confirmed the versatility of the ADOR as a method for synthesis of novel zeolites. However, the ADOR was found to be versatile method, because its pathway significantly depends on the framework and intrinsic properties of parent material. Influence of those factors was especially pronounced in the case of the treatment with 12 M HCl. While for **UTL**, CIT-13 and **IWR** germanosilicates it resulted in the rearrangement of D4Rs into S4Rs ("inverse sigma transformation"), treatment of **UOV** resulted in complete removal of D4R units.

This thesis was devoted not only to utilization of new germanosilicates in the ADOR approach but also to elaboration of this technique itself. As a result, the possibility of realization of the ADOR method under solvent-free conditions was demonstrated for the first time. It was performed by the treatment of zeolite placed on PTFE filter with hydrochloric acid vapour, i.e. without direct contact of zeolite with the respective solution. For **IWW** (Si/Ge = 2) it resulted in the formation of a new zeolite, IPC-18, the structure of which can be described as the layers of the same structure as in the parent **IWW** but connected by S4R units in contrast to D4R units in **IWW**.

As Ge-rich germanosilicates were demonstrated to be "ADORable" materials, hierarchical materials maintaining initial zeolite topology were designed from Si-rich samples. Acidic treatment of germanosilicates **ITH**, **IWW** and **UOV** resulted in extraction of Ge atoms from the framework, which was led to formation additional micro- and meso-pores. It was found that the micro-to mesopore volumes ratio (V_{micro}/V_{meso}) in final materials can be controlled by appropriate choice of zeolite chemical composition and treatment conditions (pH, temperature and duration). Treatment with 0.1M HNO_3 at 80 °C for 24 h was shown to be optimal conditions for **ITH** and **IWW** zeolites.

Post-synthesis alumination was another way of the treatment for modification of acid properties of studied zeolites. It was carried out for both Ge-poor and Ge-rich **UOV** samples. Al atoms were shown to stabilize zeolite framework and their incorporation resulted in formation of both Brønsted and Lewis acid centers. Alumination process also was accompanied with

formation of additional mesopores and development of the surface area. Altogether, it makes obtained materials perspective for investigation in catalysis.

Synthesis of zeolites **UOV** and CIT-13 in the form of aluminogermanosilicates (Si-Ge-Al) was firstly performed in this work. Method of post-synthesis alumination was shown to be more appropriate for incorporation of Al atoms in comparison with direct synthesis of zeolite samples from aluminium containing reaction mixtures. For **UTL**, **UOV**, **IWW**, **ITH** and CIT-13 germanosilicates the use of post-synthesis approach allowed incorporating of higher amount of Al atoms (up to 7%), while for direct synthesis maximum content of Al was limited only to 1%. Moreover, ^{27}Al MAS NMR study of post-synthetically obtained samples showed the presence of dominating Al (IV) signal, while directly obtained samples were characterized by dominating fraction of extra-framework (Al (V) and Al (VI)) species.

Special attention in this work was paid to the investigation of mechanism of post-synthesis substitution of Ge atoms by Al. The study was based on the treatment of germanosilicate **UOV** (Si/Ge = 0.5) with 1 M Al(NO$_3$)$_3$ at 80°C. Kinetic study made by XRD, ^{27}Al and ^{29}Si MAS NMR and ICP-OES analyses indicated a multi-stage nature of this process. On the short times, acidic hydrolysis of Ge–O–Si bonds accompanied with partial disassembly of the framework and leaching of Ge atoms was observed. In the following step, Al atoms penetrated into pores heal the silanol defects in the framework formed after hydrolysis of Ge-domains.

Fig. 46 demonstrates a summary of germanosilicate zeolites investigated in this work and methods of post-synthesis modification applied for them.
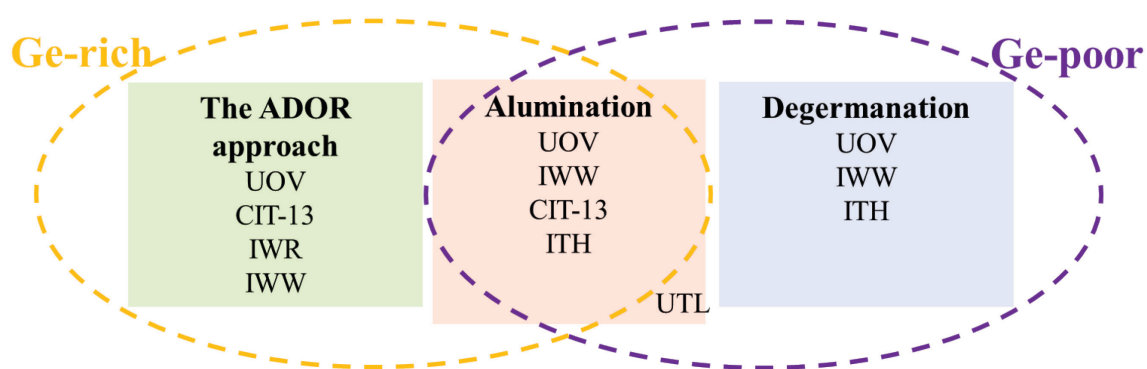

Fig. 45. Germanosilicate zeolites and respective methods of post-synthesis treatment, which were applied for them.

6. References

1.   Čejka, J.; van Bekkum, H., Zeolites and Ordered Mesoporous Materials: Progress and Prospects. *Elsevier Science* **2005**.

2.   Bellussi, G.; Carati, A.; Rizzo, C.; Millini, R., New trends in the synthesis of crystalline microporous materials. *Catalysis Science & Technology* **2013**, *3* (4), 833-857.

3.   Cundy, C. S.; Cox, P. A., The hydrothermal synthesis of zeolites: History and development from the earliest days to the present time. *Chemical Reviews* **2003**, *103* (3), 663-701.

4.   Čejka, J.; Wichterlová, B., Acid-catalyzed synthesis of mono- and dialkyl benzenes over zeolites: Active sites, zeolite topology, and reaction mechanisms. *Catalysis Reviews-Science and Engineering* **2002**, *44* (3), 375-421.

5.   Fechete, I.; Wang, Y.; Vedrine, J. C., The past, present and future of heterogeneous catalysis. *Catalysis Today* **2012**, *189* (1), 2-27.

6.   Přech, J., Catalytic performance of advanced titanosilicate selective oxidation catalysts – a review. *Catalysis Reviews. Science and Engineering* **2018**, *60* (1), 71-131.

7.   Goodwin, J. G.; Natesakhawat, S.; Nikolopoulos, A. A.; Kim, S. Y., Etherification on zeolites: MTBE synthesis. *Catalysis Reviews-Science and Engineering* **2002**, *44* (2), 287-320.

8.   Li, K. H.; Valla, J.; Garcia-Martinez, J., Realizing the Commercial Potential of Hierarchical Zeolites: New Opportunities in Catalytic Cracking. *Chemcatchem* **2014**, *6* (1), 46-66.

9.   Moliner, M., State of the art of Lewis acid-containing zeolites: lessons from fine chemistry to new biomass transformation processes. *Dalton Transactions* **2014**, *43* (11), 4197-4208.

10.   Mofarahi, M.; Gholipour, F., Gas adsorption separation of CO_2/CH_4 system using zeolite 5A. *Microporous and Mesoporous Materials* **2014**, *200*, 1-10.

11.   Kosinov, N.; Auffret, C.; Borghuis, G. J.; Sripathi, V. G. P.; Hensen, E. J. M., Influence of the Si/Al ratio on the separation properties of SSZ-13 zeolite membranes. *Journal of Membrane Science* **2015**, *484*, 140-145.

12.   Cheung, O.; Hedin, N., Zeolites and related sorbents with narrow pores for CO2 separation from flue gas. *Rsc Advances* **2014**, *4* (28), 14480-14494.

13.   Saha, D.; Bao, Z. B.; Jia, F.; Deng, S. G., Adsorption of CO_2, CH_4, N_2O, and N-2 on MOF-5, MOF-177, and Zeolite 5A. *Environmental Science & Technology* **2010**, *44* (5), 1820-1826.

14.   Gascon, J.; Kapteijn, F.; Zornoza, B.; Sebastian, V.; Casado, C.; Coronas, J., Practical Approach to Zeolitic Membranes and Coatings: State of the Art, Opportunities, Barriers, and Future Perspectives. *Chemistry of Materials* **2012**, *24* (15), 2829-2844.

15.   Gomes, G. J.; Zalazar, M. F.; Lindino, C. A.; Scremin, F. R.; Bittencourt, P. R. S.; Costa, M. B.; Peruchena, N. M., Adsorption of acetic acid and methanol on H-Beta zeolite: An experimental and theoretical study. *Microporous and Mesoporous Materials* **2017**, *252*, 17-28.

16.   Thang, H. V.; Grajciar, L.; Nachtigall, P.; Bludsky, O.; Arean, C. O.; Frydova, E.; Bulanek, R., Adsorption of CO2 in FAU zeolites: Effect of zeolite composition. *Catalysis Today* **2014**, *227*, 50-56.

17.   Khabzina, Y.; Laroche, C.; Perez-Pellitero, J.; Farrusseng, D., Xylene separation on a diverse library of exchanged faujasite zeolites. *Microporous and Mesoporous Materials* **2017**, *247*, 52-59.

18.   Davis, M. E., Ordered porous materials for emerging applications. *Nature* **2002,** *417* (6891), 813-821.

19.   Al-Jubouri, S. M.; Holmes, S. M., Hierarchically porous zeolite X composites for manganese ion-exchange and solidification: Equilibrium isotherms, kinetic and thermodynamic studies. *Chemical Engineering Journal* **2017,** *308*, 476-491.

20.   Kim, S. J.; Jones, C. W.; Nair, S.; Liu, Y.; Moore, J. S.; Dixit, R. S.; Pendergast, J. G.; Sarsani, S., Ion exchange of zeolite membranes by a vacuum 'flow-through' technique. *Microporous and Mesoporous Materials* **2015,** *203*, 170-177.

21.   Zaarour, M.; Dong, B.; Naydenova, I.; Retoux, R.; Mintova, S., Progress in zeolite synthesis promotes advanced applications. *Microporous and Mesoporous Materials* **2014,** *189*, 11-21.

22.   Sanchez, M. J.; Mauricio, J. E.; Paredes, A. R.; Gamero, P.; Cortes, D., Antimicrobial properties of ZSM-5 type zeolite functionalized with silver. *Materials Letters* **2017,** *191*, 65-68.

23.   Guntner, A. T.; Abegg, S.; Wegner, K.; Pratsinis, S. E., Zeolite membranes for highly selective formaldehyde sensors. *Sensors and Actuators B-Chemical* **2018,** *257*, 916-923.

24.   Snelders, D. J. M.; Mackenzie, F. O. V.; Boersma, A.; Peeters, R. H. M., Zeolites as coating materials for Fiber Bragg Grating chemical sensors for extreme conditions. *Sensors and Actuators B-Chemical* **2016,** *235*, 698-706.

25.   Denoual, M.; Robbes, D.; Inoue, S.; Mita, Y.; Grand, J.; Awala, H.; Mintova, S., Thermal resonant zeolite-based gas sensor. *Sensors and Actuators B-Chemical* **2017,** *245*, 179-182.

26.   Baerlocher, C.; McCusker, L. B., http://www.iza-structure.org/databases/.

27.   Barrer, R. M., Syntheses and reactions of mordenite. *Journal of the Chemical Society* **1948,** (DEC), 2158-&.

28.   Barrer, R. M.; Riley, D. W., Sorptive and molecular-sieve properties of a new zeolitic mineral. *Journal of the Chemical Society* **1948,** (FEB), 133-143.

29.   Szostak, R., Molecular Sieves. Principles of Synthesis and Identification. 2nd edition. *Blackie Academic and Professional, London* **1998**, 359 pages.

30.   Čejka, J.; Morris, R. E.; Nachtigall, P., Zeolites in Catalysis: Properties and Applications. *RSC Catalysis Series No. 28* **2017**.

31.   Introduction to Zeolite Science and Practice. In *Introduction to Zeolite Science and Practice*, Jacobs, P. A.; Flanigen, E. M.; Jansen, J. C.; van Bekkum, H., Eds. 2001; Vol. 137, pp 1-1078.

32.   Dorset, D. L.; Kennedy, G. J.; Strohmaier, K. G.; Diaz-Cabanas, M. J.; Rey, F.; Corma, A., P-derived organic cations as structure-directing agents: Synthesis of a high-silica zeolite (ITQ-27) with a two-dimensional 12-ring channel system. *Journal of the American Chemical Society* **2006,** *128* (27), 8862-8867.

33.   Eliášová, P.; Opanasenko, M.; Wheatley, P. S.; Shamzhy, M.; Mazur, M.; Nachtigall, P.; Roth, W. J.; Morris, R. l. E.; Čejka, J., The ADOR mechanism for the synthesis of new zeolites. *Chemical Society Reviews* **2015,** *44*, 7177-7206.

34.   Lorgouilloux, Y.; Dodin, M.; Mugnaioli, E.; Marichal, C.; Caullet, P.; Bats, N.; Kolb, U.; Paillaud, J.-L., IM-17: a new zeolitic material, synthesis and structure elucidation from electron diffraction ADT data and Rietveld analysis. *Rsc Advances* **2014,** *4* (37), 19440-19449.

35.   Corma, A.; Navarro, M. T.; Rey, F.; Rius, J.; Valencia, S., Pure polymorph C of zeolite beta synthesized by using framework isomorphous substitution as a structure-directing mechanism. *Angewandte Chemie-International Edition* **2001,** *40* (12), 2277-2280.

36.   Jiang, J.; Jorda, J. L.; Diaz-Cabanas, M. J.; Yu, J.; Corma, A., The Synthesis of an Extra-Large-Pore Zeolite with Double Three-Ring Building Units and a Low Framework Density. *Angewandte Chemie-International Edition* **2010,** *49* (29), 4986-4988.

37.   Sastre, G.; Vidal-Moya, J. A.; Blasco, T.; Rius, J.; Jordá, J. L.; Navarro, M. T.; Rey, F.; Corma, A., Preferential Location of Ge Atoms in Polymorph C of Beta Zeolite (ITQ-17) and Their Structure-Directing Effect: A Computational, XRD, and NMR Spectroscopic Study. *Angewandte Chemie International Edition* **2002,** *41* (24), 4722-4726.

38.   Jiang, J. X.; Yu, J. H.; Corma, A., Extra-Large-Pore Zeolites: Bridging the Gap between Micro and Mesoporous Structures. *Angewandte Chemie-International Edition* **2010,** *49* (18), 3120-3145.

39.   Sels, B.; Kustov, L., Zeolites and Zeolite-like Materials. *Elsevier Science* **2016**, 474.

40.   Čejka, J.; Corma, A.; Zones, S., Zeolites and Catalysis: Synthesis, Reactions and Applications. *John Wiley & Sons* **2010**, 918.

41.   Roth, W. J.; Nachtigall, P.; Morris, R. E.; Čejka, J., Two-Dimensional Zeolites: Current Status and Perspectives. *Chemical Reviews* **2014,** *114* (9), 4807-4837.

42.   Roth, W. J.; Čejka, J., Two-dimensional zeolites: dream or reality? *Catalysis Science & Technology* **2011,** *1* (1), 43-53.

43.   Rybicki, M.; Sauer, J., Acidity of two-dimensional zeolites. *Physical Chemistry Chemical Physics* **2015,** *17* (41), 27873-27882.

44.   Sauer, J., Bronsted activity of two-dimensional zeolites compared to bulk materials. *Faraday Discussions* **2016,** *188*, 227-234.

45.   Thang, H. V.; Rubes, M.; Bludsky, O.; Nachtigall, P., Computational Investigation of the Lewis Acidity in Three-Dimensional and Corresponding Two-Dimensional Zeolites: UTL vs IPC-1P. *Journal of Physical Chemistry A* **2014,** *118* (35), 7526-7534.

46.   Ho, T. V.; Nachtigall, P.; Grajciar, L., The Lewis acidity of three- and two-dimensional zeolites: The effect of framework topology. *Catalysis Today* **2018,** *304*, 12-21.

47.   Roth, W. J.; Chlubná, P.; Kubů, M.; Vitvarová, D., Swelling of MCM-56 and MCM-22P with a new medium - surfactant-tetramethylammonium hydroxide mixtures. *Catalysis Today* **2013,** *204*, 8-14.

48.   Chlubná , P.; Roth, W. J.; Zukal, A.; Kubů, M.; Pavlatová, J., Pillared MWW zeolites MCM-36 prepared by swelling MCM-22P in concentrated surfactant solutions. *Catalysis Today* **2012,** *179* (1), 35-42.

49.   Roth, W. J.; Čejka, J.; Millini, R.; Montanari, E.; Gil, B.; Kubů, M., Swelling and Interlayer Chemistry of Layered MWW Zeolites MCM-22 and MCM-56 with High Al Content. *Chemistry of Materials* **2015,** *27* (13), 4620-4629.

50.   Corma, A.; Diaz, U.; Garcia, T.; Sastre, G.; Velty, A., Multifunctional Hybrid Organic-Inorganic Catalytic Materials with a Hierarchical System of Well-Defined Micro- and Mesopores. *Journal of the American Chemical Society* **2010,** *132* (42), 15011-15021.

51.   Roth, W. J.; Gil, B.; Marszalek, B., Comprehensive system integrating 3D and 2D zeolite structures with recent new types of layered geometries. *Catalysis Today* **2014,** *227*, 9-14.

52.   Leonowicz, M. E.; Lawton, J. A.; Lawton, S. L.; Rubin, M. K., MCM-22 - a molecular-sieve with 2 independent multidimensional channel systems. *Science* **1994,** *264* (5167), 1910-1913.

53.   Lawton, S. L.; Fung, A. S.; Kennedy, G. J.; Alemany, L. B.; Chang, C. D.; Hatzikos, G. H.; Lissy, D. N.; Rubin, M. K.; Timken, H. K. C.; Steuernagel, S.; Woessner, D. E., Zeolite

MCM-49: A three-dimensional MCM-22 analogue synthesized by in situ crystallization. *Journal of Physical Chemistry* **1996,** *100* (9), 3788-3798.

54.   Zanardi, S.; Alberti, A.; Cruciani, G.; Corma, A.; Fornes, V.; Brunelli, M., Crystal structure determination of zeolite Nu-6(2) and its layered precursor Nu-6(1). *Angewandte Chemie-International Edition* **2004,** *43* (37), 4933-4937.

55.   Schreyeck, L.; Caullet, P.; Mougenel, J. C.; Guth, J. L.; Marler, B., PREFER: A new layered (alumino) silicate precursor of FER-type zeolite. *Microporous Materials* **1996,** *6* (5-6), 259-271.

56.   Oberhagemann, U.; Bayat, P.; Marler, B.; Gies, H.; Rius, J., A layer silicate: Synthesis and structure of the zeolite precursor RUB-15 - N(CH3)(4) (8) Si24O52(OH)4( )center dot 20H(2)O. *Angewandte Chemie-International Edition in English* **1996,** *35* (23-24), 2869-2872.

57.   Marler, B.; Camblor, M. A.; Gies, H., The disordered structure of silica zeolite EU-20b, obtained by topotactic condensation of the piperazinium containing layer silicate EU-19. *Microporous and Mesoporous Materials* **2006,** *90* (1-3), 87-101.

58.   Marler, B.; Stroter, N.; Gies, H., The structure of the new pure silica zeolite RUB-24, Si32O64, obtained by topotactic condensation of the intercalated layer silicate RUB-18. *Microporous and Mesoporous Materials* **2005,** *83* (1-3), 201-211.

59.   Wang, Y. X.; Gies, H.; Marler, B.; Muller, U., Synthesis and crystal structure of zeolite RUB-41 obtained as calcination product of a layered precursor: a systematic approach to a new synthesis route. *Chemistry of Materials* **2005,** *17* (1), 43-49.

60.   Wheatley, P. S.; Morris, R. E., Calcination of a layered aluminofluorophosphate precursor to form the zeolitic AFO framework. *Journal of Materials Chemistry* **2006,** *16* (11), 1035-1037.

61.   Ikeda, T.; Akiyama, Y.; Oumi, Y.; Kawai, A.; Mizukami, F., The topotactic conversion of a novel layered silicate into a new framework zeolite. *Angewandte Chemie-International Edition* **2004,** *43* (37), 4892-4896.

62.   Dorset, D. L.; Kennedy, G. J., Crystal structure of MCM-65: An alternative linkage of ferrierite layers. *Journal of Physical Chemistry B* **2004,** *108* (39), 15216-15222.

63.   Asakura, Y.; Takayama, R.; Shibue, T.; Kuroda, K., Topotactic Conversion of beta-Helix-Layered Silicate into AST-Type Zeolite through Successive Interlayer Modifications. *Chemistry-a European Journal* **2014,** *20* (7), 1893-1900.

64.   Park, W.; Yu, D.; Na, K.; Jelfs, K. E.; Slater, B.; Sakamoto, Y.; Ryoo, R., Hierarchically Structure-Directing Effect of Multi-Ammonium Surfactants for the Generation of MFI Zeolite Nanosheets. *Chemistry of Materials* **2011,** *23* (23), 5131-5137.

65.   Jung, J.; Jo, C.; Cho, K.; Ryoo, R., Zeolite nanosheet of a single-pore thickness generated by a zeolite-structure-directing surfactant. *Journal of Materials Chemistry* **2012,** *22* (11), 4637-4640.

66.   Choi, M.; Na, K.; Kim, J.; Sakamoto, Y.; Terasaki, O.; Ryoo, R., Stable single-unit-cell nanosheets of zeolite MFI as active and long-lived catalysts. *Nature* **2009,** *461* (7261), 246-U120.

67.   Shamzhy, M.; Mazur, M.; Opanasenko, M.; Roth, W. J.; Čejka, J., Swelling and pillaring of the layered precursor IPC-1P: tiny details determine everything. *Dalton Transactions* **2014,** *43* (27), 10548-10557.

68.   Roth, W. J.; Nachtigall, P.; Morris, R. E.; Wheatley, P. S.; Seymour, V. R.; Ashbrook, S. E.; Chlubná, P.; Grajciar, L.; Položij, M.; Zukal, A.; Shvets, O.; Čejka, J., A family of zeolites

with controlled pore size prepared using a top-down method. *Nature Chemistry* **2013,** *5* (7), 628-633.

69.   Shamzhy, M.; Opanasenko, M.; Tian, Y. Y.; Konysheya, K.; Shvets, O.; Morris, R. E.; Čejka, J., Germanosilicate Precursors of ADORable Zeolites Obtained by Disassembly of ITH, ITR, and IWR Zeolites. *Chemistry of Materials* **2014,** *26* (19), 5789-5798.

70.   Kasian, N.; Tuel, A.; Verheyen, E.; Kirschhock, C. E. A.; Taulelle, F.; Martens, J. A., NMR Evidence for Specific Germanium Siting in IM-12 Zeolite. *Chemistry of Materials* **2014,** *26* (19), 5556-5565.

71.   Chlubná , P.; Roth, W. J.; Greer, H. F.; Zhou, W. Z.; Shvets, O.; Zukal, A.; Čejka, J.; Morris, R. E., 3D to 2D Routes to Ultrathin and Expanded Zeolitic Materials. *Chemistry of Materials* **2013,** *25* (4), 542-547.

72.   Mazur, M.; Kubů, M.; Wheatley, P. S.; Eliášová, P., Germanosilicate UTL and its rich chemistry of solid-state transformations towards IPC-2 (OKO) zeolite. *Catalysis Today* **2015,** *243*, 23-31.

73.   Fan, W. B.; Wu, P.; Namba, S.; Tatsumi, T., A titanosilicate that is structurally analogous to an MWW-type lamellar precursor. *Angewandte Chemie-International Edition* **2004,** *43* (2), 236-240.

74.   Roth, W. J.; Shvets, O. V.; Shamzhy, M.; Chlubná, P.; Kubů, M.; Nachtigall, P.; Čejka, J., Postsynthesis Transformation of Three-Dimensional Framework into a Lamellar Zeolite with Modifiable Architecture. *Journal of the American Chemical Society* **2011,** *133* (16), 6130-6133.

75.   Verheyen, E.; Joos, L.; Van Havenbergh, K.; Breynaert, E.; Kasian, N.; Gobechiya, E.; Houthoofd, K.; Martineau, C.; Hinterstein, M.; Taulelle, F.; Van Speybroeck, V.; Waroquier, M.; Bals, S.; Van Tendeloo, G.; Kirschhock, C. E. A.; Martens, J. A., Design of zeolite by inverse sigma transformation. *Nature Materials* **2012,** *11* (12), 1059-1064.

76.   Wheatley, P. S.; Chlubná-Eliášová, P.; Greer, H.; Zhou, W. Z.; Seymour, V. R.; Dawson, D. M.; Ashbrook, S. E.; Pinar, A. B.; McCusker, L. B.; Opanasenko, M.; Čejka, J.; Morris, R. E., Zeolites with Continuously Tuneable Porosity. *Angewandte Chemie-International Edition* **2014,** *53* (48), 13210-13214.

77.   Paillaud, J. L.; Harbuzaru, B.; Patarin, J.; Bats, N., Extra-large-pore zeolites with two-dimensional channels formed by 14 and 12 rings. *Science* **2004,** *304* (5673), 990-992.

78.   Corma, A.; Diaz-Cabanas, M. J.; Rey, F.; Nicolooulas, S.; Boulahya, K., ITQ-15: The first ultralarge pore zeolite with a bi-directional pore system formed by intersecting 14- and 12-ring channels, and its catalytic implications. *Chemical Communications* **2004,** (12), 1356-1357.

79.   Morris, S. A.; Bignami, G. P. M.; Tian, Y.; Navarro, M.; Firth, D. S.; Čejka, J.; Wheatley, P. S.; Dawson, D. M.; Slawinski, W. A.; Wragg, D. S.; Morris, R. E.; Ashbrook, S. E., In situ solid-state NMR and XRD studies of the ADOR process and the unusual structure of zeolite IPC-6. *Nature Chemistry* **2017,** *9* (10), 1012-1018.

80.   Mazur, M.; Wheatley, P. S.; Navarro, M.; Roth, W. J.; Položij, M.; Mayoral, A.; Eliášová, P.; Nachtigall, P.; Čejka, J.; Morris, R. E., Synthesis of 'unfeasible' zeolites. *Nature Chemistry* **2016,** *8*, 58-62.

81.   Trachta, M.; Bludsky, O.; Čejka, J.; Morris, R. E.; Nachtigall, P., From Double-Four-Ring Germanosilicates to New Zeolites: In Silico Investigation. *Chemphyschem* **2014,** *15* (14), 2972-2976.

82.   Trachta, M.; Nachtigall, P.; Bludsky, O., The ADOR synthesis of new zeolites: In silico investigation. *Catalysis Today* **2015,** *243*, 32-38.

83.   Li, J. Y.; Corma, A.; Yu, J. H., Synthesis of new zeolite structures. *Chemical Society Reviews* **2015,** *44* (20), 7112-7127.
84.   Li, X.; Deem, M. W., Why Zeolites Have So Few Seven-Membered Rings. *Journal of Physical Chemistry C* **2014,** *118* (29), 15835-15839.
85.   Camblor, M. A.; Diaz-Cabanas, M. J.; Perez-Pariente, J.; Teat, S. J.; Clegg, W.; Shannon, I. J.; Lightfoot, P.; Wright, P. A.; Morris, R. E., SSZ-23: An odd zeolite with pore openings of seven and nine tetrahedral atoms. *Angewandte Chemie-International Edition* **1998,** *37* (15), 2122-2126.
86.   Xu, Y.; Li, Y.; Han, Y. D.; Song, X. W.; Yu, J. H., A Gallogermanate Zeolite with Eleven-Membered-Ring Channels. *Angewandte Chemie-International Edition* **2013,** *52* (21), 5501-5503.
87.   Hernandez-Rodriguez, M.; Jorda, J. L.; Rey, F.; Corma, A., Synthesis and Structure Determination of a New Microporous Zeolite with Large Cavities Connected by Small Pores. *Journal of the American Chemical Society* **2012,** *134* (32), 13232-13235.
88.   Deem, M. W.; Pophale, R.; Cheeseman, P. A.; Earl, D. J., Computational Discovery of New Zeolite-Like Materials. *Journal of Physical Chemistry C* **2009,** *113* (51), 21353-21360.
89.   Navarro, M.; Morris, S. A.; Mayoral, A.; Čejka, J.; Morris, R. E., Microwave heating and the fast ADOR process for preparing zeolites. *Journal of Materials Chemistry A* **2017,** *5* (17), 8037-8043.
90.   Mazur, M.; Arevalo-Lopez, A. M.; Wheatley, P. S.; Bignami, G. P. M.; Ashbrook, S. E.; Morales-Garcia, A.; Nachtigall, P.; Attfield, J. P.; Čejka, J.; Morris, R. E., Pressure-induced chemistry for the 2D to 3D transformation of zeolites. *Journal of Materials Chemistry A* **2018,** *6* (13), 5255-5259.
91.   Firth, D. S.; Morris, S. A.; Wheatley, P. S.; Russell, S. E.; Slawin, A. M. Z.; Dawson, D. M.; Mayoral, A.; Opanasenko, M.; Položij, M.; Čejka, J.; Nachtigall, P.; Morris, R. E., Assembly-Disassembly-Organization-Reassembly Synthesis of Zeolites Based on cfi-Type Layers. *Chemistry of Materials* **2017,** *29* (13), 5605-5611.
92.   Castañeda, R.; Corma, A.; Fornes, V.; Rey, F.; Rius, J., Synthesis of a new zeolite structure ITQ-24, with intersecting 10-and 12-membered ring pores. *Journal of the American Chemical Society* **2003,** *125* (26), 7820-7821.
93.   Corma, A.; Rey, F.; Valencia, S.; Jorda, J. L.; Rius, J., A zeolite with interconnected 8-, 10- and 12-ring pores and its unique catalytic selectivity. *Nat. Mater.* **2003,** *2* (7), 493-497.
94.   Corma, A.; Puche, M.; Rey, F.; Sankar, G.; Teat, S. J., A zeolite structure (ITQ-13) with three sets of medium-pore crossing channels formed by 9- and 10-rings. *Angewandte Chemie-International Edition* **2003,** *42* (10), 1156-1159.
95.   Corma, A.; Diaz-Cabanas, M. J.; Jorda, J. L.; Rey, F.; Sastre, G.; Strohmaier, K. G., A Zeolitic Structure (ITQ-34) with Connected 9-and 10-Ring Channels Obtained with Phosphonium Cations as Structure Directing Agents. *Journal of the American Chemical Society* **2008,** *130* (49), 16482-16483.
96.   Kang, J. H.; Xie, D.; Zones, S. I.; Smeets, S.; McCusker, L. B.; Davis, M. E., Synthesis and Characterization of CIT-13, a Germanosilicate Molecular Sieve with Extra-Large Pore Openings. *Chemistry of Materials* **2016,** *28* (17), 6250-6259.
97.   Moller, K.; Bein, T., Mesoporosity - a new dimension for zeolites. *Chemical Society Reviews* **2013,** *42* (9), 3689-3707.

98.   Weitkamp, J.; Sakuth, M.; Chen, C. Y.; Ernst, S., Dealumination of zeolite BETA using $(NH_4)_2SiF_6$ and $SICl_4$. *Journal of the Chemical Society-Chemical Communications* **1989,** (24), 1908-1910.

99.   Janssen, A. H.; Koster, A. J.; de Jong, K. P., Three-dimensional transmission electron microscopic observations of mesopores in dealuminated zeolite Y. *Angewandte Chemie-International Edition* **2001,** *40* (6), 1102-+.

100.   Scherzer, J., The preparation and characterization of alumunum-deficient zeolites. *Acs Symposium Series* **1984,** *248*, 157-200.

101.   Čejka, J.; Mintova, S., Perspectives of micro/mesoporous composites in catalysis. *Catalysis Reviews-Science and Engineering* **2007,** *49* (4), 457-509.

102.   Tromp, M.; van Bokhoven, J. A.; Oostenbrink, M. T. G.; Bitter, J. H.; de Jong, K. P.; Koningsberger, D. C., Influence of the generation of mesopores on the hydroisomerization activity and selectivity of n-hexane over Pt/mordenite. *Journal of Catalysis* **2000,** *190* (2), 209-214.

103.   Lupina, M. I.; Khusid, B. L.; Aliev, R. R., Effects of high-temperature treatment and steaming on properties of dealumination faujasites. *Chemistry and Technology of Fuels and Oils* **1992,** *28* (3-4), 139-144.

104.   Verboekend, D.; Perez-Ramirez, J., Design of hierarchical zeolite catalysts by desilication. *Catalysis Science & Technology* **2011,** *1* (6), 879-890.

105.   Groen, J. C.; Jansen, J. C.; Moulijn, J. A.; Perez-Ramirez, J., Optimal aluminum-assisted mesoporosity development in MFI zeolites by desilication. *Journal of Physical Chemistry B* **2004,** *108* (35), 13062-13065.

106.   Kubů, M.; Opanasenko, M.; Shamzy, M., Modification of textural and acidic properties of -SVR zeolite by desilication. *Catalysis Today* **2014,** *227*, 26-32.

107.   Perez-Ramirez, J.; Verboekend, D.; Bonilla, A.; Abello, S., Zeolite Catalysts with Tunable Hierarchy Factor by Pore-Growth Moderators. *Advanced Functional Materials* **2009,** *19* (24), 3972-3979.

108.   Groen, J. C.; Abello, S.; Villaescusa, L. A.; Perez-Ramirez, J., Mesoporous beta zeolite obtained by desilication. *Microporous and Mesoporous Materials* **2008,** *114* (1-3), 93-102.

109.   Sadowska, K.; Gora-Marek, K.; Drozdek, M.; Kustrowski, P.; Datka, J.; Triguero, J. M.; Rey, F., Desilication of highly siliceous zeolite ZSM-5 with NaOH and NaOH/tetrabutylamine hydroxide. *Microporous and Mesoporous Materials* **2013,** *168*, 195-205.

110.   Groen, J. C.; Caicedo-Realpe, R.; Abello, S.; Perez-Ramirez, J., Mesoporous metallosilicate zeolites by desilication: On the generic pore-inducing role of framework trivalent heteroatoms. *Materials Letters* **2009,** *63* (12), 1037-1040.

111.   Pavel, C. C.; Park, S. H.; Dreier, A.; Tesche, B.; Schmidt, W., Structural defects induced in ETS-10 by postsynthesis treatment with $H(2)O(2)$ solution. *Chemistry of Materials* **2006,** *18* (16), 3813-3820.

112.   Pavel, C. C.; Schmidt, W., Generation of hierarchical pore systems in the titanosilicate ETS-10 by hydrogen peroxide treatment under microwave irradiation. *Chemical Communications* **2006,** (8), 882-884.

113.   Du, S. T.; Chen, X. X.; Sun, Q. M.; Wang, N.; Jia, M. J.; Valtchev, V.; Yu, J. H., A non-chemically selective top-down approach towards the preparation of hierarchical TS-1 zeolites with improved oxidative desulfurization catalytic performance. *Chemical Communications* **2016,** *52* (17), 3580-3583.

114.   Burel, L.; Kasian, N.; Tuel, A., Quasi All-Silica Zeolite Obtained by Isomorphous Degermanation of an As-Made Germanium-Containing Precursor. *Angewandte Chemie-International Edition* **2014,** *53* (5), 1360-1363.

115.   Kasneryk, V. I.; Shamzhy, M. V.; Opanasenko, M. V.; Cejka, J., Tuning of textural properties of germanosilicate zeolites ITH and IWW by acidic leaching. *Journal of Energy Chemistry* **2016,** *25* (2), 318-326.

116.   Liu, X. L.; Kasian, N.; Tuel, A., New insights into the degermanation process of ITQ-17 zeolites. *Microporous and Mesoporous Materials* **2014,** *190*, 171-180.

117.   Shamzhy, M. V.; Eliášová, P.; Vitvarová, D.; Opanasenko, M. V.; Firth, D. S.; Morris, R. E., Post-Synthesis Stabilization of Germanosilicate Zeolites ITH, IWW, and UTL by Substitution of Ge for Al. *Chemistry-a European Journal* **2016,** *22* (48), 17377-17386.

118.   Shamzhy, M.; Ramos, F. S. d. O., Tuning of acidic and catalytic properties of IWR zeolite by post-synthesis incorporation of three-valent elements. *Catalysis Today* **2015,** *243*, 76-84.

119.   Shamzhy, M. V.; Opanasenko, M. V.; Ramos, F. S. D.; Brabec, L.; Horáček, M.; Navarro-Rojas, M.; Morris, R. E.; Pastore, H. D.; Čejka, J., Post-synthesis incorporation of Al into germanosilicate ITH zeolites: the influence of treatment conditions on the acidic properties and catalytic behavior in tetrahydropyranylation. *Catalysis Science & Technology* **2015,** *5* (5), 2973-2984.

120.   Shamzhy, M. V.; Ochoa-Hernandez, C.; Kasneryk, V. I.; Opanasenko, M. V.; Mazur, M., Direct incorporation of B, Al, and Ga into medium-pore ITH zeolite: Synthesis, acidic, and catalytic properties. *Catalysis Today* **2016,** *277*, 37-47.

121.   Gao, F.; Jaber, M.; Bozhilov, K.; Vicente, A.; Fernandez, C.; Valtchev, V., Framework Stabilization of Ge-Rich Zeolites via Postsynthesis Alumination. *Journal of the American Chemical Society* **2009,** *131* (45), 16580-16586.

122.   Fu, W. H.; Yuan, Z. Q.; Wang, Z. D.; Wang, Y. D.; Yang, W. M.; He, M. Y., Direct synthesis of hydrothermally stable Ge-IWR zeolites. *Dalton Transactions* **2017,** *46* (20), 6692-6699.

123.   Cantin, A.; Corma, A.; Diaz-Cabanas, M. J.; Jorda, J. L.; Moliner, M., Rational design and HT techniques allow the synthesis of new IWR zeolite polymorphs. *Journal of the American Chemical Society* **2006,** *128* (13), 4216-4217.

124.   Hussain, A. I.; Palani, A.; Aitani, A. M.; Čejka, J.; Shamzhy, M.; Kubů, M.; Al-Khattaf, S. S., Catalytic cracking of vacuum gasoil over -SVR, ITH, and MFI zeolites as FCC catalyst additives. *Fuel Processing Technology* **2017,** *161*, 23-32.

125.   Liu, X.; Xu, H.; Zhang, L.; Han, L.; Jiang, J. G.; Oleynikov, P.; Chen, L.; Wu, P., Isomorphous Incorporation of Tin Ions into Germanosilicate Framework Assisted by Local Structural Rearrangement. *Acs Catalysis* **2016,** *6* (12), 8420-8431.

126.   Xu, H.; Jiang, J.-g.; Yang, B.; Zhang, L.; He, M.; Wu, P., Post-Synthesis Treatment gives Highly Stable Siliceous Zeolites through the Isomorphous Substitution of Silicon for Germanium in Germanosilicates. *Angewandte Chemie International Edition* **2014,** *53* (5), 1355-1359.

127.   Rodriguez-Fernandez, A.; Llopis, F. J.; Martinez, C.; Moliner, M.; Corma, A., Increasing the stability of the Ge-containing extra-large pore ITQ-33 zeolite by post-synthetic acid treatments. *Microporous and Mesoporous Materials* **2018,** *267*, 35-42.

128.   Shvets, O. V.; Nachtigall, P.; Roth, W. J.; Čejka, J., UTL zeolite and the way beyond. *Microporous and Mesoporous Materials* **2013,** *182*, 229-238.

129.   Shvets, O. V.; Kasian, N.; Zukal, A.; Pinkas, J.; Čejka, J., The Role of Template Structure and Synergism between Inorganic and Organic Structure Directing Agents in the Synthesis of UTL Zeolite. *Chemistry of Materials* **2010,** *22* (11), 3482-3495.

130.   Přech, J.; Čejka, J., UTL titanosilicate: An extra-large pore epoxidation catalyst with tunable textural properties. *Catalysis Today* **2016,** *277*, 2-8.

131.   Shamzhy, M. V.; Shvets, O. V.; Opanasenko, M. V.; Yaremov, P. S.; Sarkisyan, L. G.; Chlubná, P.; Zukal, A.; Marthala, V. R.; Hartmann, M.; Čejka, J., Synthesis of isomorphously substituted extra-large pore UTL zeolites. *Journal of Materials Chemistry* **2012,** *22* (31), 15793-15803.

132.   Žilková, N.; Shamzhy, M.; Shvets, O.; Čejka, J., Transformation of aromatic hydrocarbons over isomorphously substituted UTL: Comparison with large and medium pore zeolites. *Catalysis Today* **2013,** *204*, 22-29.

133.   Shamzhy, M. V.; Shvets, O. V.; Opanasenko, M. V.; Kurfiřtová, L.; Kubička, D.; Čejka, J., Extra-Large-Pore Zeolites with UTL Topology: Control of the Catalytic Activity by Variation in the Nature of the Active Sites. *Chemcatchem* **2013,** *5* (7), 1891-1898.

134.   Kang, L. H.; Deng, W. Q.; Zhang, T.; Liu, Z. M.; Han, K. L., Theoretical studies of IM-12 zeolite for acidic catalysts. *Microporous and Mesoporous Materials* **2008,** *115* (3), 261-266.

135.   Xu, H.; Jiang, J. G.; Yang, B. T.; Wu, H. H.; Wu, P., Effective Baeyer-Villiger oxidation of ketones over germanosilicates. *Catalysis Communications* **2014,** *55*, 83-86.

136.   Kasian, N.; Verheyen, E.; Vanbutsele, G.; Houthoofd, K.; Koranyi, T. I.; Martens, J. A.; Kirschhock, C. E. A., Catalytic activity of germanosilicate UTL zeolite in bifunctional hydroisomerisation of n-decane. *Microporous and Mesoporous Materials* **2013,** *166*, 153-160.

137.   Gao, Z. H.; Chen, F. J.; Xu, L.; Sun, L.; Xu, Y.; Du, H. B., A Stable Extra-Large-Pore Zeolite with Intersecting 14-and 10-Membered-Ring Channels. *Chemistry-a European Journal* **2016,** *22* (40), 14367-14372.

138.   Sastre, G.; Pulido, A.; Castañeda, R.; Corma, A., Effect of the Germanium Incorporation in the Synthesis of EU-1, ITQ-13, ITQ-22, and ITQ-24 Zeolites. *Journal of Physical Chemistry B* **2004,** *108* (26), 8830-8835.

139.   Yuan, R. T.; Claes, N.; Verheyen, E.; Tuel, A.; Bals, S.; Breynaert, E.; Martens, J. A.; Kirschhock, C. E. A., Synthesis of an IWW-type germanosilicate zeolite using 5-azonia-spiro 4,4 nonane as a structure directing agent. *New Journal of Chemistry* **2016,** *40* (5), 4319-4324.

140.   Corma, A.; Llopis, F. J.; Martinez, C.; Sastre, G.; Valencia, S., The benefit of multipore zeolites: Catalytic behaviour of zeolites with intersecting channels of different sizes for alkylation reactions. *Journal of Catalysis* **2009,** *268* (1), 9-17.

141.   Moliner, M.; Martinez, C.; Corma, A., Multipore Zeolites: Synthesis and Catalytic Applications. *Angewandte Chemie-International Edition* **2015,** *54* (12), 3560-3579.

142.   Liu, X. L.; Ravon, U.; Bosselet, F.; Bergeret, G.; Tuel, A., Probing Ge Distribution in Zeolite Frameworks by Post-Synthesis Introduction of Fluoride in As-Made Materials. *Chemistry of Materials* **2012,** *24* (15), 3016-3022.

143.   Chlubná-Eliášová, P.; Tian, Y. Y.; Pinar, A. B.; Kubů, M.; Čejka, J.; Morris, R. E., The Assembly-Disassembly-Organization-Reassembly Mechanism for 3D-2D-3D Transformation of Germanosilicate IWW Zeolite. *Angewandte Chemie-International Edition* **2014,** *53* (27), 7048-7052.

144.   Pinar, A. B.; McCusker, L. B.; Baerlocher, C.; Schmidt, J.; Hwang, S. J.; Davis, M. E.; Zones, S. I., Location of Ge and extra-framework species in the zeolite ITQ-24. *Dalton Transactions* **2015,** *44* (13), 6288-6295.

145.   Jorda, J. L.; Cantin, A.; Corma, A.; Diaz-Cabanas, M. J.; Leiva, S.; Moliner, M.; Rey, F.; Sabater, M. J.; Valencia, S., Structural study of pure silica and Gecontaining zeolite ITQ-24. *Zeitschrift Fur Kristallographie* **2007**, 393-398.

146.   Castañeda, R.; Corma, A.; Fornes, V.; Martinez-Triguero, J.; Valencia, S., Direct synthesis of a 9 x 10 member ring zeolite (Al-ITQ-13): A highly shape-selective catalyst for catalytic cracking. *Journal of Catalysis* **2006,** *238* (1), 79-87.

147.   Buchanan, J. S.; Dakka, J. M.; Feng, X.; Santiesteban, J. G., Aromatics conversion with ITQ-13. *US7081556 B2*.

148.   Llopis, F. J.; Sastre, G.; Corma, A., Isomerization and disproportionation of m-xylene in a zeolite with 9-and 10-membered ring pores: Molecular dynamics and catalytic studies. *Journal of Catalysis* **2006,** *242* (1), 195-206.

149.   Zeng, P. H.; Guo, X. Z.; Zhu, X. C.; Guo, Q. X.; Wang, Y. D.; Ren, S. Y.; Shen, B. J., On the synthesis and catalytic cracking properties of Al-ITQ-13 zeolites. *Microporous and Mesoporous Materials* **2017,** *246*, 186-192.

150.   Li, L. P.; Chen, Y. Y.; Xu, S. T.; Li, J. F.; Dong, M.; Liu, Z. W.; Jiao, H. J.; Wang, J. G.; Fan, W. B., Oriented control of Al locations in the framework of Al-Ge-ITQ-13 for catalyzing methanol conversion to propene. *Journal of Catalysis* **2016,** *344*, 242-251.

151.   Zeng, P.; Zhang, L.; Guo, X.; Li, M.; Guo, Q.; Niu, C.; Shen, B., Catalytic performances of Al-ITQ-13 zeolites with different SiO_2/Al_2O_3 ratios in the conversion of methanol to propene. *Journal of Fuel Chemistry and Technology* **2017,** *45* (11), 1349-1355.

152.   Xu, G. L.; Zhu, X. X.; Li, X. J.; Xie, S. J.; Liu, S. L.; Xu, L. Y., Synthesis of pure silica ITQ-13 zeolite using fumed silica as silica source. *Microporous and Mesoporous Materials* **2010,** *129* (1-2), 278-284.

153.   Vidal-Moya, J. A.; Blasco, T.; Rey, F.; Corma, A.; Puche, M., Distribution of fluorine and germanium in a new zeolite structure ITQ-13 studied by F-19 nuclear magnetic resonance. *Chemistry of Materials* **2003,** *15* (21), 3961-3963.

154.   Bats, N.; Rouleau, L.; Paillaud, J. L.; Caullet, P.; Mathieu, Y.; Lacombe, S., Recent developments in the use of hexamethonium salts as structure directing agents in zeolite synthesis. In *Recent Advances in the Science and Technology of Zeolites and Related Materials, Pts a - C*, VanSteen, E.; Claeys, M.; Callanan, L. H., Eds. 2004; Vol. 154, pp 283-288.

155.   Ren, X.; Liu, J.; Li, Y.; Yu, J.; Xu, R., Hydrothermal synthesis of an ITH-type germanosilicate zeolite in a non-concentrated gel system. *Journal of Porous Materials* **2013,** *20* (4), 975-981.

156.   Liu, X. L.; Ravon, U.; Tuel, A., Effect of HF concentration on the composition and distribution of Ge species in the framework of ITQ-13 and ITQ-17 zeolites. *Microporous and Mesoporous Materials* **2013,** *170*, 194-199.

157.   Liu, X. L.; Chu, Y. Y.; Wang, Q.; Wang, W. Y.; Wang, C.; Xu, J.; Deng, F., Identification of double four-ring units in germanosilicate ITQ-13 zeolite by solid-state NMR spectroscopy. *Solid State Nuclear Magnetic Resonance* **2017,** *87*, 1-9.

158.   Brunauer, S.; Emmett, P. H.; Teller, E., Adsorption of Gases in Multimolecular Layers. *J. Am. Chem. Soc* **1938,** *60 (2)*, pp 309–319.

159.   Lippens, B. C.; Deboer, J. H., Studies on pore systems in catalysts V.T. method. *Journal of Catalysis* **1965,** *4* (3), 319-&.

160.   Barrett, E. P.; Joyner, L. G.; Halenda, P. P., The determination of pore volume and area distributions in porous substances. 1. Computations from nitrogen isotherms. *Journal of the American Chemical Society* **1951,** *73* (1), 373-380.

161.   Emeis, C. A., Determination of integrated molar extinction coefficients for infrared-absorption bands of pyridine adsorbed on solid acid catalysts. *Journal of Catalysis* **1993,** *141* (2), 347-354.

162.   Johnson, O. H., Germanium and its inorganic compounds. *Chemical Reviews* **1952,** *51* (3), 431-469.

163.   Kasneryk, V.; Shamzhy, M.; Opanasenko, M.; Wheatley, P. S.; Morris, S. A.; Russell, S. E.; Mayoral, A.; Trachta, M.; Cejka, J.; Morris, R. E., Expansion of the ADOR Strategy for the Synthesis of Zeolites: The Synthesis of IPC-12 from Zeolite UOV. *Angewandte Chemie-International Edition* **2017,** *56* (15), 4324-4327.

7. Enclosures

1. <u>Kasneryk, V.</u>; Shamzhy, M.; Opanasenko, M.; Wheatley, P. S.; Morris, S. A.; Russell, S. E.; Mayoral, A.; Trachta, M.; Čejka, J.; Morris, R. E., Expansion of the ADOR Strategy for the Synthesis of Zeolites: The Synthesis of IPC-12 from Zeolite UOV. *Angewandte Chemie-International Edition* **2017,** *56* (15), 4324-4327.

2. <u>Kasneryk, V</u>.; Opanasenko, M.; Shamzhy, M.; Musilová, Z.; Avadhut, Y. S.; Hartmann, M.; Čejka J., Consecutive interlayer disassembly–reassembly during alumination of UOV zeolites: insight into the mechanism. *Journal of Materials Chemistry A* **2017**, *5*, 22576-22587.

3. <u>Kasneryk, V.</u>; Shamzhy, M.; Opanasenko, M.; Wheatley, P. S.; Morris, R. E.; Čejka, J., Insight into the ADOR zeolite-to-zeolite transformation: the UOV case. *Dalton Transactions* **2018**, *47*, 3084-3092.

4. <u>Kasneryk, V. I.</u>; Shamzhy, M. V.; Opanasenko, M. V.; Čejka, J., Tuning of textural properties of germanosilicate zeolites ITH and IWW by acidic leaching. *Journal of Energy Chemistry* **2016,** *25* (2), 318-326.

5. Shamzhy, M. V.; Ochoa-Hernandez, C.; <u>Kasneryk, V. I.</u>; Opanasenko, M. V.; Mazur, M., Direct incorporation of B, Al, and Ga into medium-pore ITH zeolite: Synthesis, acidic, and catalytic properties. *Catalysis Today* **2016,** *277*, 37-47.